

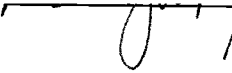
AN ABSTRACT OF THE THESIS OF

Peng-Cheng Lin for the degree of Doctor of Philosophy in
Mechanical Engineering presented on November 8, 1988.

Title: An Experimental Study of Natural Convection from Protruding
Arrays on A Vertical Plate with and without An Opposing Wall for
Various Fluids

Redacted for privacy

Abstract approved:

 Dwight J. Bushnell

Natural convection from six rectangular protruding heated arrays on a vertical plate with and without an unheated shrouding wall was experimentally investigated. The protruding arrays with square cross sectional areas were evenly spaced and mounted horizontally on the vertical plate. The boundary conditions were all uniform at equal heat flux for the vertical surfaces of the protruding arrays. The variation of the uniform heat flux surface condition among the heated array surfaces was less than 5%. Air, distilled water, and Chevron multi-machine oil 68 were employed as the bath fluids to vary the Prandtl numbers in the range of 0.72 to 1,009. The modified Rayleigh numbers based on the array height were between 1.6×10^5 and 3.8×10^8 . The channel spacing-to-height ratios, b/H , were 0.104, 0.167, 0.358, 0.567, and ∞ , respectively.

The heated array vertical surface temperature was the lowest in the water bath, the second lowest in the oil, and the highest in the ambient air for a fixed uniform heating. Maximum heat transfer rates were attainable in the vertical channel with $b/H = 0.104$. For a given modified Rayleigh number, the inequality relation of local Nusselt number, $Nu_{x,oil} > Nu_{x,air} >$

Nu_{x,H_2O} , prevailed for all data. Three distinct flow regions: a buoyancy driven boundary layer flow region, a stagnant fluid region, and a reversed flow region were observed in the channel. The penetration depth of the reversed flow into the channel top varies with the kind of working fluids used. Comparisons of heat transfer results with a smooth vertical heated wall and a smooth vertical channel with one wall heated are discussed. The percent uncertainty in the heat transfer coefficient is about 5%. The best correlations for the natural convection from protruding arrays on a vertical plate with all fluids combined is

$$Nu_B = 7.5021 (Ra_B^*)^{-0.1930} \quad \text{for } 0.72 < Pr < 974$$

with a 18% average deviation. The best correlation for the vertical channels with protruding arrays on one wall with all fluids combined is

$$Nu_b = 4.9884 (b/H)^{0.7657} (Ra_b^*)^{0.1480} \quad \text{for } 0.72 < Pr < 1,009$$

with a 28% average deviation.

An Experimental Study Of Natural Convection From
Protruding Arrays On A Vertical Plate With And Without
An Opposing Wall For Various Fluids

by

Peng-Cheng Lin

A THESIS

submitted to

Oregon State University

in partial fulfillment of
the requirements for the
degree of

Doctor of Philosophy

Completed November 8, 1988

Commencement June 1989

APPROVED:

Redacted for privacy

Professor of Mechanical Engineering in charge of major

Redacted for privacy

Head of department of Mechanical Engineering

Redacted for privacy

Dean of Graduate School

Date thesis is presented November 8, 1988

Typed by Sue-May Jin for Peng-Cheng Lin

ACKNOWLEDGEMENTS

I wish to express my appreciation to my major advisor Professor Dwight J. Bushnell for his help and encouragement. His efforts were a direct and indispensable contribution to the completion of the research reported herein.

The inspiration furnished by Professor Robert O. Warrington, Head of the Mechanical Engineering Department at Louisiana Technology Institute is hereby cited as contributing to this research. Exposure to his contagious enthusiasm during the author's early years as a graduate student contributed indirectly but substantially to the realization of this thesis.

The moral support from Dr. Milton B. Larson and Dr. Peter Burke are greatly appreciated. I would like to express my appreciation to each member of my committee: Professors Milton B. Larson, Timothy C. Kennedy, Alan H. Robinson, and Edward R. Kolbe, for the time they spent.

I would also like to extend my appreciation to Professor Robert E. Wilson for his treatise in fluid mechanics and complex variables.

I would like to thank The Mechanical Engineering Department at Oregon State University for providing me a teaching assistantship during my graduate program.

I acknowledge Hewlett Packard for the use of their computer and other equipment.

Without the devotion of my parents, my goals could not be accomplished. Many others have also given of themselves in my behalf. Without their efforts in the form of support, guidance, and encouragement, this work would not have been possible.

Finally, I would like to express my gratitude to my wife, Sue-May, and my son, Eugene, who have suffered such a long student life with me.

NOMENCLATURE

<u>Symbol</u>	<u>Description</u>
A	Each discrete heating surface area, m^2
B	Protruding discrete heating element height, cm
b	Channel spacing, cm
Bo_L	Boussinesq number $Pr \times Ra_L$
C	Arbitrary constant
C_p	Specific heat at constant pressure, $kJ/(kg \cdot ^\circ K)$
C_f	Friction coefficient
D	Hydrodynamic Diameter, cm
d_p	Penetration depth, cm
$El_{ba,b}$	Elenbaas number, $(b/H) Ra_b$
G	Volumetric flow rate, M/ρ , m^3/sec
Gr_L	Grashof number, $g\beta\Delta TL^3/\nu^2$
Gr_L^*	Modified Grashof number, $Gr_L \times Nu_L$
Gr_x	Local Grashof number, $g\beta\Delta T x^3/\nu^2$
g	Acceleration of gravity, m/sec^2
H	Channel height, m
h	Convective heat transfer coefficient, $q''/(T_h - T_c)$, $W/(m^2 \cdot ^\circ K)$
I	Current, A
k	Thermal conductivity $W/(m \cdot ^\circ K)$
L	Arbitrary characteristic length, m
M	Mass flow rate, Kg/sec
m	Slope of a line
Nu_L	Nusselt number, hL/k
Nu_x	Local Nusselt number, hx/k
Pr	Prandtl number, ν/α
Q	Heat flux by convection, W
Q_{cond}	Heat transfer by conduction, W
Q_{conv}	Heat transfer by convection, W
Q_{rad}	Heat transfer by radiation, W
Q_{tot}	Total power input, I V, W
q''	Heat flux per unit area, Q/A , W/m^2
R	Electrical resistance, Ω
Ra_L	Rayleigh number, $Pr \times Gr_L$ or $g\beta\Delta TL^3/\nu^2$

Ra_B^*	Modified Rayleigh number, $g\beta q'' B^4/(\alpha \nu k)$
Ra_b^*	Modified Rayleigh number, $g\beta q'' b^4/(\alpha \nu k)$
Ra_L^*	Modified Rayleigh number, $g\beta q'' L^4/(\alpha \nu k)$
Re_L	Reynolds number, uL/ν
Ra_x^*	Local modified Rayleigh number
s	Spacing between protruding elements, cm
T_B	Protruding block center surface temperature, °K
T_C	Chamber or ambient fluid temperature, °K
T_h	Heated surface temperature, $T_h = T_B$, °K
T_i	i th row protruding heated array temperature, °K
T_m	Arithmetic mean fluid temperature, $(T_B + T_\infty)/2$, °K
T_s	Shroud wall center surface temperature, °K
T_w	Wall temperature, °K
T_∞	Ambient temperature, $T_\infty = T_C$, °K
u	Traverse velocity component, m/sec
V	Voltage, V
v	Streamwise velocity component, m/sec
x	Streamwise or vertical direction
y	Traverse or horizontal direction
α	Thermal diffusivity, $k/(\rho C_p)$, m^2/sec
β	Thermal expansion coefficient, $1/^\circ K$
δ	Hydrodynamic boundary layer, mm
δ_t	Thermal boundary layer, mm
γ	Angle tilted from horizontal, °
μ	Dynamic viscosity, Pa.sec
ν	Momentum diffusivity, μ/ρ , m^2/sec
ρ	Fluid density, kg/m^3
θ	Dimensionless temperature, $T_i - T_C/(T_{max} - T_C)$

TABLE OF CONTENTS

Chapter	Page
1. INTRODUCTION	1
2. LITERATURE REVIEW	6
2.1 Scope	6
2.2 Natural Convection from Vertical Plate	6
2.3 Natural Convection in Vertical Channels	11
2.4 Heat Transfer in Electronic Equipment	21
3. THEORETICAL ANALYSIS	22
3.1 Scope	22
3.2 Principles of Conservation	22
3.3 Scaling Analysis	23
3.4 Prandtl Number Effects	25
3.5 Geometric Variation	26
4. EXPERIMENTAL APPARATUS AND PROCEDURE	28
4.1 Scope	28
4.2 Experimental Apparatus	29
4.2.1 Test Section	29
4.2.1.1 Inner Chamber and Water Jacket	29
4.2.1.2 Vertical Channel	33
4.2.1.3 Discrete Heat Sources Arrangement	33
4.2.2 Power Supply	36
4.2.3 Cooling Water System	36
4.2.4 Instrumentation	39
4.2.4.1 Power Measurement	39
4.2.4.2 Surface Temperature Measurement	39
4.2.4.3 Channel Inlet/Outlet Fluid Temperature	39
4.2.4.4 Data Acquisition System	40
4.2.5 Flow Visualization	40
4.3 Experimental Procedures	41
4.3.1 Experimental Set-up	41
4.3.2 Data Calibration	42
4.3.3 Data Collection	42
4.3.4 Heat Transfer Coefficient Calculations	43
4.3.5 Uncertainty Analysis	44
4.3.6 Flow Visualization	45

5. RESULTS AND DISCUSSIONS	47
5.1 Scope	47
5.2 Temperature Distribution of Discrete Heating Surfaces	47
5.3 Fluid Property Effects	51
5.4 Prandtl Number Effect	57
5.5 Heat Transfer Results Comparison	61
5.6 Flow Visualization Results	80
5.7 Empirical Equation	86
6. CONCLUSION AND RECOMMENDATIONS	94
6.1 Conclusions	94
6.2 Recommendations	97
BIBLIOGRAPHY	98
APPENDICES	
A TEMPERATURE DATA ACQUISITION PROGRAM	107
B RADIATION CORRECTION	109
C AVERAGE HEAT FLUX	117
D HEAT TRANSFER DATA REDUCTION PROGRAM	118
E UNCERTAINTY ANALYSIS	129
F SAMPLE OF EXPERIMENTAL DATA LOG	132
G RAW HEAT TRANSFER DATA	133
H FLUID PROPERTY VARIATION WITH TEMPERATURE	144
I CORRELATION PROGRAM	149

LIST OF FIGURES

Figure		Page
1.1	Schematic of Vertical Plate with Protruding Discrete Heat Sources	2
1.2	Schematic of 2-D Vertical Channel with Protruding Discrete Heat Sources	3
4.1	Overall Heat Transfer Test Apparatus	30
4.2	Schematic of Test Set-Up and Microcomputer Based Data Acquisition System	31
4.3	Schematic of Experimental Set Up for Free Convection in a Vertical Channel	32
4.4	Schematic of Vertical Protruding Array Plate with Discrete Heat Sources	34
4.5	Heating Element Arrangement and Thermocouple Locations	35
4.6	Schematic of Heater Tape Arrangement and Thermocouple Locations on Heated Surface	37
4.7	Protruding Heated Array Center Cutaway View	38
5.1	Q versus x/H for Various b/H	
(a)	Air; $Q = 5.86W$	48
(b)	Air; $Q = 7.33W$	48
5.2	Q versus x/H for Various b/H	
(a)	H ₂ O; $Q = 7.33W$	49
(b)	H ₂ O; $Q = 33.71W$	49
5.3	Q versus x/H for Various b/H	
(a)	Oil; $Q = 7.33W$	50
(b)	Oil; $Q = 33.71W$	50
5.4	Q versus x/H for Various Q	
(a.1)	b/H - Infinite; $Pr = 0.72$	52

5.4		
(a.2)	b/H - Infinite; $586 < Pr < 974$	52
(b.1)	b/H - 0.567; $Pr = 0.72$	53
(b.2)	b/H - 0.567; $586 < Pr < 974$	53
(c.1)	b/H - 0.358; $Pr = 0.72$	54
(c.2)	b/H - 0.358; $586 < Pr < 974$	54
(d.1)	b/H - 0.167; $Pr = 0.72$	55
(d.2)	b/H - 0.167; $586 < Pr < 974$	55
(e.1)	b/H - 0.104; $Pr = 0.72$	56
(e.2)	b/H - 0.104; $586 < Pr < 974$	56
5.5	Momentum Diffusivity-Temperature Variation	58
5.6		
(a)	Thermal Diffusivity-Temperature Variation	59
(b)	Thermal Diffusivity-Temperature Variation; Water and Oil	60
5.7		
(a)	Prandtl Number-Temperature Variation	62
(b)	Prandtl Number-Temperature Variation; Water and Air	63
5.8	h versus B/b	
(a)	Air; Row 1	64
(b)	Air; Row 6	64
(c)	Air; Row 4	65
5.9	Comparison of h versus B/b for Various Fluids	
(a)	$Q = 7.33W$; Row 1	66
(b)	$Q = 7.33W$; Row 6	66
(c)	$Q = 7.33W$; Row 4	67
5.10	Comparison of Local Nu and $Ra \times Pr$ for Various Fluids	69
5.11	Comparison of Air Data with Dotson for Protruding Arrays without Shrouding	71
5.12	Comparison of Water Data with Vliet & Liu [76] for Protruding Arrays without Shrouding	72
5.13	Comparison of Oil Data with Fujii & Fujii [78] for Protruding Arrays without Shrouding	73

5.14	Comparison of Air Data with Churchill & Chu [57] for Protruding Arrays without Shrouding	74
5.15	Comparison of Water Data with Churchill & Chu [57] for Protruding Arrays without Shrouding	75
5.16	Comparison of Oil Data with Churchill & Chu [57] for Protruding Arrays without Shrouding	76
5.17	Comparison of Air Data with Fujii & Fujii [78] for Protruding Arrays with Shrouding	77
5.18	Comparison of Water Data with Fujii & Fujii [78] for Protruding Arrays with Shrouding	78
5.19	Comparison of Oil Data with Fujii & Fujii [78] for Protruding Arrays with Shrouding	79
5.20	Comparisons of Flow Patterns in Vertical Channels with Same Heat Flux, $Q = 5.86W$	
(a)	Air; $b/H = 0.357$; $Ra_b^* = 3.5 \times 10^7$	81
(b)	Distilled Water; $b/H = 0.357$; $Ra_b^* = 9.2 \times 10^8$	81
(c)	Distilled Water; $b/H = 0.167$; $Ra_b^* = 4.6 \times 10^7$	81
5.21	Typical Flow Pattern in Vertical Channels with Protruding Heated Arrays for $b/H = 0.567$ & 0.358	82
5.22	Anticipated Velocity Profile adjacent to the Channel Outlet with Protruding Heated Arrays for $b/H = 0.567$ & 0.358	84
B.1	Schematic of 2-D Vertical Channel with Protruding Discrete Heat Sources for Radiation Correction	110
G.1	Q and ΔT Variation on Protruding Arrays without Shrouding for Various Fluids	134
G.2	Q and ΔT Variation on Protruding Arrays with Shrouding for Various Fluids	
(a)	$b/H = 0.567$	135
(b)	$b/H = 0.358$	136
(c)	$b/H = 0.167$	137

G.2		
(d)	$b/H = 0.104$	138
G.3	Q and ΔT Variation on a Protruding Array for Various b/H Values	
(a)	For First Row	140
(b)	For Fourth Row	141
(c)	For Sixth Row	142
H		
(a)	Thermal Conductivity-Temperature Variation	144
(b)	Thermal Expansion Coefficient-Temperature Variation	145
(c)	Specific Heat-Temperature Variation	146
(d)	Density-Temperature Variation	147
(e)	Dynamic Viscosity-Temperature Variation	148

LIST OF TABLES

Table		Page
1.1	Range of Dimensionless Parameters	5
2.1	Convection Heat Transfer in Vertical Channels	12
5.1	Range of Correlating Parameter	88
5.2	Correlation for Vertical Plate Case	89
5.3	Correlation for Vertical Channel Case	90
5.4	Correlation for Protruding Array Plate with shrouding	91

AN EXPERIMENTAL STUDY OF NATURAL CONVECTION FROM PROTRUDING ARRAYS ON A VERTICAL PLATE WITH AND WITHOUT AN OPPOSING WALL FOR VARIOUS FLUIDS

CHAPTER 1

INTRODUCTION

During this decade, natural convection heat transfer from a vertical plate or in a vertical channel with discrete protruding heat sources has been receiving increasing research activities. This is due to the interest in heat removal from microelectronic systems and communication systems, high performance heat exchange systems, energy efficient buildings, manufacturing processes, and many other applications. The study of natural convection from a vertical plate and in vertical channels with discrete heat sources in air, water, and oil is proposed for this thesis project.

Figures 1.1 and 1.2 illustrate the arrangement of an array of square blocks attached to an unheated vertical wall with and without an unheated shrouding wall for the proposed investigation. A buoyancy driven flow would occur when the vertical surfaces of the blocks are heated. Each heated surface induces an upward buoyancy boundary layer flow. In turn, each protruding block has a rising flow which may impinge on the neighboring rising flow at a point downstream. The overall rising flow accelerates as it proceeds downstream. The overall boundary layer, hence, is building up and is thickening near the upper block surface. The buoyancy flows may be modified when an unheated shrouding wall is placed parallel and opposite to the protruding element plate with certain finite spacing. The interaction of thermal energy spreading and the momentum diffusion in the boundary layer region for this geometric arrangement make accurate analytic prediction of natural convection processes difficult.

Owing to the lack of quantitative data, it is difficult to predict whether such interactions will enhance or reduce the natural convection heat transfer.

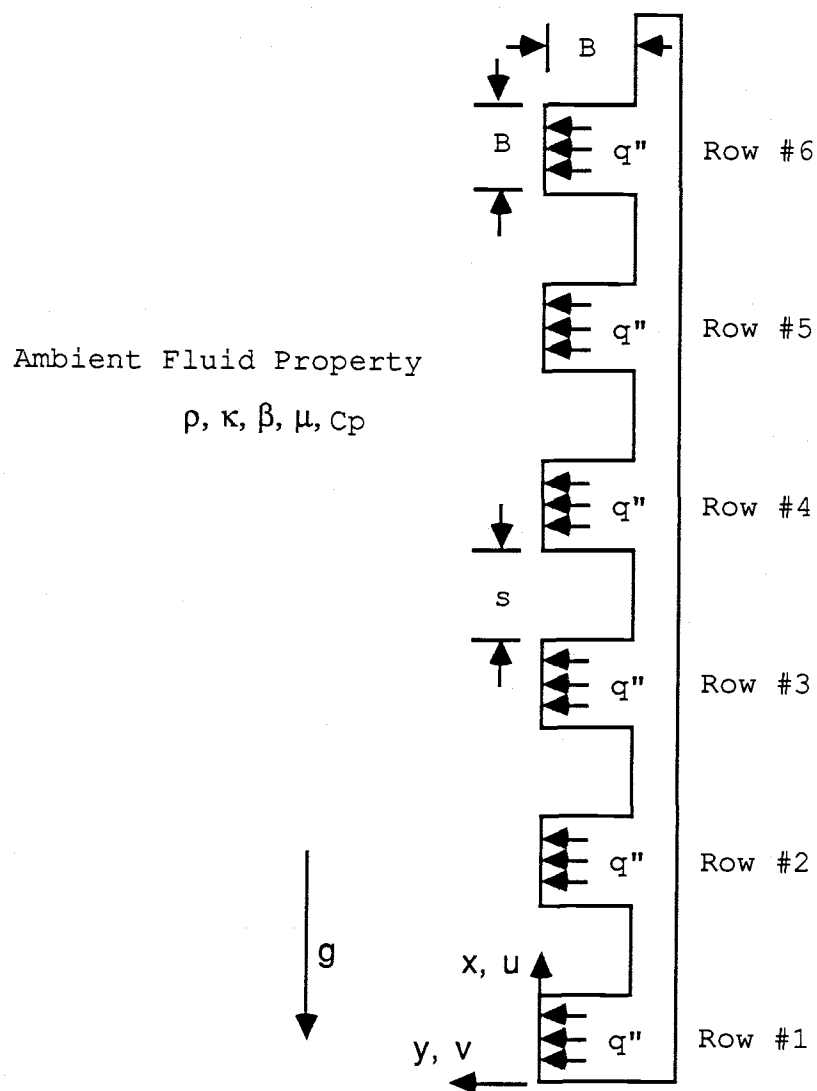


Figure 1.1 Schematic of Vertical Plate with Protruding Discrete Heat Sources

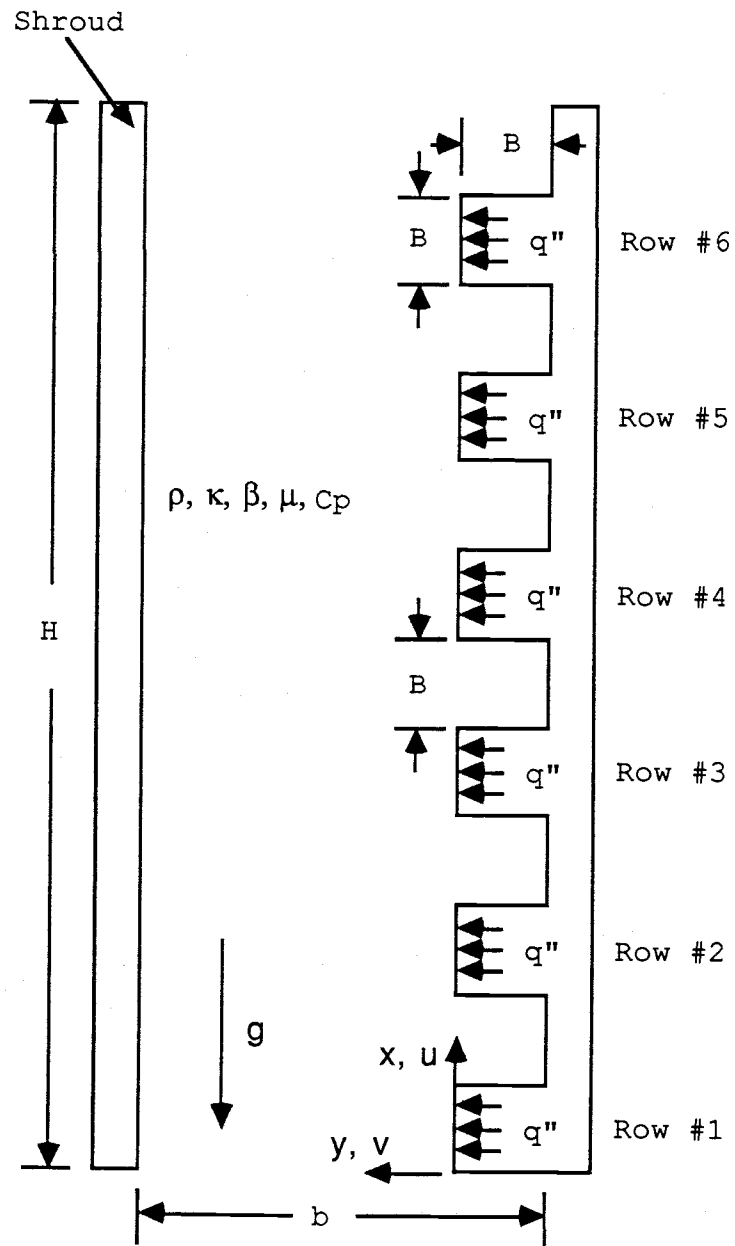


Figure 1.2 Schematic of 2-D Vertical Channel with Protruding Discrete Heat Sources

Strong natural convection heat transfer may be achieved at certain interplate spacing. Natural convection also depends upon the fluid property variation. The present work is to develop an experimental model for the study of two-dimensional natural convective processes from a vertical plate with protruding discrete heated elements with and without a shrouding wall. The objective of this experimental study is

1. to determine the natural convection heat transfer characteristic of the block,
2. to identify the effects of the shrouding wall,
3. to understand the effects of the geometric parameters on the heat transfer,
4. to obtain flow patterns with the aid of flow visualization, and
5. to propose empirical correlations in the form of $Nu = f(b/H, Ra^*)$.

Table 1.1 shows the range of parameters achieved in the experiment. The modified Rayleigh number based on the element height was less than 4.0×10^8 . The Prandtl number varied from 0.7 to 1,009 by use of air, distilled water, and Chevron multi-machine oil 68 (base oil) as working fluids. The interplate spacing to plate height ratios (b/H) are 0.104, 0.167, 0.358, 0.567, and ∞ . The element height to interplate spacing ratios (B/b) are 0.8, 0.525, 0.233, 0.167, and 0.

Table 1.1 Range of Dimensionless Parameters

Dimensionless Parameter	Minimum	Maximum
Pr	0.72	1009
Rax*	6000	1. 1E+11
b/H	0.104	Infinite
B/b	0	0.8

CHAPTER 2

LITERATURE REVIEW

2.1 Scope

When a vertical surface is heated, a buoyancy driven flow will rise along the surface due to density differences in the adjacent fluid. This driven flow is a natural convection phenomenon caused by the diffusion of surface heating in the gravitational field. The natural convection flow and heat transfer rate may be altered depending on the specific boundary conditions, geometric configuration and its orientation, variable fluid properties, and the gravitational intensity. The field of natural convection has been broad and diverse. Recent textbooks authored by Bejan [1], Arpaci and Larsen [2], and Jaluria [3] are recommended for reviewing the fundamentals of this field. Particularly comprehensive reviews of both experimental and theoretical studies for the field of natural convection have been compiled by Kakac et al. [4] and Gebhart et al. [5] most recently.

As a result, in this chapter it is only necessary to highlight some important methods and findings and describe some details of work related to the present thesis work. Hence, the following review of natural convection is categorized into three sections: natural convection from vertical plates, natural convection in vertical channels, and heat transfer in electronic equipment. The last section lists sources for reviewing heat transfer research pertinent to electronic equipment. Only a few selected papers will be discussed in Sections 2.2 and 2.3.

2.2 Natural Convection from Vertical Plates

Classical examples of natural convection on smooth vertical plates and cylinders have been studied and well documented in literature. Similarity solutions and local nonsimilarity solutions for natural convection from a

vertical surface have been discussed by Sparrow and Gregg [6], Yang [7], and Minkowycz and Sparrow [8]. This solution procedure requires the transformation of relevant two-dimensional boundary layer equations to a set of ordinary differential equations in terms of a similarity variable. These simultaneous ordinary differential equations with appropriate boundary conditions are then solved for velocity and temperature profiles. The heat transfer rate is then determined. The methodology of similarity solutions for this subject may be found in work by Kays and Crawford [9], White [10], and Dresner [11].

Ostrach [12] analyzed the free convection flow along a vertical flat plate. Grashof number was found to be an important parameter for determining the type of flow. For large Grashof numbers the flow was of the boundary-layer type. Velocity and temperature profiles were calculated for Prandtl numbers ranging from 0.01 to 1000.

Sparrow [13] analyzed laminar free convection on a vertical plate with prescribed nonuniform wall heat flux and wall temperature boundary conditions. Local heat transfer coefficients were determined for Prandtl numbers in the range of 0.01 to 1000.

Sparrow and Gregg [14] derived an exact solution of the laminar boundary layer equations for free convection from a vertical plate with uniform heating. The resulting average Nusselt number correlation was given by

$$Nu_H = [-(2/5)^{1/5} / \theta(0)]^{5/4} Gr_H^{1/4} \quad (2.1)$$

where θ represents as a temperature variable which is defined as

$(Gr_x^* / 5x^4)^{1/5} (T_w - T_\infty) / (x^{1/5} q''/k)$. This equation was applicable to the uniform wall temperature case when $Nu_H / Gr_H^{1/4}$ was based on $T_w - T_\infty$ at the plate center.

Sparrow and Gregg [15] analyzed laminar free convection on an

isothermal vertical flat plate including the effects of variable fluid properties. Solutions of the boundary layer equations with variable fluid properties were achieved. For gases, the fluid properties were evaluated at reference temperature, $T_r = T_w - 0.38 (T_w - T_\infty)$ except that β was replaced by $1/T_\infty$. For liquid mercury, T_r was used to evaluate all the properties.

Yang and Jerger [16] presented a first order perturbation method for characterizing two-dimensional laminar natural convection along a vertical surface. The results showed good agreement with experimental data.

Sparrow and Husar [17] performed flow visualization studies of free convection from a vertical surface with non-horizontal leading edges. Their flow visualization photographs indicated that the dye stripes were parallel vertical lines, even adjacent to the lateral edges. It was apparent that there were no spanwise velocity components present in the flow field along the vertical plates. With the evidence of no spanwise velocities, the problem was treated as quasi two-dimensional; because additional shear and heat conduction terms in spanwise direction were negligible compared with the shear and heat conduction terms of two-dimensional boundary layer equations.

Vliet and Liu [76] experimentally investigated turbulent natural convection boundary layers in water for a uniform heat flux condition. Their heat transfer results were in agreement with the uniform wall temperature condition data of Eckert and Jackson [83] and Bayley [84], but showed a much earlier transition point due to different heating modes.

Fujii and Fujii [78] recommended a simple and accurate correlation to predict local Nusselt number for a vertical surface with uniform heat flux condition. The equation is

$$Nu_x = C Ra_x^{* 1/5} \quad (2.2)$$

where $C = [Pr / (4 + 9 Pr^{1/2} + 10 Pr)]^{1/5}$ for any range of Prandtl number

fluids. This equation may be evaluated at the mid-height ($H/2$) of the vertical surface, then multiplied by $2b/H$ to obtain an equation suitable for the vertical channel case:

$$Nu_x = C (Ra_x^* b/H)^{1/5} \quad (2.3).$$

A general correlation of laminar and turbulent natural convection from an isothermal vertical surface was developed by Churchill and Chu [57]. This correlation is

$$Nu_H = 0.68 + 0.15 Ra_H^{1/3} / [1 + (0.437/Pr)^{9/16}]^{16/27} \quad (2.4)$$

which may be applied to the entire range of Rayleigh numbers. Although this equation is useful for most engineering calculations, better accuracy can be attained for laminar flow by using

$$Nu_H = 0.68 + 0.67 Ra_H^{1/4} / [1 + (0.492/Pr)^{9/16}]^{4/9} \quad (2.5)$$

for $Ra < 10^9$. The two resulting equations may be applied for uniform heat flux conditions as well as for uniform surface temperature conditions.

Hwang [18] discussed the effect of flow direction on mixed convection heat transfer from a vertical flat plate with and without square protuberances. His experiment indicated that the Nusselt number increased with Grashof number for local Reynolds number $\leq 2 \times 10^5$ for upward forced flow but decreased with Grashof number for downward forced flow. For $Re_x > 2 \times 10^5$, the Nusselt number, however, increased with Grashof number for downward and upward forced flows.

Jaluria [19] numerically studied the natural convection phenomena induced by finite sized multiple thermal sources on a vertical adiabatic wall with an explicit finite difference method. Time dependent two dimensional laminar boundary layer equations with Boussinesq approximations were formulated with a uniform heat flux condition for heated elements. Temperature and velocity profiles were determined. His study showed that the heat transfer coefficient for the upper element was lowered due to the upstream element for small spacing and increased in correlation with the

increase of spacing.

Jaluria [20] conducted an experimental study of natural convection flow from two discrete line heat sources on a vertical adiabatic surface. The insulated wall temperature decreased downstream of the lower heat source and then increased significantly as the upper heat source was approached, followed by a decay beyond the second source. The spacing between the heat sources was an important parameter in determining the resulting temperature levels. The upper heat source caused the temperature level to rise and caused the thermal boundary layer thickness to increase.

Jaluria [21] numerically investigated the interaction of natural convection wakes arising from discrete uniform heated sources on a vertical adiabatic surface with a horizontal, isothermal surface at the leading edge. A two dimensional vorticity transport equation similar to the derivation of Roache [22] and an energy equation were employed to analyze the problem. His results indicated that the horizontal, isothermal surface at the leading edge had significantly affected the flow due to the importance of axial conduction for low Grashof numbers $Gr_b \leq 10^4$. Although a lower velocity level was adjacent to the leading edge, the flow accelerated rapidly downstream and the boundary-layer characteristics were approached asymptotically downstream. His numerical results of a single heat source with and without a horizontal boundary showed agreement with the boundary layer solution particularly in higher Grashof numbers.

Kishinami and Seki [23] conducted a numerical and experimental study of 2-D natural convection heat transfer from a vertical plate with air. The vertical plate consisted of the upper section unheated and the lower section heated and maintained at an isothermal condition. Heat conduction in the unheated plate and thermal radiation effects were discussed. Their investigation showed that the surface temperature tends to increase rapidly for the smaller ratios of plate-to-fluid thermal conductivity. As the

emissivity of the plate approached unity, the temperature profile in the thermal boundary layer region decreases appreciably near the unheated portion.

2.3 Natural convection in Vertical Channels

Better understanding of natural convection in vertical channels may contribute to the research of combined free and forced convection for low Reynolds number flow heat exchangers as mentioned by Shah [89]. The study of natural convection in vertical channels has received attention in recent years as shown in Table 2.1. Abbreviations that appear in Table 2.1 are defined here. FDF is for fully developed flow, UHF is for a uniform heat flux condition, UWT is for a uniform wall temperature condition, and LWT is for a linear wall temperature condition.

Elenbaas [24] pioneered the semi-empirical studies of natural convection between vertical parallel square plates in air. Heat transfer as affected by the plate size (5.95 cm, 12 cm, 24 cm) and the channel spacing (0 to 3.3 cm) was discussed. His study showed that the heat dissipation increased significantly as the channel spacing decreased. This is due to the increase of flow velocity as the channel spacing decreased. The resulting equation for the symmetrically heated uniform surface temperature conditions was

$$Nu_b = 1/24 Eb_b [1 - \exp (-35 /Eb_b)]^{3/4} \quad (2.6)$$

where Eb_b the Elenbaas number defined as $(b/H) Ra_b$, is less than 10^5 .

Ostrach [25] analytically studied combined natural and forced convection with, laminar fully developed flow in vertical channels with and without heat sources. Both channel wall temperatures were assumed to be linearly varying along the walls but they were not required to be equal. The conservation equations of mass, momentum, and energy with boundary conditions were normalized and transformed to a boundary value problem.

Table 2.1 Convection Heat Transfer in Vertical Channels

Investigator	Considerations	Heating	Pr	Method	Year	Reference	Remark
Elenbaas	UHF	Symmetric	0.7	Semi-Empirical	1942	[24]	
Ostrach	FDF, UWT	Asymmetric		Series Expansion	1952	[25]	
Ostrach	FDF, LWT	Asymmetric		Eigen Function	1954	[26]	
Ostrach	FDF, LWT	Friction		Mechanical Analogy	1955	[27]	
Siegel & Norris	UHF	Asymmetric	0.7	Experiment	1957	[40]	
Tao	FDF, LWT	Symmetric		Complex Function	1960	[28]	
Bodoia & Osterle	UWT	Symmetric	0.7	Finite Difference	1962	[29]	
Agrawal	LWT	Symmetric		Variational Principle	1962	[30]	
Lauber & Welch	FDF, UHF	Asymmetric		Experiment	1966	[47]	
Levy	UWT	Symmetric		Calculus	1971	[48]	
Aung	FDF, UWT/UHF	Asymmetric		Separation variables	1972	[31]	
Aung, Fletcher & Sernas	UWT/UHF	Asymmetric		Finite Difference	1972	[32]	
Aung, Kessler & Beitin	UHF	Symmetric		Experiment	1973	[33]	
Miyatake & Fujii	UHF	Asymmetric	0.7-10	Finite Difference	1972	[36]	
Miyatake & Fujii	UWT	Asymmetric	0.7-10	Finite Difference	1973	[38]	
Miyatake & Fujii	UHF	Asymmetric	0.7-10	Finite Difference	1974	[39]	
Sparrow, Shah & Prakash	UWT	Asymmetric		Finite Difference	1980	[42]	
Sparrow & Prakash	UWT	Symmetric		Finite Difference	1980	[44]	Discrete plate
Prakash & Sparrow	UWT	Symmetric		Finite Difference	1980	[45]	Discrete plate
Sparrow & Bahrami	UWT	Symmetric		Experiment	1980	[41]	
Bar-Cohen & Rohsenow	FDF, UWT/UHF	Sym. & Asym.		Approximation	1981	[83]	
Cebeci, Khattab & LaMont	UWT	Symmetric		Finite Difference	1982	[86]	
Wirtz & Stutzman	UWT	Asymmetric		Experiment	1982	[49]	
Yao	UWT/UHF	Symmetric		Perturbation	1983	[87]	
Aung & Chimah	UWT/UHF	Asymmetric		Finite Difference	1983	[10]	
Sparrow, Chrysler & Azevedo	UWT	Asymmetric	10	Experiment	1984	[88]	
Burch, Rhodes & Acharya	UWT	Symmetric		Finite Difference	1985	[51]	
Azevedo & Sparrow	UWT	Asymmetric	10	Experiment	1985	[52]	
Ortega & Moffat	UHF	Asymmetric	0.7	Experiment	1985	[56]	3-D Discrete Bumps
Aung & Worku	UHF	Asymmetric		Finite Difference	1986	[35]	
Aung & Worku	FDF, UWT	Asymmetric		Finite Difference	1986	[82]	
Yan & Lin	UWT	Asymmetric		Finite Difference	1987	[58]	Discrete Plate

Solutions were then derived in terms of universal functions. Velocity and temperature distributions were also presented. Unstable convection in vertical channels with heating from below was also studied by Ostrach [26]. Boundary conditions with linearly varying wall temperatures and insulated walls were considered. The effects of heat sources and frictional heating were discussed.

Ostrach [27] analyzed laminar natural convection processes in vertical channels with and without heat sources. The channel wall temperatures were maintained constant but not necessarily equal. Fully developed velocity and temperature profiles in tall narrow channels resulted. The effects of heat sources and frictional heating were discussed. His analytical results showed that the heat sources and the frictional heating tended to increase the velocities and temperatures in the channel. Increased the ratio of two wall-to-ambient temperature differences for each channel also indicated similar results.

Tao [28] proposed an analytical method by introducing a complex function into the conservation equations to tackle the problem of two-dimensional, fully developed laminar combined free and forced convection in vertical channels with a linearly varying wall temperature. The real and imaginary parts of the complex function were directly related to the velocity and temperature fields. This combination of the momentum and energy equations led to an inhomogeneous Helmholtz wave equation with homogeneous boundary conditions. He claimed the method was more direct and powerful than those of conventional approaches.

Bodoia and Osterle [29] numerically investigated the development of two-dimensional, laminar, natural convection between symmetrically heated vertical plates. They analyzed this subject by solving the conservation equations of mass, momentum, and energy with finite difference methods. Their results showed that the heat transfer was invariant along the flow

direction in the fully developed region. The fully developed heat transfer correlation was given by

$$\text{Nu}_b = 8/3 \text{ Ra}_b \quad (2.7)$$

for $\text{Pr} \times \text{Gr}_b < 10^4$ and $0.7 < \text{Pr} < 10$. Their numerical result appeared in agreement with the experimental work of Elenbaas except for $\text{Gr}_b < 3 \times 10^2$ where side leakage effects in the vertical channels was important.

Agrawal [30] used a variational method for the analysis of combined free and forced convection in channels. The inhomogeneous Helmholtz wave equation derived by Tao [28] was substituted by the variational principle of the Ritz method. The complexities of the solution to the problem were substantially reduced.

Aung [31] presented closed form analytical solutions for fully developed laminar free convection in a vertical channel with asymmetric heating. Boundary conditions of uniform but different levels of heat flux and wall temperatures were considered. Aung et al. [32] conducted a numerical and experimental study of the developing laminar free convection heat transfer in vertical plate channels with asymmetrical heating. Different ratios of the wall fluxes and wall temperatures and temperatures differences were discussed. Later Aung et al. [33] included the influence of discrete heated components in the experimental investigation. The effects of channel flow restrictions, staggered cards, and baffles in a simulated electronic cabinet were also discussed. Aung and Chimah [34] developed a finite difference numerical method for the analysis of two-dimensional, laminar convection heat transfer in vertical channels. These results were applied in the design of electronic cooling systems.

Aung and Worku [35] analytically studied mixed convection laminar fully developed flow in parallel-plate vertical channels. Their theoretical results indicated that flow reversal would occur at a certain threshold value

of buoyancy parameter Gr_b/Re_b when unequal channel wall temperatures were present. There would be no reversed flow situation with symmetrical heating wall conditions.

Miyatake et al. [36-37] used an implicit finite difference method to study free convection in vertical channels with one wall uniformly heated and the other insulated. A parabolic inlet velocity profile was assumed to generate the solution. Heat transfer correlations were

$$Nu_b = 0.613 (b/H Ra_b)^{0.25} \quad \text{for } Pr = 0.7 \quad (2.8)$$

and

$$Nu_b = 0.68 (b/H Ra_b)^{0.25} \quad \text{for } Pr = 10 \quad (2.9)$$

with $3 \times 10^2 < (b/H) Ra_b < 10^3$.

Miyatake and Fujii [38-39] numerically analyzed the subject but with different levels of uniform heat flux and uniform temperature boundary conditions. For the case of uniform temperature boundary conditions and a uniform inlet velocity, the heat transfer correlation was

$$Nu_b = C (b/H Ra_b)^{0.25} \quad (2.10)$$

where $C = 0.58 (1 + 0.165 R^{0.36})$ for $Pr = 0.7$ and $C = 0.64 (1 + 0.089 R^{0.45})$ for $Pr = 10$. R was a dimensionless opposed plate temperature defined as $(T - T_\infty)/(T_w - T_\infty)$. For the case of a uniform heat flux boundary condition, the local heat transfer correlation was given by

$$Nu_x = \Phi / [24(1+R)]^{1/2} \{1 - \exp[-k(1+R)^{3/4} \Phi^n]\} \quad (2.11)$$

where $k = 2.84$, $n = -3/5$ for $Pr = 0.7$ and $k = 3.63$, $n = -2/3$ for $Pr = 10$. R was defined as the ratio of wall heat fluxes and $\Phi = (b/x) Ra_b^* / [(b/H) Ra_b^*]^{1/2}$.

Siegel and Norris [40] experimentally investigated free convection between uniformly heated parallel vertical plates with either an enclosed or open bottom. The channel spacing and the distance between the floor and

either enclosed or open bottom channel inlet were varied to determine the heat transfer effects. The Grashof number was on the order of 10^{10} .

Sparrow and Baharmi [41] experimentally studied natural convection from vertical parallel plates with either open or closed edges. A naphthalene sublimation technique was utilized to obtain mass transport results that are analogous to natural convection heat transfer. They concluded that the edge effects become significant when Elenbaas number $(b/H) Ra_b$ is less than 10. In other words, fluid flow through the lateral edge gaps is important at small spacings, and such flows between vertical plates are essentially three-dimensional in nature.

Bar-Cohen and Rohsenow [85] presented the first order analysis of two-dimensional, fully developed laminar natural convection in a vertical channel. Isothermal and constant heat flux boundary conditions with symmetric and asymmetric heating were included in the analysis. Optimum channel spacing was discussed.

Cebeci, Khattab, and LaMont [86] numerically studied combined natural and forced convection in vertical ducts. Velocity and temperature profiles were calculated.

Yao [87] used a perturbation method to analyze combined convection in the entrance of a vertical channel. The results of local Nusselt numbers agree with the available data.

Sparrow, Chrysler, and Azevedo [88] conducted an experimental study of natural convection in a one side heated vertical channel with water. A thymol blue technique was employed for the flow visualization. A downward flow with recirculation pocket at the channel top was observed adjacent to the unheated wall.

Sparrow et al. [42] numerically analyzed natural convection in a vertical channel with the Patankar-Spalding method [43] but with some modification. The effects of thermal boundary conditions, the wall radiative

transfer and the shrouding were discussed. For pure convection, the rate of heat transfer in a channel was generally higher for the case of isothermal equi-temperature walls than for the case of one isothermal wall and one adiabatic wall. With radiation present, the rate of convective heat transfer was enhanced. The heat transfer in the presence of shrouding was greater than that for the unshrouded plate for the pure convection case.

Nevertheless, when significant radiation is contributed, the heat transfer for the shrouded case is lower than for the unshrouded case.

Sparrow and Prakash [44-45] analytically investigated the enhancement of natural convection heat transfer using a staggered or in-line array of discrete vertical plates. Their numerical finite difference solutions showed that the heat transfer was enhanced for discrete plates instead of continuous plates when $(D/L) Ra_D > 2 \times 10^3$. The heat transfer enhancement achieved was as high as 80 - 90%. They suggested that the enhancement of heat transfer can be accomplished by larger transverse spacing and by relatively short system heights. This enhancement of heat transfer was unattainable at small $(D/L) Ra_D$ due to a decrease in mass thru-flow relative to that for the parallel plate array. The wall-to-ambient temperature difference could be significantly decreased with the use of a discrete-plate array when $(D/L) Ra_D^* > 100$. They concluded that the sensitivity due to the number of discrete plates and the arrangement of either in-line or staggered discrete plates does not play a significant role in the extent of the heat transfer enhancement.

Sobel, Landis, and Mueller [46] performed an experimental study of natural convection heat transfer with air in short vertical channels with uniform heat flux boundary conditions. Both straight and staggered channels were considered. Their results agreed with those of Elenbaas inspite of the different boundary conditions. Their investigation led to the following heat

transfer correlations:

for the case of straight channel

$$Nu_{b/2} = 0.666 (Ra_{b/2}^*)^{0.2} \quad \text{for } 5 < Ra_{b/2}^* < 3,500 \quad (2.12)$$

and for the case of staggered channel

$$Nu_{b/2} = 0.547 (Ra_{b/2}^*)^{0.3} \quad \text{for } 5 < Ra_{b/2}^* < 200 \quad (2.13)$$

$$Nu_{b/2} = 0.927 (Ra_{b/2}^*)^{0.2} \quad \text{for } 200 < Ra_{b/2}^* < 3,500 \quad (2.14).$$

The case of a staggered channel would result in a 20% increase in thermal effectiveness compared with the case of a straight channel.

Lauber and Welch [47] analyzed fully developed buoyant flow between vertical parallel plates in oil with an asymmetrically uniform heating condition. However, their analytical results were only applicable for Rayleigh numbers below 150.

Levy [48] presented the study of optimum plate spacings for laminar natural convection heat transfer from parallel vertical isothermal flat plates. His minimum plate spacing was determined based on the minimum temperature difference between the plate and the fluid for a given heat flux. This optimum spacing differed from those of Elenbaas [24] and Bodoia et al. [29] whose optimum spacings were based on the condition of maximum heat transfer rate in the channel.

Wirtz and Stutzman [49] experimentally investigated free convection between vertical plates with symmetric heating. Their experimental results were in agreement with those of Aung et al. [33].

Lehmann and Wirtz [50] performed an experimental study of forced convection from horizontal surface mounted repeated ribs in a vertical channel. Both uniform heat flux and uniform wall temperature boundary conditions were considered. The uniform heat flux boundary condition was accomplished by using a Kapton encapsulated thin film heater attached to the face of a plexiglas rib. The uniform wall temperature was furnished by

outfitting a copper rib with a heater buried on its underside. Local heat transfer on a rectangular rib in a fully developed flow region was measured by the use of a Mach-Zehnder interferometer. The uniform surface temperature case resulted in slightly higher heat transfer rates than did uniform heat flux surfaces. Variations in the channel wall-to-wall spacing indicated a relatively weak effect on the heat transfer. A flow visualization study was carried out by using a smoke wire with oil droplets.

Burch et al. [51] employed a finite difference method with an iterative solution scheme to analyze laminar natural convection heat transfer between finitely conducting vertical plates. The conservation of mass, momentum, and energy equations were used to depict the convective flow in the channel. Additionally, a homogeneous two-dimensional steady-state heat conduction equation was used to account for the conduction effect of channel walls. They found that the influence of wall conduction on the natural convection heat transfer between finitely conducting vertical walls was significant, particularly at higher Grashof numbers and lower conductivity ratio k_s/k_f (fluid to solid thermal conductivity ratio). The velocity and temperature profiles at various streamwise locations were substantially influenced by wall conduction.

Azevedo and Sparrow [52] experimentally investigated natural convection in open-ended inclined channels with water as the working fluid. Each heated channel wall was maintained at a uniform wall temperature and the channel spacing was varied. No backflow was observed for the case of a bottom heated channel with inclinations of 30° and 45° . For the vertical channel case, the following heat transfer correlations were obtained

$$Nu_b = 0.675 \left[(b/H) Ra_b \right]^{0.25} \quad \text{both sides heated channel} \quad (2.15)$$

$$Nu_b = 0.642 \left[(b/H) Ra_b \right]^{0.25} \quad \text{one side heated channel} \quad (2.16)$$

for $2 \times 10^2 < Ra_b < 1.5 \times 10^5$ and $0.043 < (b/H) < 0.11$. Water properties

were evaluated at $(T_w + T_\infty)/2$.

Chu et al. [53] analyzed two dimensional laminar natural convection in enclosure with concentrated heat sources by employing finite difference techniques with the ADI method to solve non-dimensionalized vorticity and energy equations. The effects of the heater size, location, enclosure aspect ratio, and wall boundary conditions were discussed. Their numerical solution agreed with the experimental observation of smoke flow patterns in a 2.54 cm square enclosure.

Turner and Flack [54-55] experimentally investigated natural convection heat transfer in rectangular enclosures with concentrated energy sources. The optimum heater location was determined.

Ortega and Moffat [56] conducted an extensive experimental study to characterize natural convection heat transfer from an array of simulated electronic components. These components were fixed on a vertical wall and were studied with and without a shroud. Their unshrouded array heat transfer data were compared to the Kays and Crawford's laminar correlation [9] and Churchill and Chu's turbulent correlation [57]. The unshrouded array case resulted in significantly higher heat transfer rates when it was compared to a smooth vertical plate case at an equivalent Grashof number. This suggested that the unshrouded array is similar to the smooth plate in turbulent natural convection. When a shrouding wall is present opposite the array wall, the heat transfer behavior is altered significantly if the channel spacing to the block height ratio is less than or equal to 4. The shrouded array case resulted in a 40 to 50 percent higher plate-average heat transfer coefficient than those of the equivalent smooth, parallel plane channel.

Yan and Lin [58] presented a numerical study of natural convection heat transfer in a smooth vertical channel with two discrete heat sources. Their finite difference solution led to the following conclusions. The temperature profile in the channel was modified when the unheated to heated

length ratio was varied; however, the velocity profile seems to remain unchanged. A higher heated wall surface temperature was observed when the discrete heating case was compared to the continuously distributed heating case. The average Nusselt number, however, decreased as the unheated to heated length ratio increased. This is to say that the heat transfer by natural convection in the channel is higher for the continuous heating boundary condition.

2.4 Heat Transfer in Electronic Equipment

This section is not intended to present an exhaustive review of the heat transfer in electronic equipment, rather a compilation of some references in the field. A comprehensive report of thermal design in miniaturized electronic equipment was presented by the Navy Department [59] in the early 1950s. Current progress of the submicron integrated circuit technology has created the ever-increasing higher power density for electronic components and systems as pointed out by Kraus, Chu, and Bar-Cohen [79] and Oktay et al. [80]. To assure a lower device temperature, thermal constraints of microelectronic equipment is one of the vital factors to be considered in the reliability analysis as reported by Simons [81]. Books written by Seely and Chu [60], Steinberg [61], Ellison [62], and Kraus and Bar-Cohen [63] describe thermal analysis of electronic equipment. A bibliography of heat transfer in electronic equipment before 1985 has been compiled by Antonetti and Simons [64]. Some annual bound conference volumes of the ASME [65-70] and others [71] are good references for reviewing recent research interests in the broad field of heat transfer in electronic equipment.

CHAPTER 3

THEORETICAL ANALYSIS

3.1 Scope

Functional forms are of importance when analyzing and correlating experimental data. In reviewing the publications in Chapter 2, the dimensionless parameters have yielded important roles in interpreting the natural convection heat transfer results. But there is still no convincing argument as to why there is no universal functional relationship available. If there is such a functional form, what would it be? A much simpler approximation method is used in search of basic and general functional forms. This approximation is called scale analysis, which was devised by Bejan [1] and is employed for the analysis of natural convection heat transfer from a vertical plate and in vertical channels. By scaling analysis, functional relationships in terms of dimensionless parameters are derived for specific sets of boundary conditions and three extreme cases of the Prandtl number.

3.2 Principles of Conservation

Before applying the scale analysis, it is necessary to take a closer look at the conservation equations of mass, momentum, and energy for their physical meanings. These equations written in the following differential form are for steady state, two-dimensional, laminar, incompressible buoyancy flow on a flat surface inclined with an angle of γ from horizontal. The representation of these equations are:

Continuity equation:

$$\frac{\partial u}{\partial x} + \frac{\partial v}{\partial y} = 0 \quad (3.1)$$

which is the balance of the mass flow.

Momentum equation in x, streamwise direction:

$$\rho(u \frac{\partial u}{\partial x} + v \frac{\partial u}{\partial y}) = \mu(\frac{\partial^2 u}{\partial x^2} + \frac{\partial^2 u}{\partial y^2}) + \rho g \beta (T_s - T_\infty) \sin \gamma \quad (3.2)$$

Momentum equation in y, traverse direction:

$$\rho(u \frac{\partial v}{\partial x} + v \frac{\partial v}{\partial y}) = \mu(\frac{\partial^2 v}{\partial x^2} + \frac{\partial^2 v}{\partial y^2}) + \rho g \beta (T_s - T_\infty) \cos \gamma \quad (3.3)$$

which are the balance of inertia, friction, and buoyancy forces in the x and y directions, respectively.

Energy equation:

$$\rho C_p (u \frac{\partial T}{\partial x} + v \frac{\partial T}{\partial y}) = k(\frac{\partial^2 T}{\partial x^2} + \frac{\partial^2 T}{\partial y^2}) \quad (3.4)$$

which is the balance of convective energy and conductive energy. These aforementioned equations were simplified by invoking the Boussinesq approximation for free convection flow. This approximation involved neglecting all variable fluid property effects except for density variation with the approximation of $\rho g \beta (T - T_\infty)$.

3.3 Scale Analysis

Now consider the conservation of mass, momentum, and energy, particularly, in the thermal boundary layer region, where the heating effect of the vertical plate is manifested. The characteristic length of the thermal boundary layer in the horizontal, y, direction can be expressed as δ_t . The significant streamwise length for the plate can be the plate height, which denotes H. Nevertheless, we choose L as some arbitrary characteristic length preceeding the following analysis. At the steady state, the heat transfer conducted from the wall horizontally into the fluid is moving upwards as an enthalpy stream. The energy eqn. (3.4) expresses a balance between convection and conduction terms. The convection terms are of the order $u \Delta T/L$ and $v \Delta T/\delta_t$ and the conduction terms are of the order $\alpha \Delta T/L^2$ and $\alpha \Delta T/\delta_t^2$. α is the thermal diffusivity defined as $k/(\rho C_p)$ and $\Delta T = T_w - T_\infty$

is the scale of $T - T_\infty$. Since $L > \delta_t$ so that $\Delta T/\delta_t^2 \ll \Delta T/L^2$ thus, there is no doubt that the first expression of the conduction term is negligible. Any terms with $1/L^2$ will then be dropped in the subsequent analysis.

Mass conservation in the thermal boundary layer yields

$$u/L \sim v/\delta_t \quad (3.5).$$

Balancing the convection and conduction terms in the energy equation gives

$$u \Delta T/L \sim \alpha \Delta T/\delta_t^2 \quad (3.6)$$

which means that these two terms are of the same order of magnitude. \sim is a symbol which represents "the same order of magnitude." Simplifying the terms will yield the following relationship

$$u \sim \alpha L/\delta_t^2 \quad (3.7).$$

Still focusing on the thermal boundary layer region, it is recognized that the momentum equations represent the interplay between inertia, friction, and buoyancy forces. Performing a similar analysis on the momentum equations, gives

$$u^2/L, vu/\delta_t \sim v u/\delta_t^2 \sim g\beta \Delta T \sin\gamma \quad (3.8)$$

Inertia	Friction	Buoyancy	
$uv/L, v^2/\delta_t$	$\sim v v/\delta_t^2$	$\sim g\beta \Delta T \cos\gamma$	(3.9)

where ν is the momentum diffusivity defined as μ/ρ . Because the traverse velocity, v , is extremely small in comparison with the streamwise velocity, u ; i.e., $u \gg v$. This was also observed by the flow visualization study of Sparrow and Husar [17]. Thus, the inertia term of eqn. (3.9) is eliminated. With the boundary layer approximation the friction term in eqn. (3.9) is negligible small. These arguments lead to the conclusion of a negligible buoyancy term in the y momentum equation. This may imply that the buoyancy effect, indeed, does not play any significant role in the traverse direction even with the inclined heated surface.

3.4 Prandtl Number Effects

It is necessary to consider three extreme cases of the Prandtl number, Pr , for the analysis of the natural convective processes.

Case I. $Pr \gg 1$:

For $Pr \gg 1$ its significant physical meaning suggests that the friction force dominates and the inertia force is less significant; i.e., friction \gg inertia or $\delta \gg \delta_t$. Balancing the friction and bouyancy terms of eqn. (3.8) gives

$$\nu u / \delta_t^2 \sim g\beta \Delta T \sin\gamma.$$

Substituting the relationship of $u \sim \alpha L / \delta_t^2$ into the previous form yields the expression $u \propto L / \delta_t^4 \sim g\beta \Delta T \sin\gamma$. Rearranging, gives

$$(L / \delta_t)^4 \sim Ra_L \sin\gamma \text{ or}$$

$$L / \delta_t \sim (Ra_L \sin\gamma)^{1/4}.$$

Since $h \Delta T \sim k \Delta T / \delta_t$ gives $\delta_t \sim k/h$ which can be substituted into the last expression and yields the heat transfer expression

$$Nu_L \sim (Ra_L \sin\gamma)^{1/4} \quad (3.10).$$

Case II. $Pr \ll 1$:

For $Pr \ll 1$ the friction effect is diminished and the inertia plays a significant role in the natural convection processes. Balancing the inertia and buoyancy terms in the momentum equations using a similar approach as the case of $Pr \gg 1$, yields $u^2 / L \sim g\beta \Delta T \sin\gamma$. Introducing $u \sim \alpha L / \delta_t^2$, gives

$$L / \delta_t \sim (Pr Ra_L \sin\gamma)^{1/4} \text{ or}$$

$$L / \delta_t \sim (Bo_L \sin\gamma)^{1/4} \quad \text{where } Bo_L = Pr \times Ra_L.$$

Again applying $\delta_t \sim k/h$ we then have the heat transfer relationship as

$$Nu_L \sim (Pr Ra_L \sin\gamma)^{1/4} \quad (3.11).$$

Case III. $Pr = 1$ or is close to 1:

For $Pr = 1$ or close to 1 the final heat transfer relationships for each of the previous cases are effectively the same. Therefore, the simpler form is recommended, that is,

$$Nu_L \sim (Ra_L \sin \gamma)^{1/4} \quad (3.12).$$

The foregoing resultant relationships are convenient for the analysis of natural convection problems with a uniform wall temperature (UWT) condition. For a uniform heat flux (UHF) wall boundary condition, ΔT is not known before the solution or the experiment is done. Thus the use of $q'' \sim k \Delta T / \delta_t$ to eliminate ΔT , yields $\Delta T \sim q'' \delta_t / k$. Substituting this relation into $L / \delta_t \sim (Ra_L)^{1/4}$ and then rearranging, gives $L / \delta_t \sim (Ra_L^*)^{1/5}$. Modified Rayleigh number, Ra_L^* denotes $\rho g \beta q'' L^4 / \alpha \nu k$, and with similar manipulation gives

$$Nu_L \sim (Ra_L^*)^{1/5} \quad \text{for } Pr \gg 1 \quad (3.13)$$

and

$$Nu_L \sim (Bo_L^*)^{1/5} \quad \text{for } Pr \ll 1 \quad (3.14).$$

The derived relationships, so far, are for the natural convection resulting from a smooth boundary surface such as a flat plate or a cylindrical wall. These may not be applicable for the case of natural convection in the vertical channels because it fails to include the significance of any geometric variation. To account for this deficiency, the next section provides some insight.

3.5 Geometric Variations

For the case of vertical channels, b is designated as the characteristic length. To account for the geometric variation of the vertical channel, the channel spacing-to-height ratio (b/H) is included and the characteristic length L is replaced by channel spacing (b). Thus the following functional forms

are proposed for natural convection in an inclined channel with various conditions.

For $Pr \gg 1$ or $= 1$

$$Nu_b \sim (b/H Ra_b \sin\gamma)^{1/4} \quad \text{for UWT} \quad (3.15)$$

and

$$Nu_b \sim (b/H Ra_b^* \sin\gamma)^{1/5} \quad \text{for UHF} \quad (3.16).$$

For $Pr \ll 1$

$$Nu_b \sim (b/H Bo_b \sin\gamma)^{1/4} \quad \text{for UWT} \quad (3.17)$$

and

$$Nu_b \sim (b/H Pr Ra_b^* \sin\gamma)^{1/5} \quad \text{for UHF} \quad (3.18).$$

For the case of a vertical heated surface with orientation, $\gamma = \pi/2$ so that $\sin\gamma = 1$. The foregoing functional relationships reduce to

For $Pr \gg 1$ or $= 1$

$$Nu_b \sim (b/H Ra_b)^{1/4} \quad \text{for UWT} \quad (3.19)$$

and

$$Nu_b \sim (b/H Ra_b^*)^{1/5} \quad \text{for UHF} \quad (3.20).$$

For $Pr \ll 1$

$$Nu_b \sim (b/H Bo_b)^{1/4} \quad \text{for UWT} \quad (3.21)$$

and

$$Nu_b \sim (b/H Bo_b^*)^{1/5} \quad \text{for UHF} \quad (3.22).$$

The functional expressions derived in this chapter may be applicable for the protruding discrete heating case; however, the 1/5th power is likely to be altered.

CHAPTER 4

EXPERIMENTAL APPARATUS AND PROCEDURE

4.1 Scope

This experimental study was developed to gain an understanding of thermal energy dissipation from microelectronic systems. Rather than attempt to match the characteristics of a complex system of electronic components on a host circuit board in a laboratory environment, the present approach has centered on obtaining accurate experimental data using a two dimensional model which displays some of the essential natural convection processes affected by geometric features and fluid properties for electronic systems. A flat surface which serves to dissipate heat, is widely encountered on varieties of microelectronic devices. This flat surface primarily dissipates the majority of heat generation from the integrated chip into an adjacent environment. The heat may be directly rejected, or rejected by a fin-like sink into the adjacent environment. The flat surface case will be the main focus of this investigation. The heat conduction through the chip's pin is small, thus, it will be neglected.

The main objective of the study has been to provide part of this data base, by temperature measurements and flow visualization, in an experimental model, over a range of the parameters of interest. A heat transfer apparatus was designed to study the natural convective processes for the following geometric arrangements:

- (1) a vertical flat plate with protruding discrete heat sources and
- (2) a vertical channel with protruding heat sources on one wall.

Additionally, the vertical channel spacing can be varied. Four channel spacings, 1.98 cm (0.781"), 3.18 cm (1.25"), 6.82 cm (2.686"), and 10.8 cm (4.25") were considered in this investigation. The channel spacing-to-height ratios (b/H) were 0.104, 0.167, 0.358, and 0.567. The variation of Prandtl

numbers was achieved in the range from 0.7 to 1,009 by utilizing air, distilled water, and Chevron multi-machine oil 68 (base oil) as the working fluids. The following sections are organized into two parts. The first part describes the design of the test apparatus and the arrangement of the instrumentation. The second part describes the experimental procedures.

4.2 Experimental Apparatus

Figure 4.1 depicts the photograph of the overall heat transfer test apparatus. Figure 4.2 shows the entire heat transfer test set-up and microcomputer based data acquisition system. This is the implementation of Warrington and Weaver [91] and Mussulman, Warrington, and Lin [92]. The assembled apparatus as shown in Figure 4.3 includes a vertical test channel, an inner chamber, and a water jacket tank located in an insulated room. The setting isolated the experiment from the possibility of interfering draft and ventilation. The instrumentation and the temperature controlling and monitoring systems were located outside the insulated room. The following sections describe each component of the test apparatus, the peripheral components, and the instrumentation in detail.

4.2.1 Test Section

4.2.1.1 Inner Chamber and Water Jacket Tank:

The test chamber consisted of an inside horizontal square cross sectional area 43.48 cm (17") in length on each side and 53.34 cm (21") in height. It was fabricated from a 1.27 cm (0.5") thick clear sheet of plexiglas. The 60.96 cm (24") cubical water jacket chamber surrounding the test chamber was partitioned off from a 0.61 m by 0.61m by 1.83 m (2' by 2' by 6') transparent glass tank. The partition was made of a 11.83 m (2') square sheet of plexiglas. This water jacket consisted of a 7.62 cm (3") wide rectangular channel for each face of the test chamber except the top face which was exposed to the ambient temperature in the insulated room. The

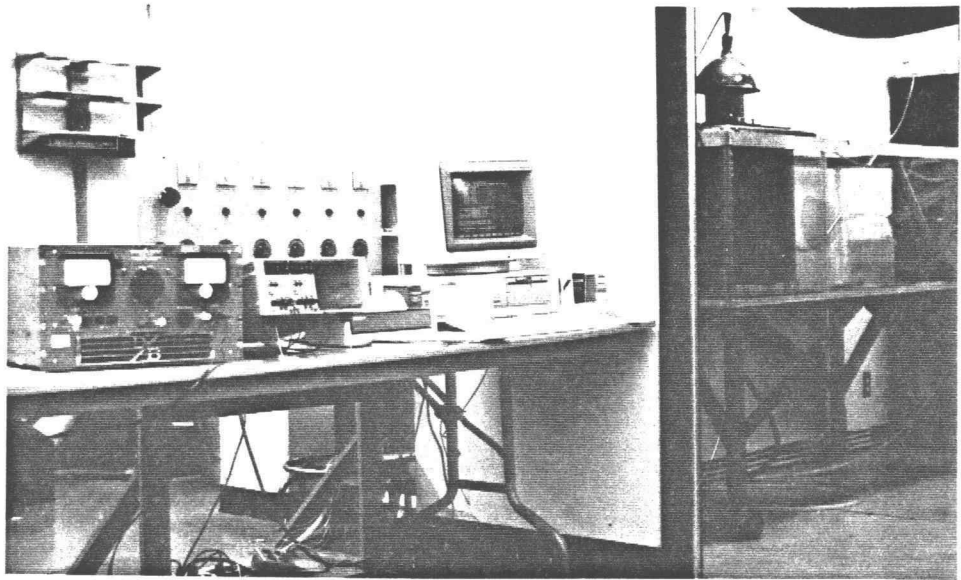


Figure 4.1 Overall Heat Transfer Test Apparatus

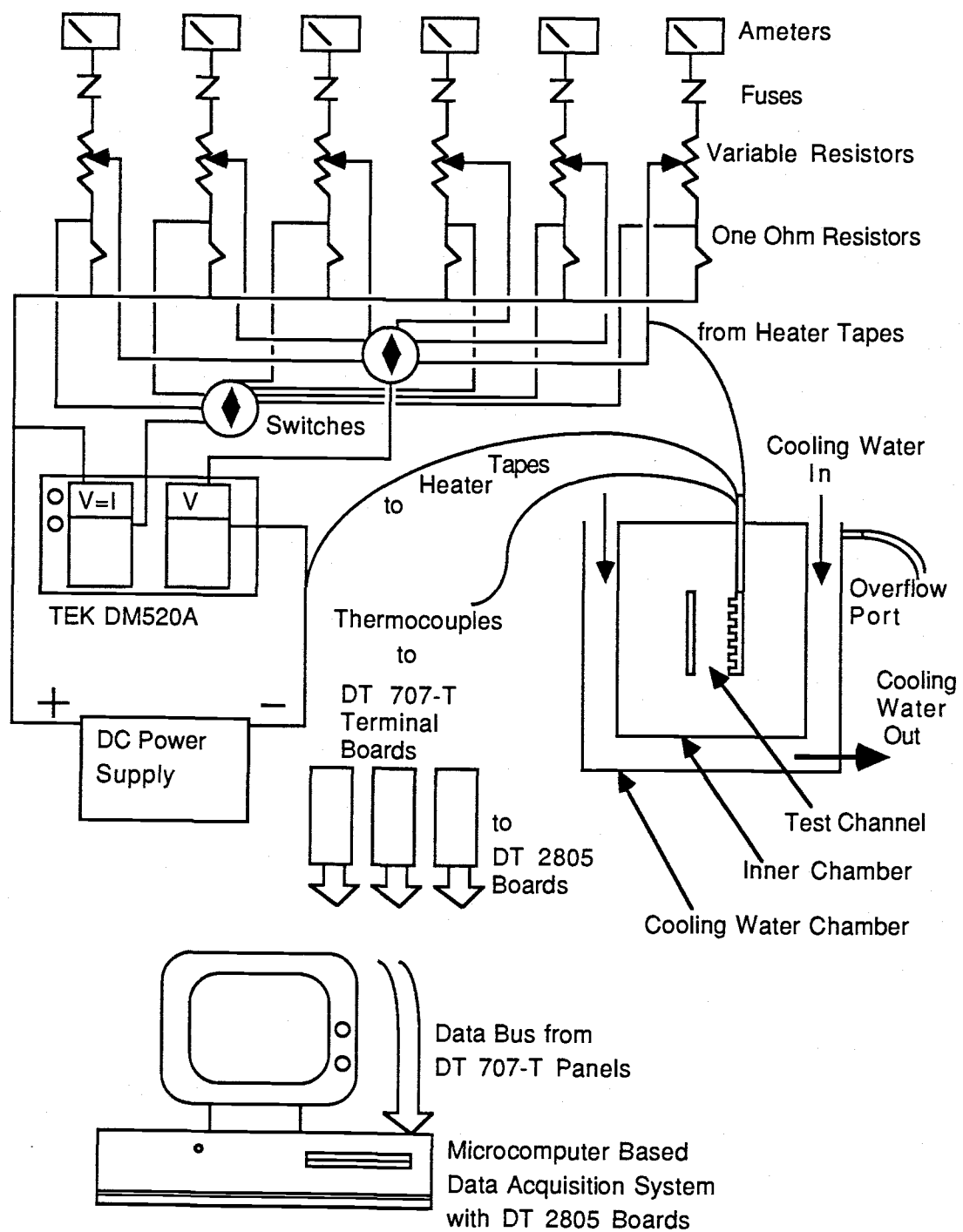


Figure 4.2 Schematic of Test Set-Up and Microcomputer Based Data Acquisition System

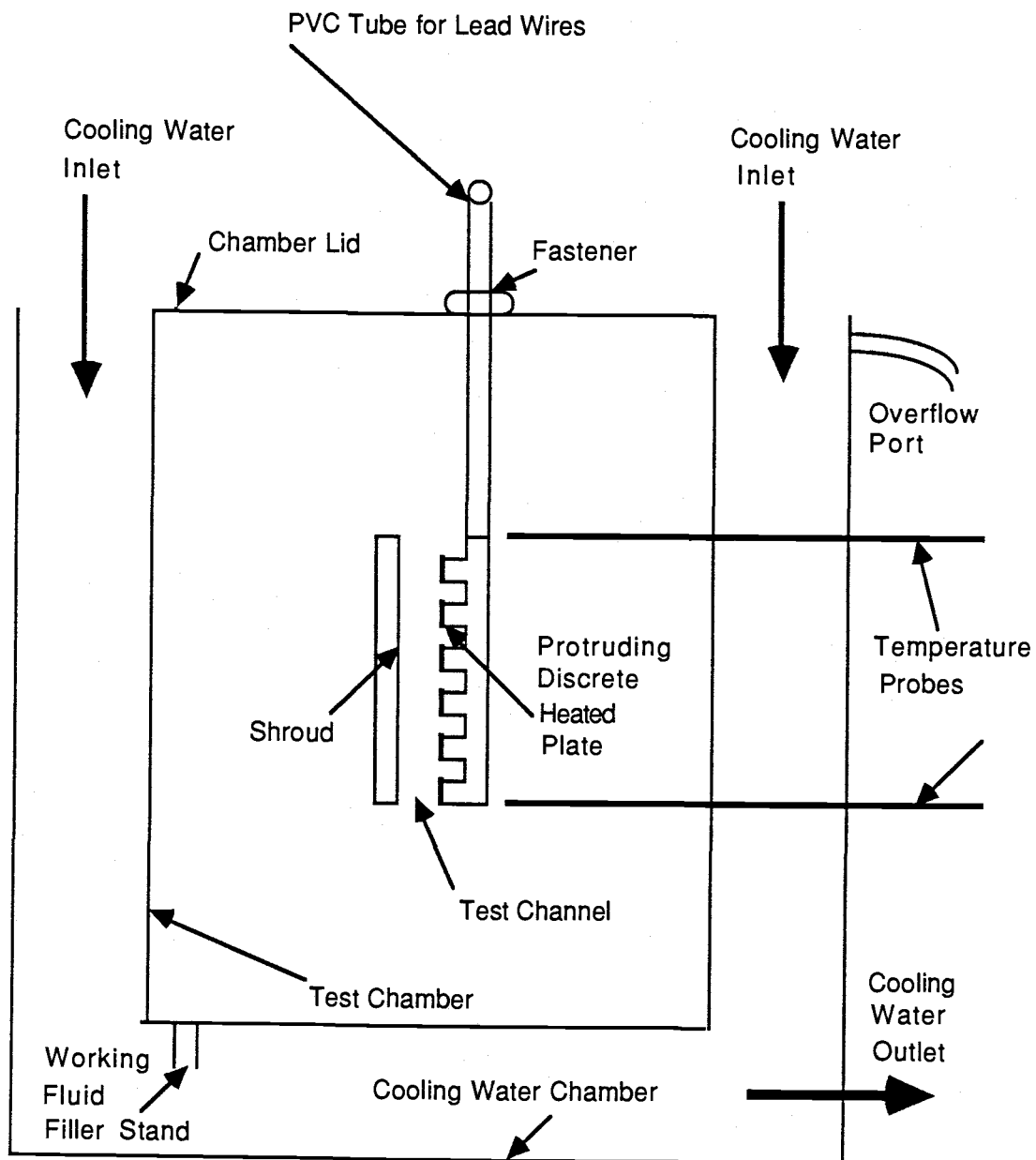


Figure 4.3 Schematic of Experimental Set Up for Free Convection in Vertical Channel

test chamber was fastened with machine screws and sealed with silicone sealant to prevent the possibility of leakage. The test chamber rested on equally sized circular rods which were located at the corners of the chamber bottom.

4.2.1.2 Vertical Channel:

The vertical test channel was formed by an electrically heated protruding array plate and a 1.27 cm (0.5") thick plexiglas shroud. The protruding array plate was constructed from a 2.54 cm (1") thick plexiglas sheet with dimensions of 30.48 cm by 19.05 cm (12" by 7.5"). The six slots were 25.4 cm (10") long, 1.588 cm (0.625") wide, and 1.588 cm (0.625") deep and were machined by a numerically controlled milling machine. Each slot was separated by a protruding element. The protruding surface was milled out 2.39 mm (0.094") deep except for a 0.79 mm (0.031") thick lip left around the protruding element edges. This design allowed sufficient space for the heating element with lead wires and thermocouple wires to be embedded. The protruding array plate is shown in Figure 4.4.

The channel sides were enclosed by plexiglas spacer plates. The spacer plates were fastened on the stabilized plexiglas plate so that the channel inlet was 17.78 cm (7") from the chamber floor. This arrangement assured two dimensional flow in the test channel. The channel spacing was varied by simply exchanging different size spacer plates.

4.2.1.3 Discrete Heat Sources Arrangement:

Figure 4.5 illustrates the protruding array heating element arrangement and thermocouple locations. Electrical resistance heat tape provided the heating for the discrete heat sources. The heat tape, 3.18 mm (0.125") wide and 0.64 mm (0.0252") thick consisted of an electrical resistance wire sandwiched between an adhesive back fabric and a metallic insulative foil. This electrically resistant wire was rated at 7.0 ohms/ft and a maximum power of 40 Watts/ft. One set of heater tapes was attached to a

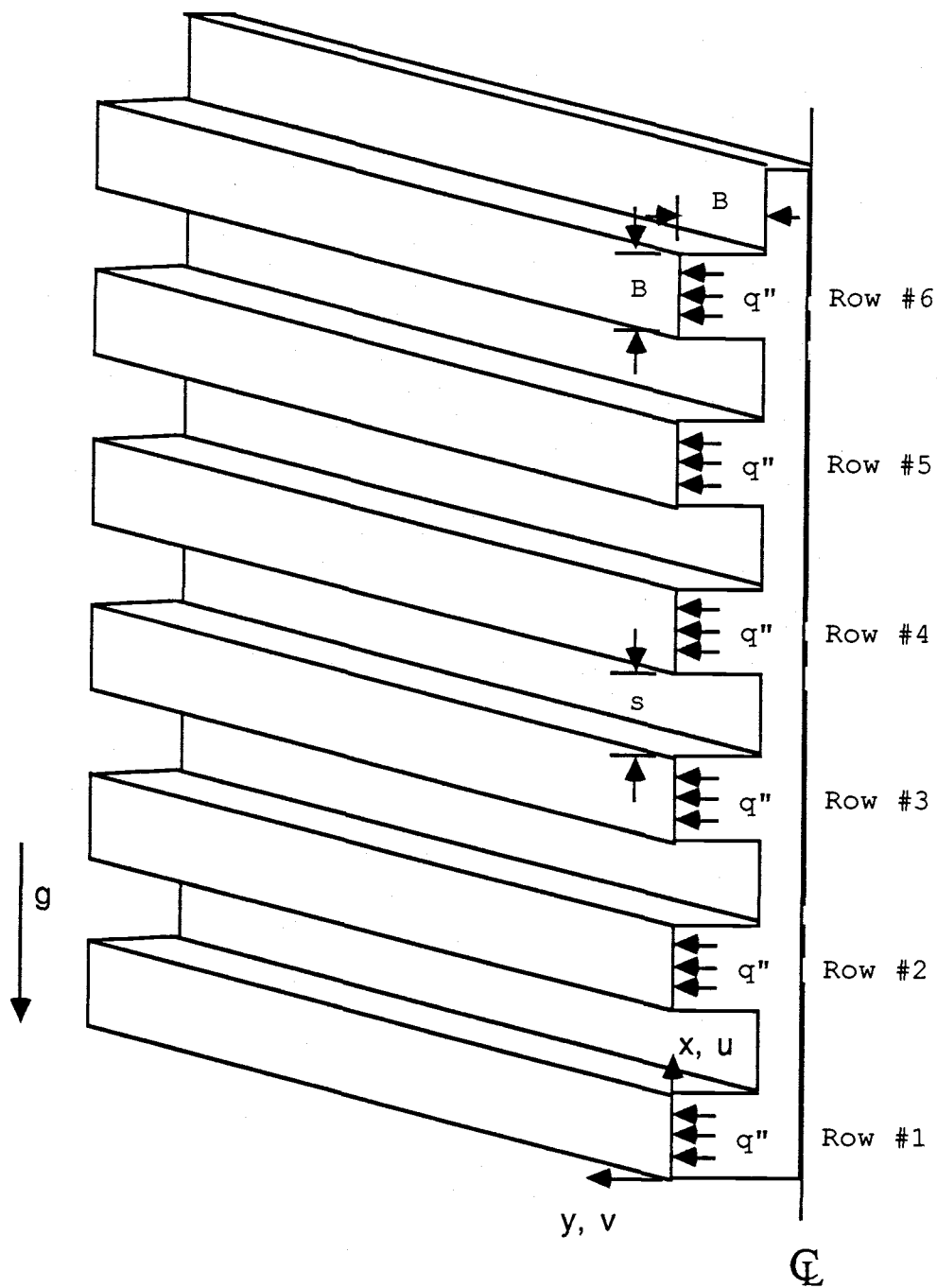


Figure 4.4 Schematic of Vertical Protruding Array Plate with Discrete Heat Sources

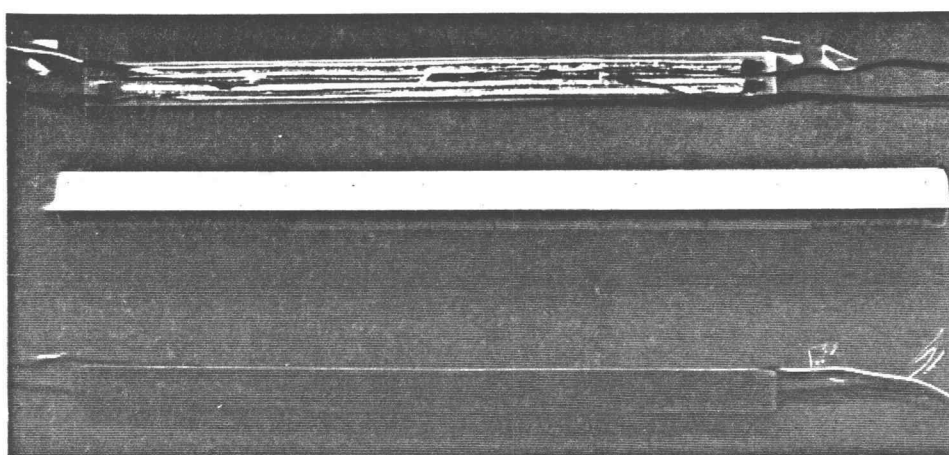


Figure 4.5 Heating Element Arrangement and Thermocouple Locations

of heater tapes, were connected in series. Thus the total length of the heater tapes on each aluminum strip surface was about 91.44 cm (3') long. Figure 4.6 shows the heater tape arrangement and thermocouple location. Figure 4.7 depicts the protruding array center cutaway view.

4.2.2 Power Supply

Power was supplied to the heater tapes by a DC power supply which was rated at 0-15 Amperes and 0-40 Volts (Model 62-121) manufactured by Dressen & Barnes. The power supply was connected to a panel of Rheostats (0-50 Ohms, 150 Watts, 1.73 Amperes maximum). Input power to the heater was individually controlled by means of Rheostats connected in series with each set of heater tapes.

4.2.3 Cooling Water System

The cooling system is of the open loop design and consisted of a supply manifold system, a water jacket tank, and a drain manifold system. This provided water to cool the test chamber. The cooling water source was city water for the supply manifold system. Water was collected from the water jacket to the drain manifold system. The discharge of the cooling water was then siphoned to the drain. A uniform flow rate through each channel of the water jacket was insured by a regulating valve on the faucet which fed the five inlet ports and the five outlet ports. This arrangement permitted the variation of temperature in the top portion of the test chamber while providing a constant temperature on the remaining faces of the test space. Since the cooling water flow rate for a given valve setting may fluctuate depending on the water consumption in the building, an overflow port was built to maintain a constant water level in the water jacket. This water jacket tank contains about 17 gallons of water. A slender L-shaped stainless steel rod surrounded by a Tygon tube was utilized to sweep off air bubbles developed in the water jacket.

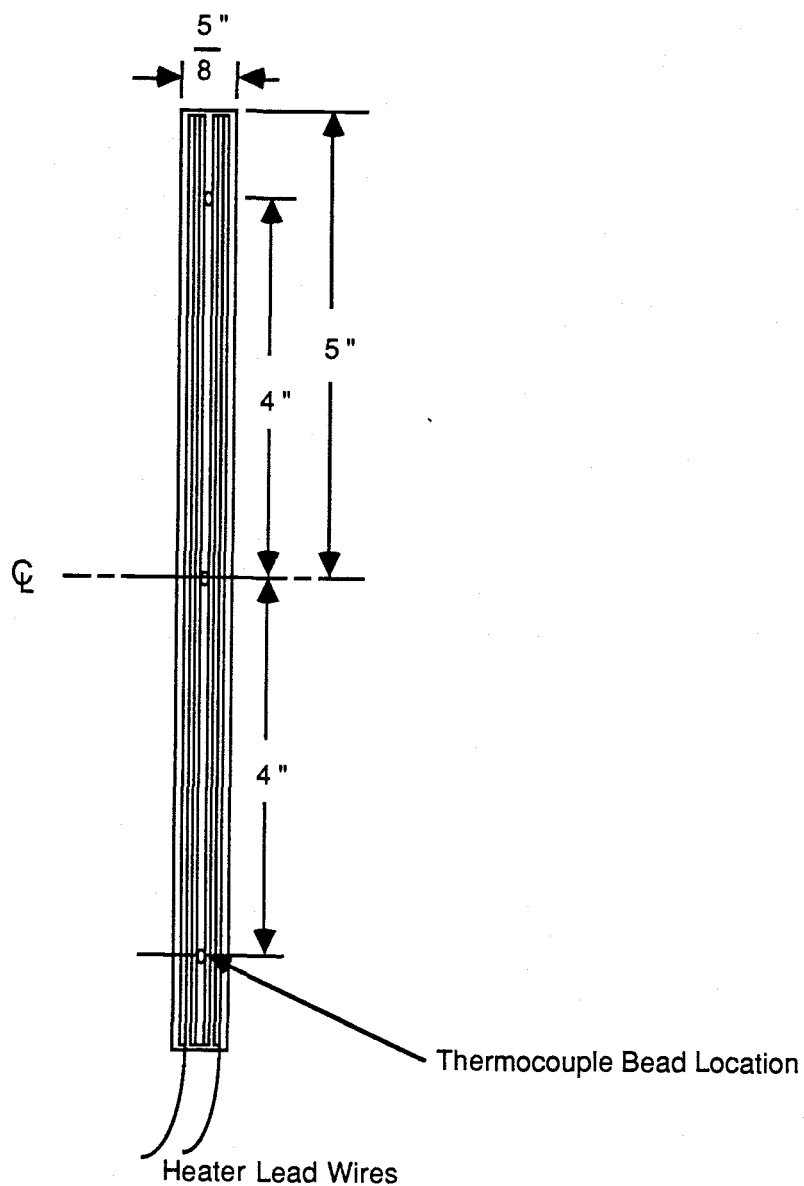


Figure 4.6 Schematic of Heater Tape Arrangement and Thermocouple Bead Location on Heated Surface

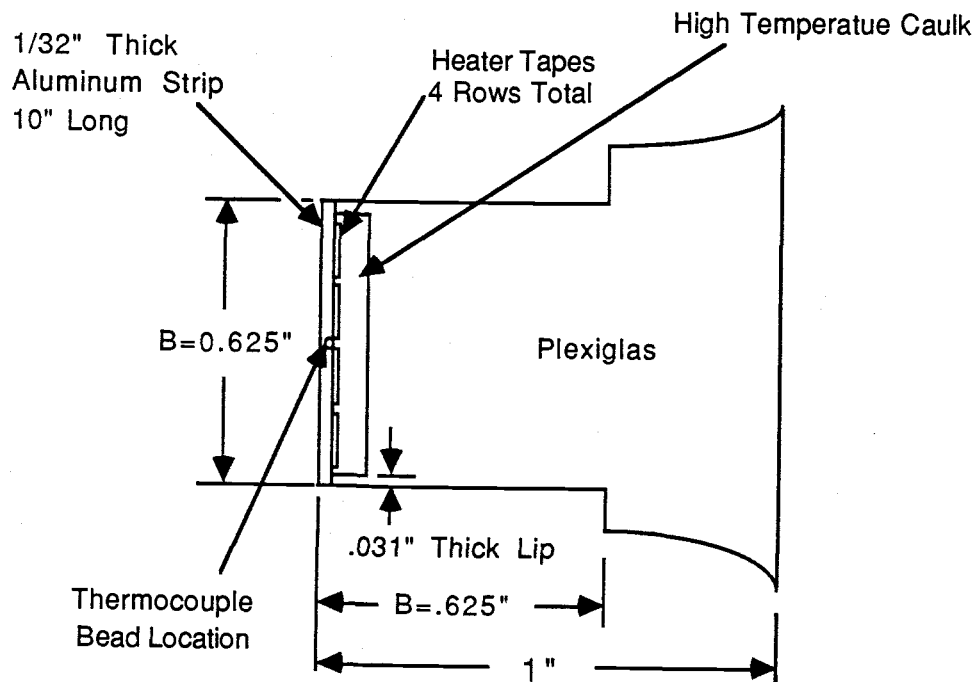


Figure 4.7 Protruding Heated Array Center Cutaway View

4.2.4. Instrumentation

4.2.4.1 Power Measurement:

Digital multimeters were used to measure the current and voltage drop across each set of electrical resistance heating element wire simultaneously for the calculation of the power input.

4.2.4.2 Surface Temperature Measurement:

The surface temperature of each protruded heating element was monitored by using three copper-constantan thermocouples epoxied 1.588 cm (0.0625") from the inner surface. These three thermocouple beads were placed on a line bisecting the aluminum strip lengthwise as shown in Figure 4.3. One was on the center, the other two were 10.16 cm (4") away from the center, one on each side. The thermocouple leads and the heat tape leads passed through holes in the sides of the discrete heat source plate with one lead per hole, and were brought upward inside cylindrical holes in the sides of the plate. The holes were sealed with silicone rubber cement. The leads were directed toward the plexiglas ceiling where they exited through two PVC tubes. The PVC tubes passed through a hole in the top of the inner chamber.

To account for the heat conduction loss, the hot wall rear face center temperature was monitored using a thermocouple. The shroud surface center temperature was also monitored with a thermocouple. Additionally, the inner chamber surface temperatures were monitored.

4.2.4.3 Channel Inlet/Outlet Fluid Temperature:

Local fluid temperatures in the entrance and the exit of the vertical channel were measured using two thermocouple probes to traverse the mid-plane of the vertical channel. These probes consisted of a copper-constantan thermocouple coated with insulation and sheathed with a 3.16 mm (0.125") diameter stainless tube. The area between each thermocouple bead and tubing end was streamlined with an epoxy cone.

This combination tended to limit heat conduction along the probe shaft from the measuring point. Two holes 1.27 cm (0.5") diameter were drilled and threaded in the plexiglas wall of the inner chamber. To each hole, a bushing unit was inserted and sealed with silicone cement. The bushing units included a sleeve, an O-ring, and a cap nut. This design enabled the probe to be traversed through the test space without seepage of the working fluid or cooling water.

4.2.4.4 Data Acquisition System:

The main data acquisition system consisted of the following:

1. Tektronix DM 502A autoranging digital multimeters for voltage and current measurements.
2. Three DT 2805 data acquisition boards used as interfaces between the computer and the thermocouple screw terminal boards.
3. Three DT 707-T screw terminal panels for connecting thermocouple lead wires.
4. A Hewlett Packard (HP) Vectra computer with one 20 megabyte hard disk and one 640 Kilobyte floppy disk driver.

A computer program written in BASIC, as listed in Appendix A was developed for the temperature data acquisition.

4.2.5 Flow Visualization Equipment

The test chamber and the vertical channel were both painted flat black for better lighting effects. A lighting system equipped with one 300 watt, high intensity lamp provided a thin collimated beam of light necessary for flow visualization.

The tracer fluid in the test chamber mid-plane was illuminated through a slit in the center of the top. Flow patterns were observed and photographed through the clear front face.

4.3 Experimental Procedures

4.3.1 Experimental Set-Up

For experimentation, the following steps were followed:

1. The vertical channel was centered in the inner chamber.
2. After the chamber lid was secured, each protruding PVC tube was sealed off with an O-ring and a 1.27 cm (0.5") thick plexiglas ring which was fastened by three machine screws on the lid.
3. The thermocouple leads were fastened on the DT 707-T screw terminal panels. The panels were mounted to a wooden board on the wall in the insulated room. There were seven thermocouple lead wires per each panel.
4. Twelve heating element lead wires from the PVC tubes were brought outside through a hole in the wall and fastened to the screw terminal strip. The Rheostat panel was then connected to this terminal strip.
5. Digital multimeters were connected to the voltage ports and amperage ports.
6. A DC power supply system was connected to the power input ports on the Rheostat panel.
7. The cooling system plumbing was connected and the hoses exited through a hole in the wall to the cooling water faucet and the sump.

To run the experiment, the cooling water system was first activated and water flow rate adjusted and maintained around 150 ml/sec. When the test chamber water temperature reached the chamber cooling water temperature, the input power was then supplied to the discrete heat sources and adjusted until the desired uniform heat flux condition was achieved. The establishment of the thermal equilibrium condition in the test space was of primary importance. It was noted that two hours time was sufficient to attain thermal equilibrium. The subsequent temperature readings for any

particular position on the test section or in the test space were nearly constant.

4.3.2 Data Calibration

To minimize errors in the data, all instruments were calibrated before or periodically checked during the experiment. Thermocouple temperature readings were calibrated using distilled ice water and distilled boiling water temperatures with a high accuracy thermometer. The calibrated distilled ice water and distilled boiling water temperatures should be accurate, because any extraneous error due to the impurity of water is not large. The maximum error for the temperature reading was plus or minus 0.25 °C. Measurement of the power input at each protruded heating element was accurate to within plus or minus 0.1 percent. All the data was collected at room temperature condition in the range of 22 °C to 24.5 °C and the pressure was one atmosphere.

During the initial stages of experimentation, it was found that temperature readings drifted from the standard calibration temperatures. In order to preserve the consistency of temperature readings throughout the experiment, necessary precautions were taken. The standard temperature calibration was performed before and after each set of experimental run. If the standard temperature calibration was not attained, that particular set of data would be discarded. Otherwise, each set of temperature readings was utilized for further heat transfer data reduction. The experimental data was checked and the experiment was proven repeatable.

4.3.3 Data Collection

Once the thermal equilibrium state was reached, the following data were recorded for each run:

1. The input voltage to each protruding heat source.
2. The input amperage to each protruding heat source.
3. The temperature readings on each protruding heating surface, the

shroud, the test chamber, and the inlet and outlet cooling water.

A minimum of 10 heat transfer data points were recorded with each channel spacing per each working fluid. In addition, temperature profiles in the channel inlet and outlet were recorded in conjunction with each data run. Each of two thermocouple probes was inserted into the test space until it contacted the shroud surface. It was then withdrawn in small increments until the probe tip was flush with the hot wall surface. The temperature readings and positions along the traverse were recorded at each step of withdrawal. Positions were measured within 0.04 cm (0.016").

4.3.4 Heat Transfer Coefficient Calculations

Heat transfer by natural convection is a function of the temperature difference between the heated surface and the fluid or a cold surrounding temperature and the surface area. The Newton's law of cooling gives the relation as

$$Q_{\text{conv}} = h A (T_h - T_c) \quad (4.1).$$

The quantity Q_{conv} is determined by

$$Q_{\text{conv}} = Q_{\text{tot}} - Q_{\text{cond}} - Q_{\text{rad}} \quad (4.2).$$

Q_{tot} represents the total power input which is the product of measuring current (I) and voltage for each heating element. Q_{cond} is the amount of heat conduction loss through the hot wall and the lead wires. A one-dimensional heat conduction analysis is utilized to compute Q_{cond} . The conduction heat loss is less than 1% for all the tests. Radiation heat loss, Q_{rad} is estimated only when air was employed as the working fluid.

The approach to calculate radiation heat loss is presented in Appendix B. The maximum radiation heat loss for the present experiment is less than 25%. Since distilled water and viscous oil are opaque to radiation, radiation heat loss would be negligible for these fluids.

When the convective heat transfer rate is determined, the average convection heat transfer coefficient is then computed by

$$h = q'' / (T_h - T_c) \quad (4.3).$$

q'' denotes Q_{conv} / A . T_h is the center surface temperature for each protruded element, and T_c is the chamber surface temperature. Note that the average heat flux over the entire hot plate for the present geometries is calculated to be $0.5 q''$ as shown in Appendix C. The fluid properties were evaluated at the mean fluid temperature which is defined by

$$T_m = 0.5 (T_h + T_c) \quad (4.4).$$

A subroutine written in FORTRAN and listed in Appendix D was used in calculating the fluid properties based on T_m .

4.3.5 Uncertainty Analysis

An attempt was made to achieve a uniform heat flux boundary conditions for each heated block surface; however, the theoretical uniform heat flux boundary condition is difficult to attain in the experimental setting. The variation of the constant heat flux surface conditions among the heated block surfaces was minimized and was about 5%. The percentage of the heat flux variation for each protruded heating element was defined as

$$\text{Heat Flux Variation \%} = \frac{P_{\text{max}} - P_{\text{local row}}}{P_{\text{max}}} \times 100 \quad (4.5)$$

where $P_{\text{local row}}$ represents the input power for the particular row of the protruded heating element which was evaluated. P_{max} represents the maximum input power for the protruded heating element.

The uncertainty analysis of the experiment is presented in Appendix E. The uncertainty for the convection heat transfer coefficient was about 5% for the present experiment. A sample of experimental data log is seen in

Appendix F.

4.3.6 Flow Visualization

In order to eliminate any fluid motion disturbance caused by the heating effect of an illuminating light beam, the light beam was passed through a 15.24 cm (6") layer of distilled water in a 2,500 c.c. beaker before entering the test plane. The water in the beaker served the purpose of cooling the light source because part of the lamp was immersed in the water. The water also served to focus and amplify the light. The beaker was of a light-tight design except for a 0.79 mm (1/32") clear slit on the bottom which permitted the intensified light beam to enter the test space.

Cigar smoke was utilized as the tracer fluid when air was the working fluid. The cigar smoke was collected in a flexible bottle (500 c.c.). By gently squeezing the bottle twice or thrice, the smoke was sufficient and it traveled 5.94 m (18') in distance up and down along a 1.905 cm (0.75") diameter tygon tube before reaching the honeycomb strainer located at the bottom corner of the test chamber. It is noted that the last 0.914 m (3') of the tube was submersed in the cooling water jacket. This allowed the smoke temperature to be as close to or below the working fluid in the test space. The smoke was then dispersed in the test space through the strainer. By the time it reached the channel, the smoke and test fluid were nearly in thermal equilibrium. Three minutes of elapsed time was sufficient to re-establish the steady state condition although no noticeable fluctuation in temperature readings was detected before, during, or after the smoke was introduced.

The use of milk in the dye mixture provided high contrast of dye lines and stabilized filaments relative to a rapid diffusion. This approach was also used by Merzkirch [72]. The dyed solution was then chosen as the tracer fluid when using distilled water as the working fluid. The dye mixture was released into the test space by an injection device. The injection device was composed of a 0.0125 cm diameter hypodermic needle, a 3.18 mm (1/8")

o.d. and 35.56 cm (14") long stainless steel tube, a syringe, a 3.18 mm (1/8") o.d. and 6.35 mm (1/4") long latex sealing tube, and a 0.508 m (20") long latex tube. Before using the dye in the flow visualization experiment, the dyed solution was performance tested. It was observed that a stream of stable dye could be injected 10" away from the needle tip without turbulence. The diffusion of the mixed dye solution tended to be retarded in comparison with the diffusion of one dye solution itself. This effect was also observed in Simpson's study [73]. It would take 3 hours approximately to allow the dye to precipitate to the bottom.

Different locations of introduced dyed solution into the test chamber seemed to add insignificant disturbance in the steady state flow patterns. Three to five minutes was allowed to re-establish the steady state although no noticeable fluctuations in temperature readings were detected before, during, and after the dyed tracer fluid was introduced for each flow visualization experiment. Each tracer fluid would recirculate and then increasingly contaminate each working fluid in the test space. Thus, the test chamber had to be emptied and refilled with the working fluid after each test run.

The steady state flow patterns at the channel mid-plane were photographed with a 35 mm Nikon camera on a ASA 1600 high speed slide film at f/1.8 aperture setting. It was found that one minute to two minutes exposure time would produce high contrast photographs with the present lighting condition and the camera setting. It was noted that the photographs of steady state flow patterns for each experimental run were reproducible.

CHAPTER 5

RESULTS AND DISCUSSION

5.1 Scope

This chapter reports and discusses heat transfer results and flow visualization results. The graphic representation of heat transfer data is presented. The effects of variable fluid properties on heat transfer are discussed. The flow observation of natural convection processes in vertical channels is also presented. The heat transfer results are expressed with functional forms in terms of dimensionless parameters, $Nu_L = f(b/H, Ra_L^*)$.

5.2 Temperature Distribution of Discrete Heating Surfaces

The comparisons of protruding array heated surface temperature profile data with various channel spacing-to-height ratios at approximately the same heat flux are shown in Figures 5.1 to 5.3 for each working fluid, respectively. These plots use a dimensionless temperature, θ , and a dimensionless length, x/H . The dimensionless temperature is defined as

$$\theta = (T_i - T_c) / (T_{i,max} - T_c)$$

where T_i is the local array heated surface center temperature measured at any protruding array center position, x/H , along the streamwise direction. $T_{i,max}$ is the maximum temperature of the protruding array heated surface. For a given heat flux, θ increases as x/H increases from 0.04 to 0.71 and decreases as x/H increases from 0.71 to 0.88 with air as the working fluid. This indicates that the upper row of protruding arrays, being in the wake, tend to decrease θ . The decrease of θ from the 5th to 6th row may be contributed to their location near the protruding array plate trailing edge. Generally, θ decreases as the channel spacing-to-height ratio decreases. This is true for the arrays from the first row to the fourth row.

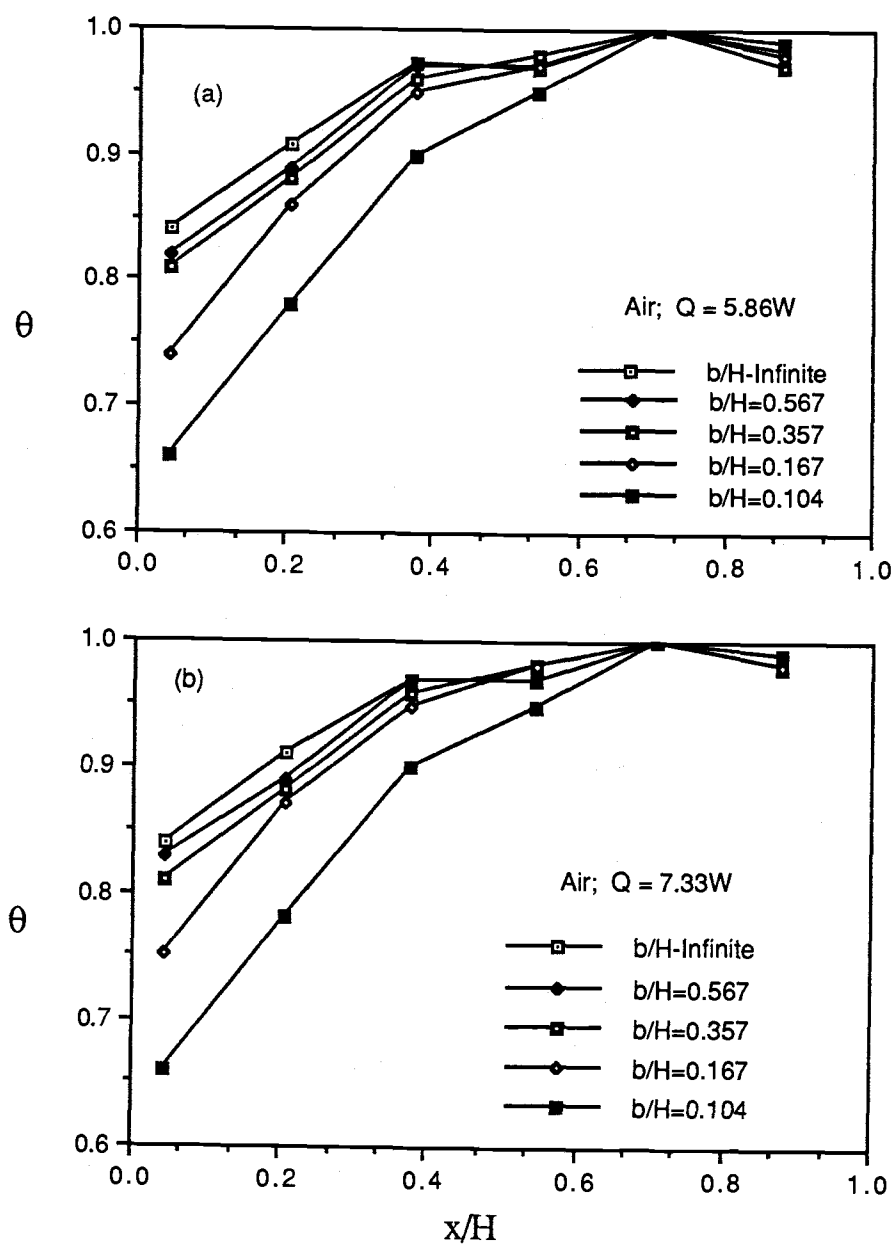


Figure 5.1 θ versus x/H for Various b/H

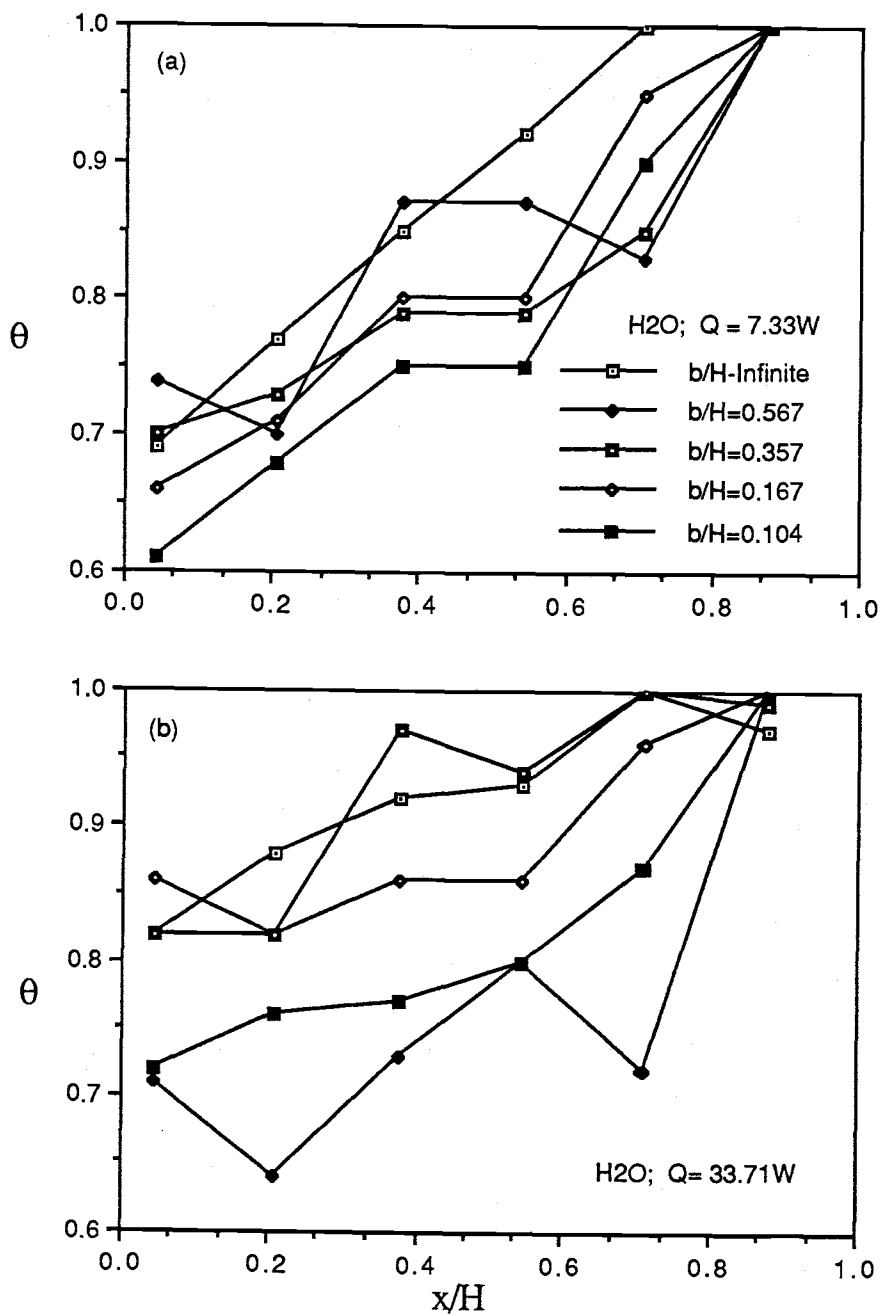


Figure 5.2 θ versus x/H for Various b/H

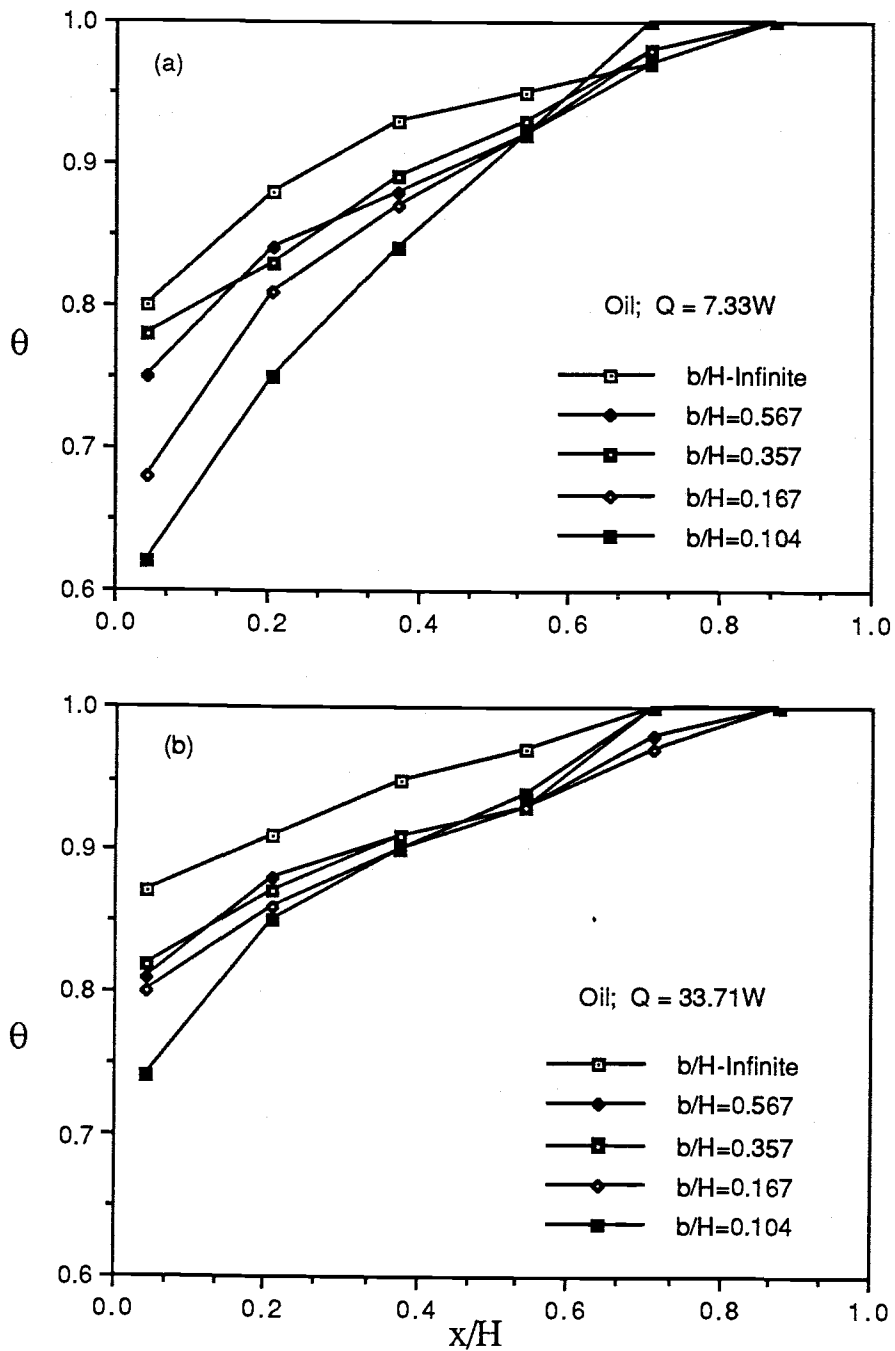


Figure 5.3 θ versus x/H for Various b/H

The upper protruding array surface temperature is usually higher than the lower protruding array surface temperature. This is attributed to the fact that the upper protruding arrays are in the wakes of the lower ones similar to Larson's cylinder array case [90]. In other words, the higher upper array temperatures are caused by the preheating effect from the rising warm buoyancy flow and the effect of thermal boundary layer thickening.

A fully developed temperature profile seems to be present for the vertical channels with $b/H=0.167$ and 0.104 as shown in Figures 5.4 (d)-(e). This may imply that the dimensionless temperature profile in the traverse direction is geometrically similar, varying only by a stretching factor.

5.3 Fluid Property Effects

To determine how the fluid properties affect the relation between Q and ΔT , the fluid property-temperature variations for air, water, and oil must be analyzed. The fluid thermophysical properties referred to come from Liley [74] for air and water and from Chevron [75] for oil.

Figures H (a)-(e) show the fluid properties in the range of $10\text{ }^{\circ}\text{C}$ to $100\text{ }^{\circ}\text{C}$ as seen in Appendix H. In the temperature range from $10\text{ }^{\circ}\text{C}$ to $87\text{ }^{\circ}\text{C}$, the fluid properties for air, distilled water, and oil have the following relations:

$$k_{\text{H}_2\text{O}} > k_{\text{oil}} > k_{\text{air}}, \beta_{\text{H}_2\text{O}} < \beta_{\text{oil}} < \beta_{\text{air}}, C_{p\text{H}_2\text{O}} > C_{p\text{oil}} > C_{p\text{air}},$$

$$\rho_{\text{H}_2\text{O}} > \rho_{\text{oil}} > \rho_{\text{air}}, \mu_{\text{oil}} > \mu_{\text{H}_2\text{O}} > \mu_{\text{air}}, \nu_{\text{oil}} > \nu_{\text{air}} > \nu_{\text{H}_2\text{O}},$$

$$\text{Pr}_{\text{oil}} > \text{Pr}_{\text{H}_2\text{O}} > \text{Pr}_{\text{air}}.$$

By examining these fluid property values, it was found that the fluid thermal conductivity and thermal expansion coefficient regulate the relation of Q and ΔT . It may be stated that the slope (m) of the line in Figures G.1 and G.2 (a) to (d) increases with the increase of fluid thermal conductivity, k_f , or specific heat, C_p , or the decrease of thermal expansion coefficient, β_f .

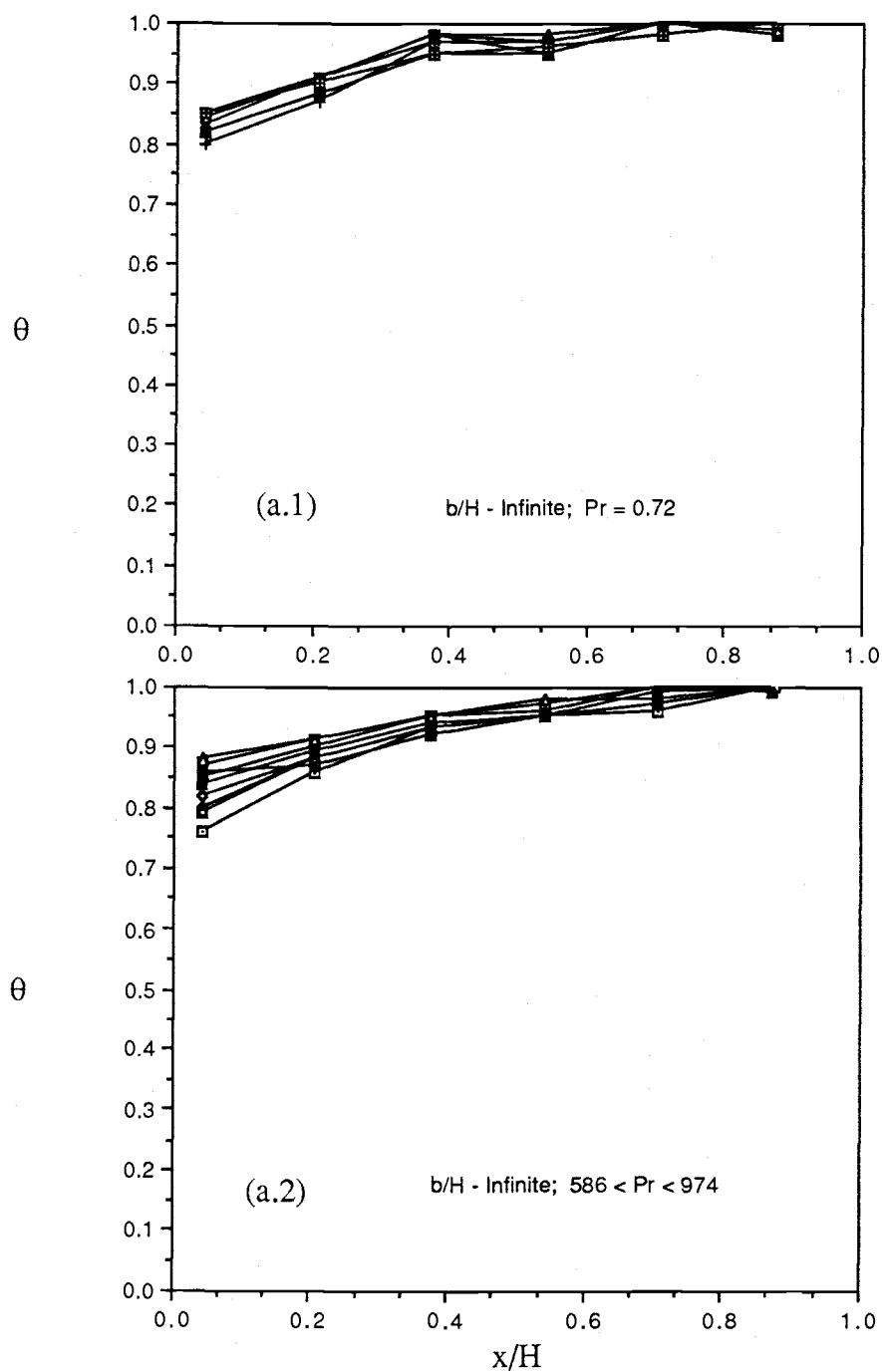


Figure 5.4 θ versus x/H for Various Q

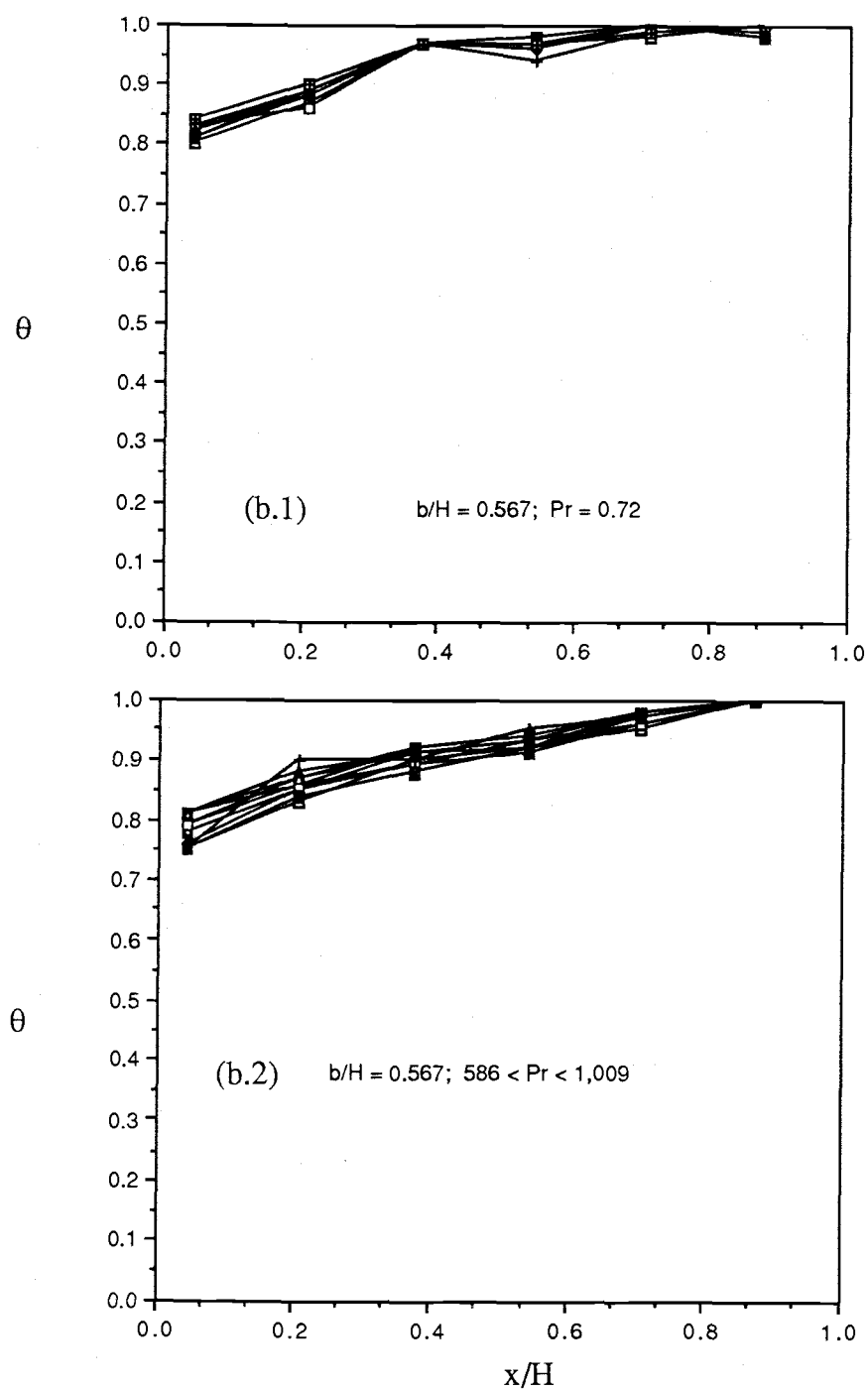


Figure 5.4 θ versus x/H for Various Q

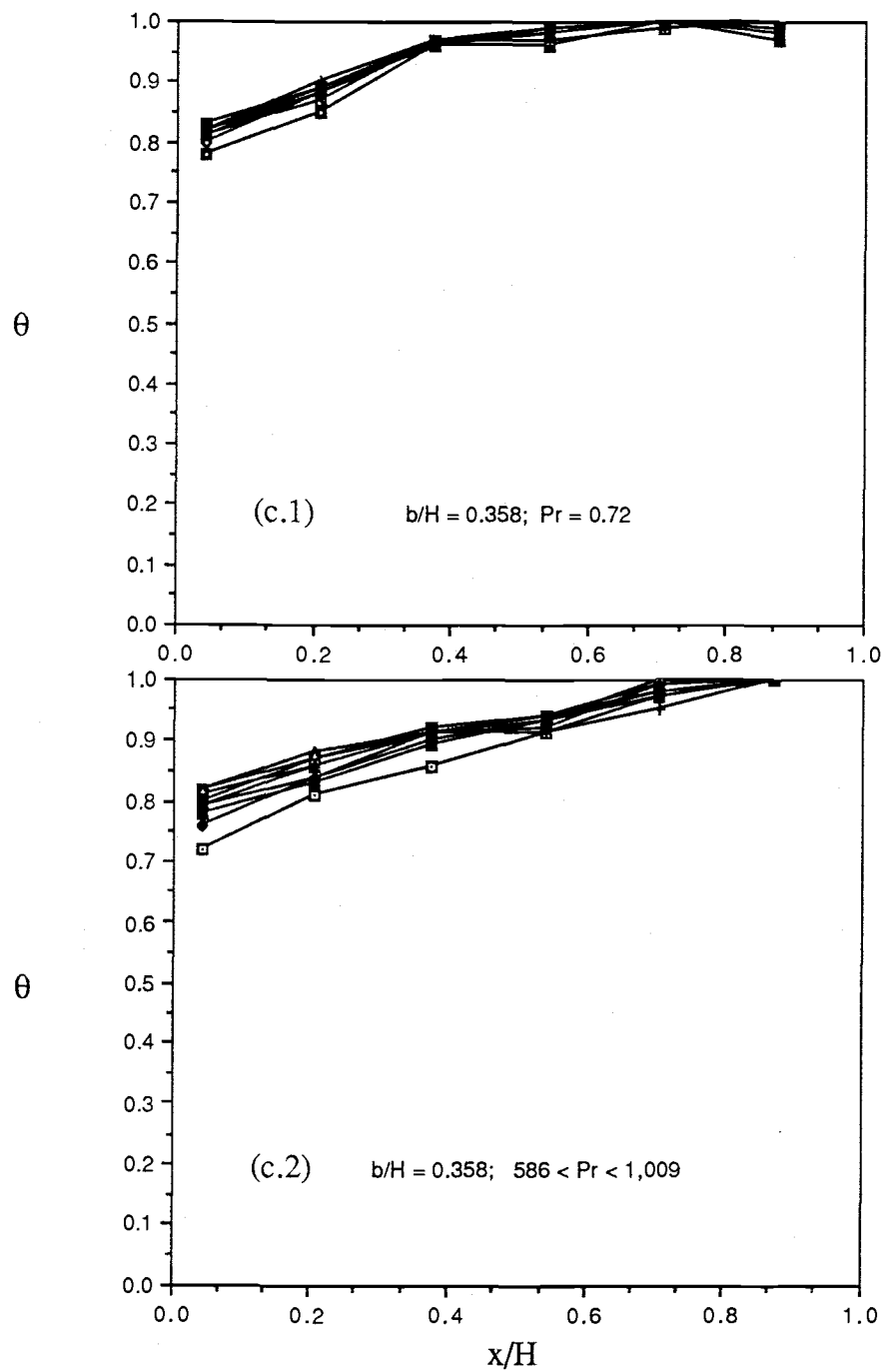


Figure 5.4 θ versus x/H for Various Q

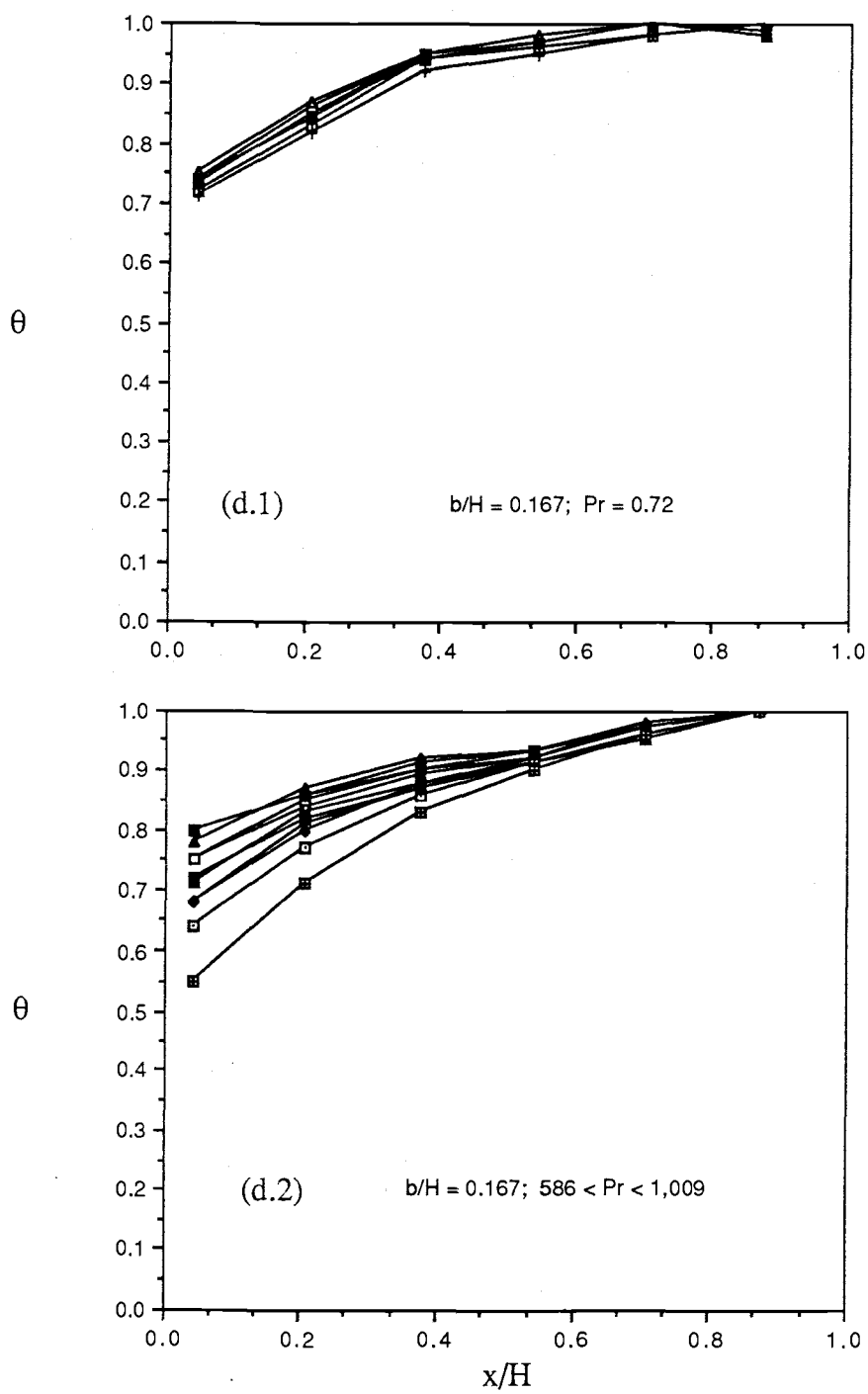
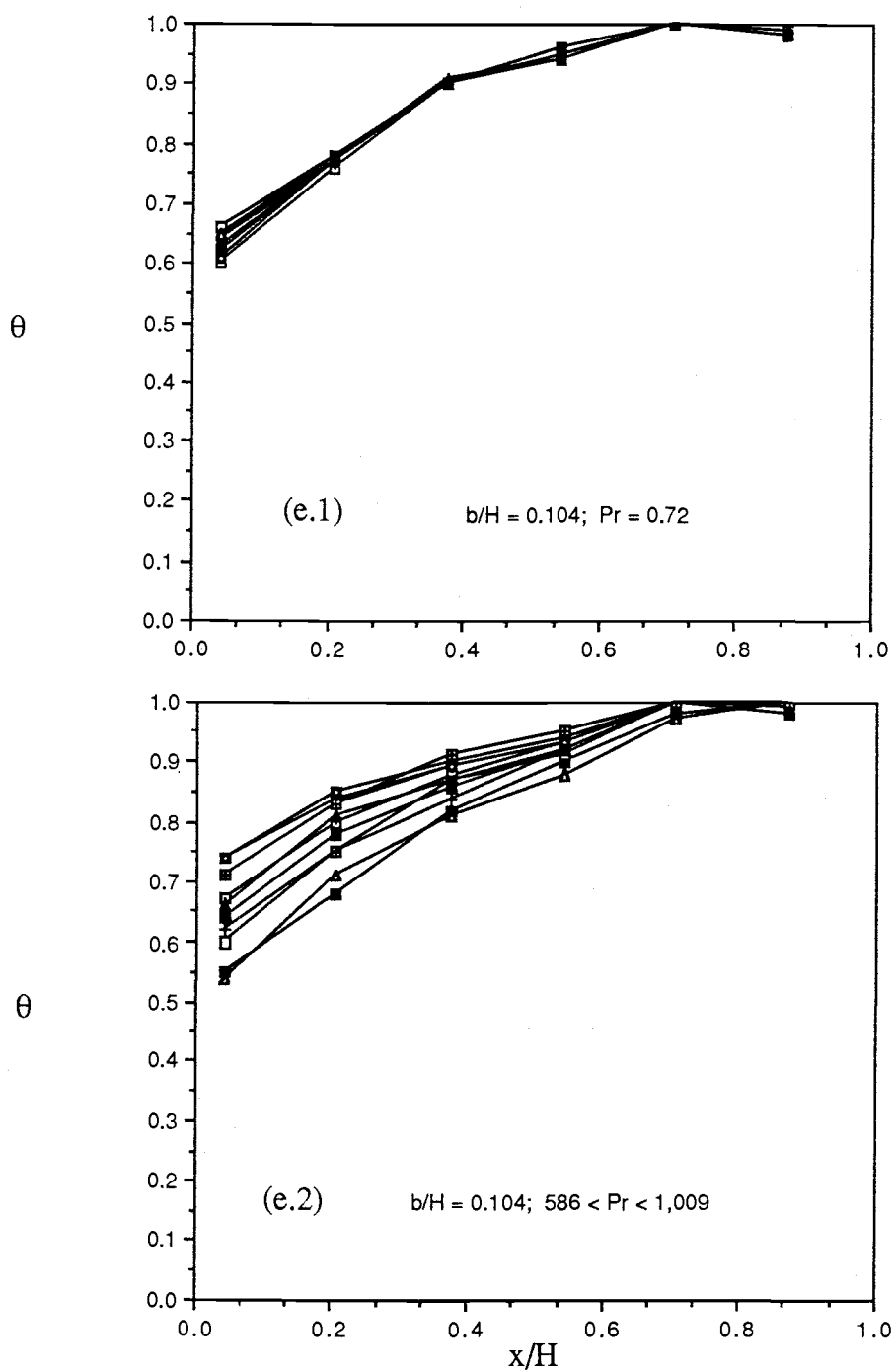


Figure 5.4 θ versus x/H for Various Q

Figure 5.4 θ versus x/H for Various Q

For a given heat flux condition, a vertical heated surface temperature is lower for a fluid with a higher thermal conductivity. With the present experiment at a given heat flux condition, a higher protruding heated surface temperature is observed for air.

The properties k , β , and C_p are important parameters in determining the heat transfer mechanism in the thermal boundary layer near a vertical heated surface. Other fluid properties, ρ and μ play significant roles in the momentum boundary layer region to govern the velocity field or mass exchange adjacent to the heated surfaces. All fluid property variation with temperature are presented in Appendix H.

5.4 Prandtl Number Effects

Reviewing the definition of Prandtl number will help to interpret the heat transfer results. The Prandtl number is defined as the ratio of the momentum diffusivity, ν to the thermal diffusivity, α . Comparisons of momentum diffusivity and thermal diffusivity variation with temperature on various fluids are presented in Figures 5.5 and 5.6 (a)-(b) for the analysis. Figure 5.5 indicates that in the temperature range from 10 °C to 87 °C,

$$\nu_{oil} > \nu_{air} > \nu_{H_2O}$$

This suggests that the hydrodynamic boundary layer, δ , is the thickest for oil, the second thickest for air, and the thinnest for water. Figures 5.6 (a) and (b) for the same temperature range, the following holds true

$$\alpha_{oil} < \alpha_{H_2O} < \alpha_{air}$$

This reveals that the thermal boundary layer, $\delta_{t,oil}$ is the thinnest, δ_{t,H_2O} is the second thinnest, and $\delta_{t,air}$ is the thickest among the three types of fluids used. For viscous fluids, $Pr \gg 1$, the velocity profile develops more rapidly than the temperature profile; i.e., the hydrodynamic boundary layer is much thicker than the thermal boundary layer or $\delta \gg \delta_t$. Thus, thermal

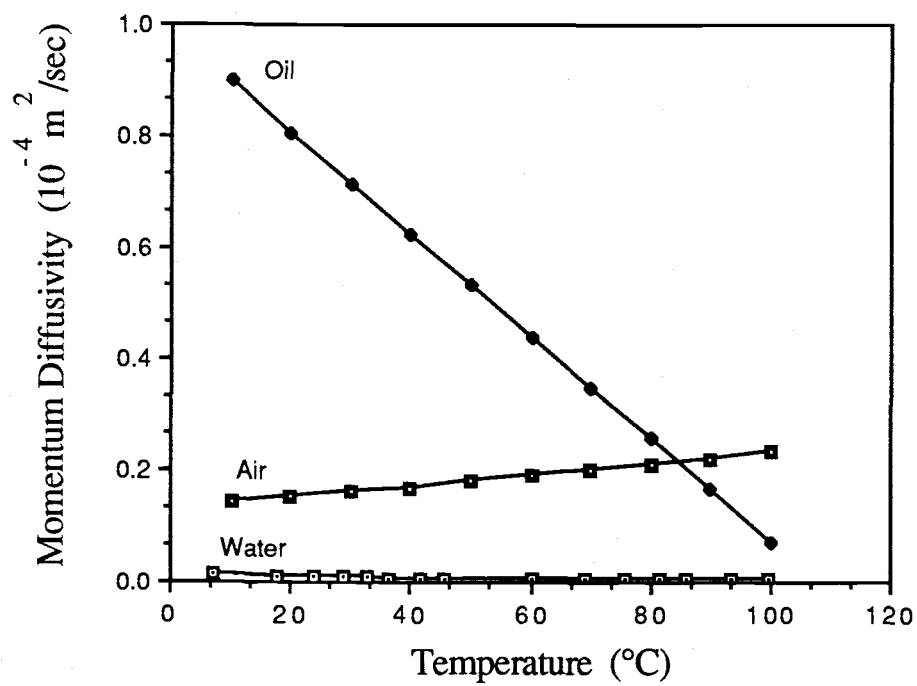


Figure 5.5 Momentum Viscosity-Temperature Variation

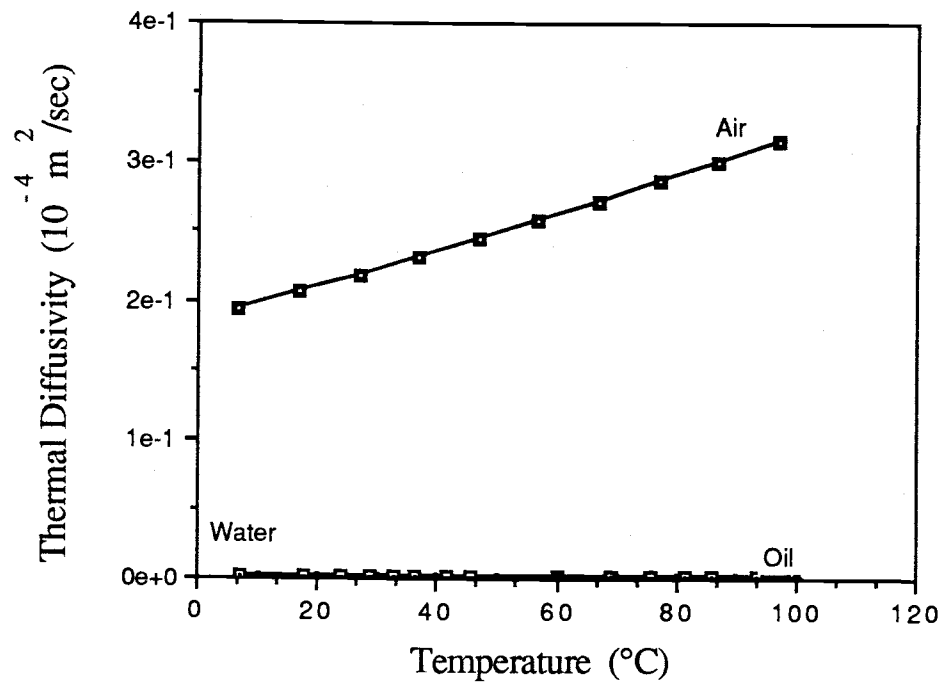


Figure 5.6 (a) Thermal Diffusivity-Temperature Variation

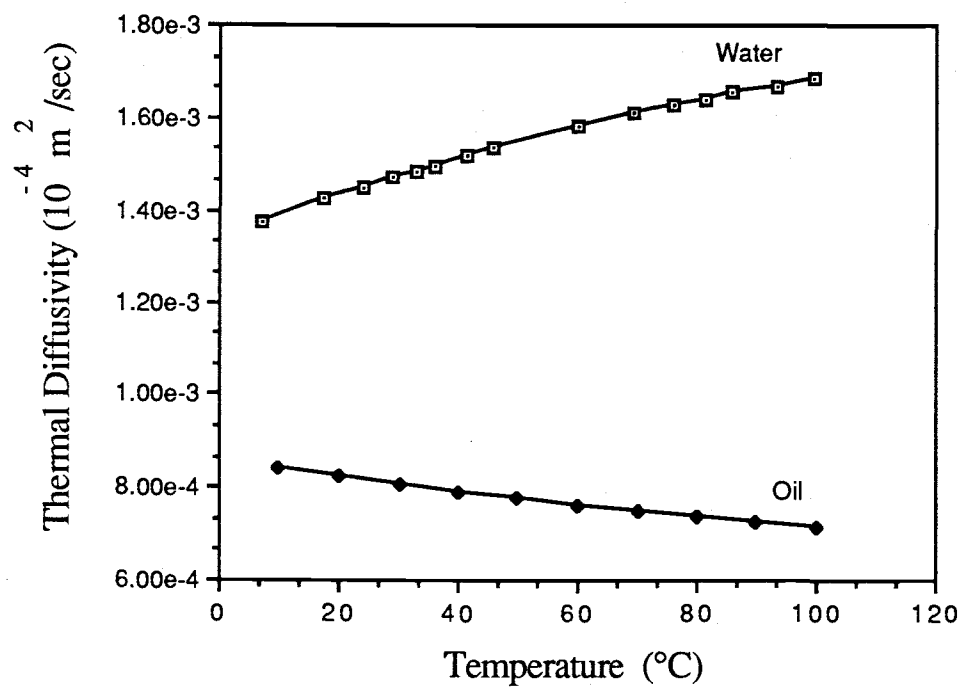


Figure 5.6 (b) Thermal Diffusivity-Temperature Variation

or spreading is manifested in the thermal boundary layer close to the heated discrete surfaces in the channel. The friction heat dominates in the higher viscous fluid. The balance of friction and buoyancy forces in the thermal boundary layer is expected. For water, $Pr > 1$, a similar trend as seen in oil would occur but with a much smaller magnitude. For air, $Pr < 1$, the onset of the thermal boundary layer is relatively rapid compared to the onset of the momentum boundary layer. For the case of air, however, the heated surface temperature is much higher for the same amount of heat flux than for other fluids. This is due to the low air thermal conductivity and the low air density and the less heat convected away from the surface. Figures 5.7 (a) and (b) depict the Prandtl number variation with temperature for the three different fluids. The values of ν , α and Pr in variation with temperature are also listed in Appendix H.

5.5 Heat Transfer Results Comparison

The plots of heat transfer coefficient versus the ratio of protruding array height to channel spacing for various heat fluxes are shown in Figures 5.8 and 5.9. Figure 5.8 (a) shows that the heat transfer coefficient increases as the channel spacing decreases for the first row. Figures 5.8 (b) and (c) illustrate that h decreases rapidly as the channel spacing narrows. These Figures suggest that a higher heat transfer coefficient occurs at the first row with the middle and top rows being opposite.

For a fixed heat flux, comparisons of h versus B/b with various fluids are shown in Figures 5.9 (a) to (c). The fluctuation of the heat transfer coefficient for distilled water in Figures 5.9 (a) to (c) is due to the formation of a flow circulation cell in the channel central region. The heat transfer coefficient is the highest for the distilled water, the second highest for the oil, and the lowest for air.

A typical variation of heat transfer coefficient for protruding arrays

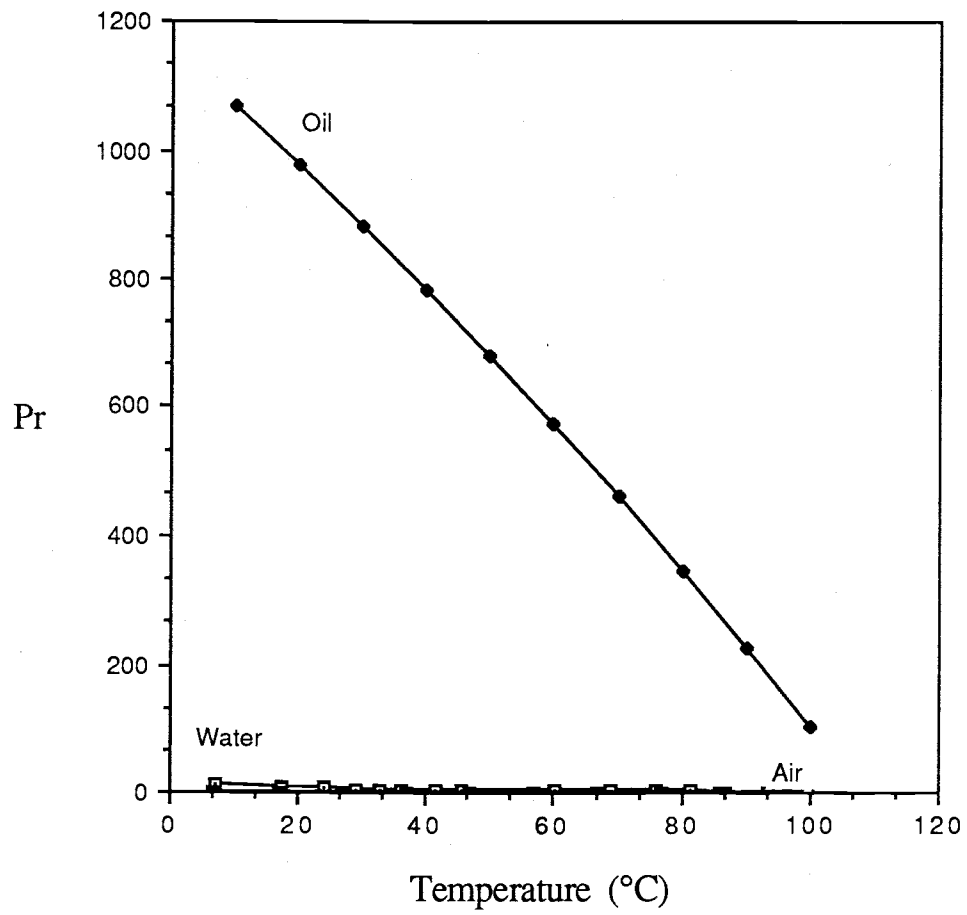


Figure 5.7 (a) Prandtl Number-Temperature Variation

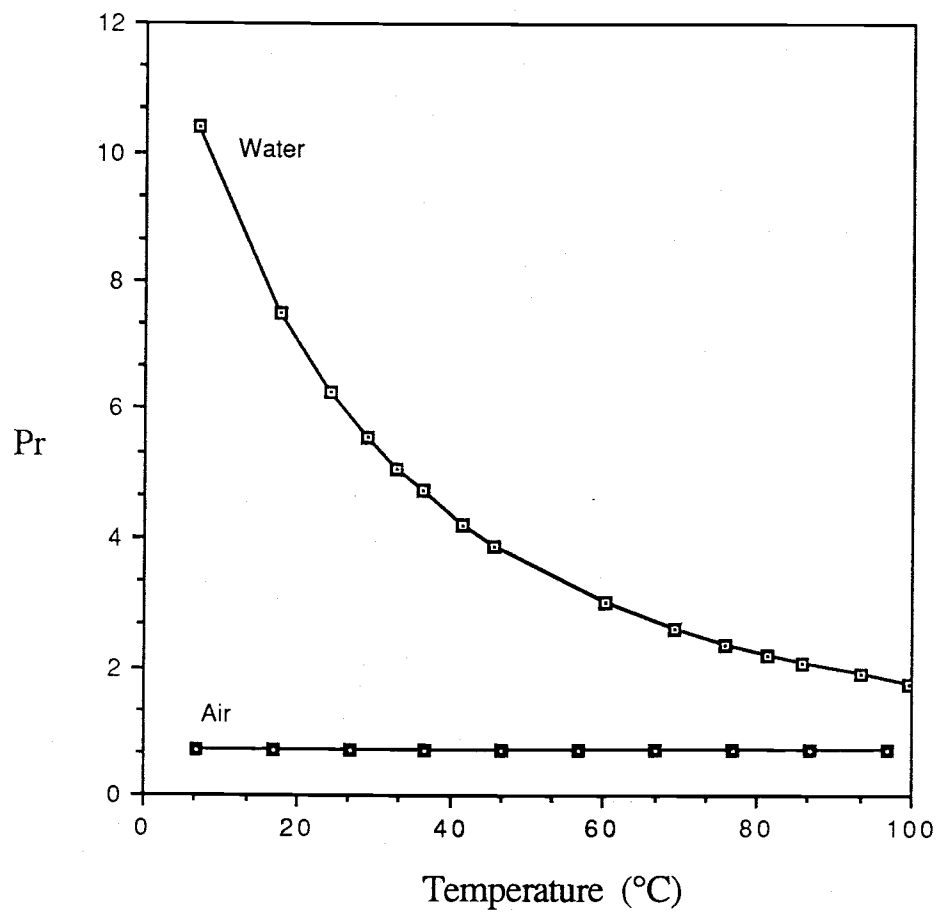
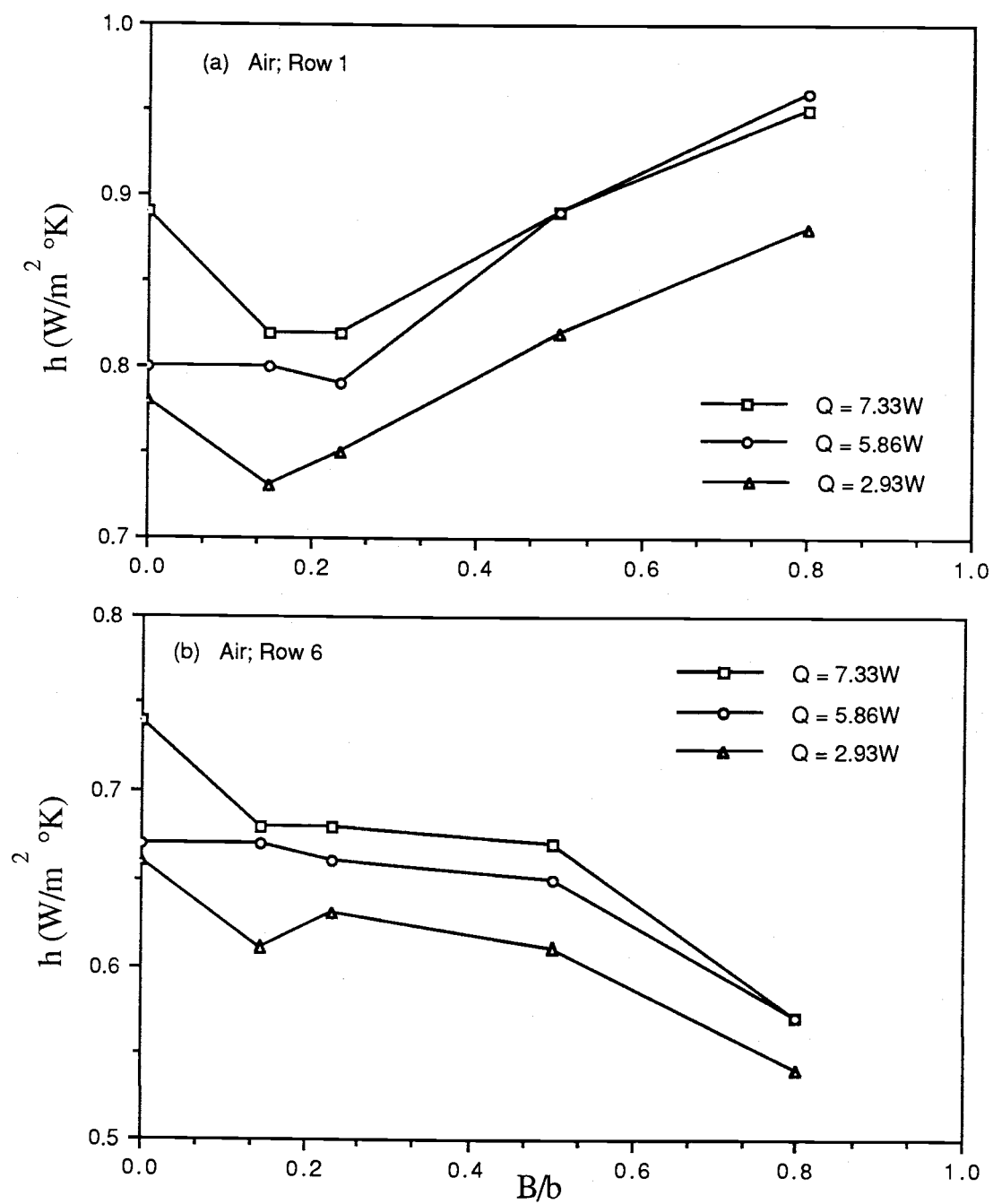
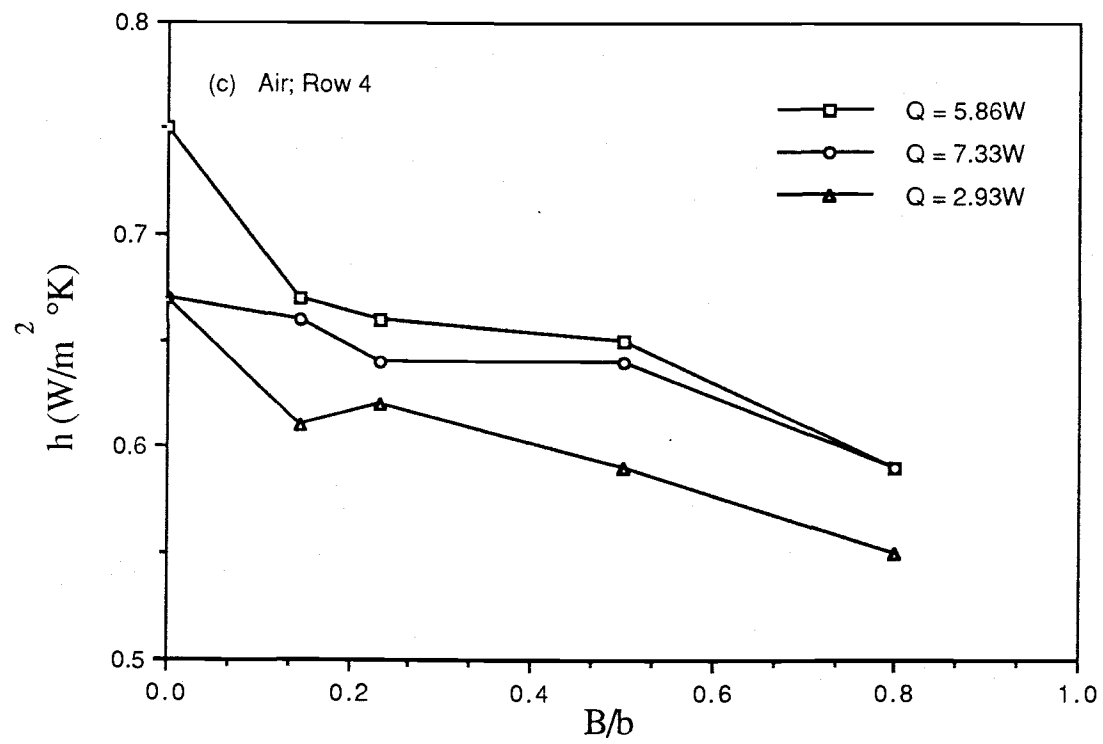


Figure 5.7 (b) Prandtl Number-Temperature Variation

Figure 5.8 h versus B/b

Figure 5.8 h versus B/b

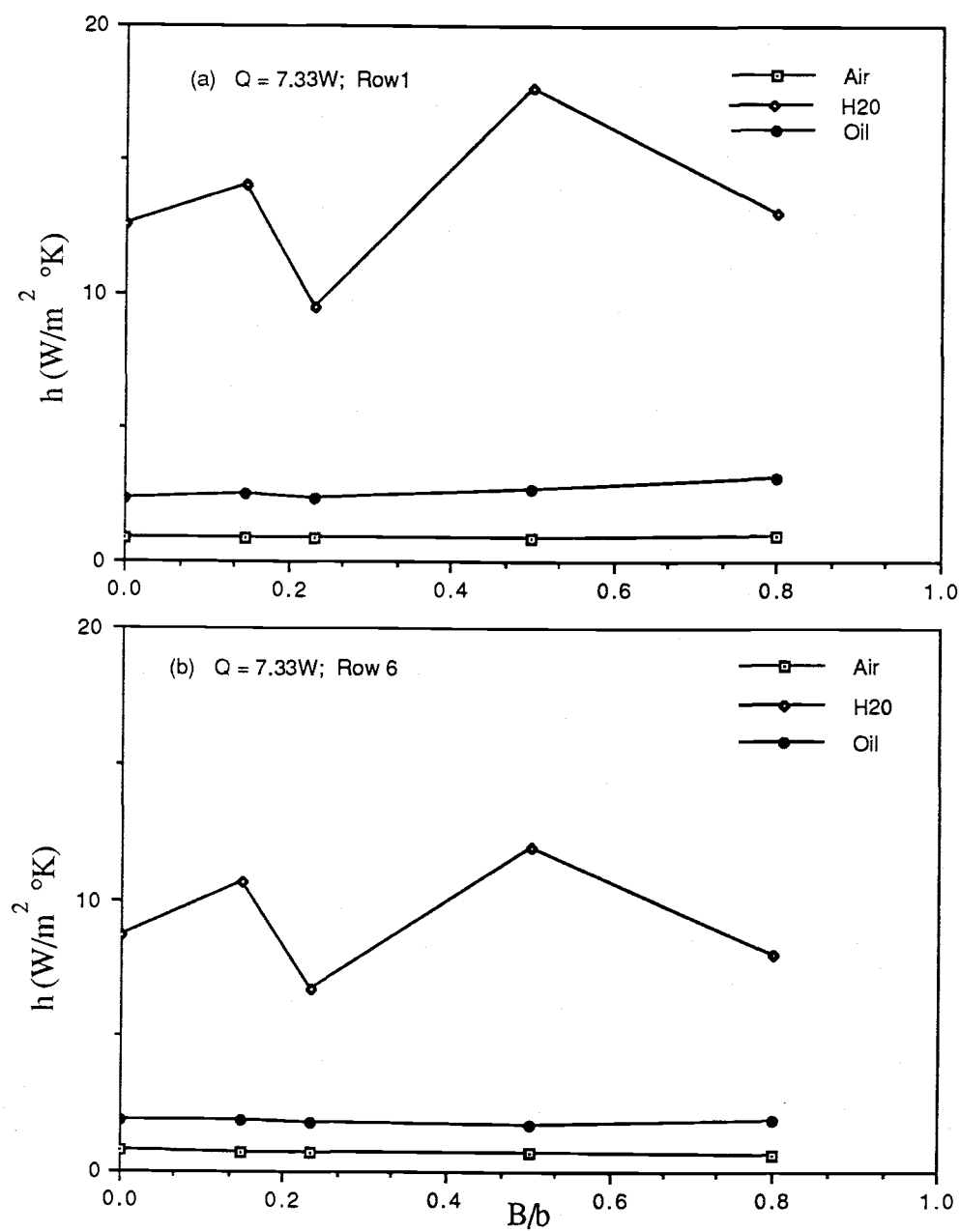


Figure 5.9 Comparison of h versus B/b for Various Fluids

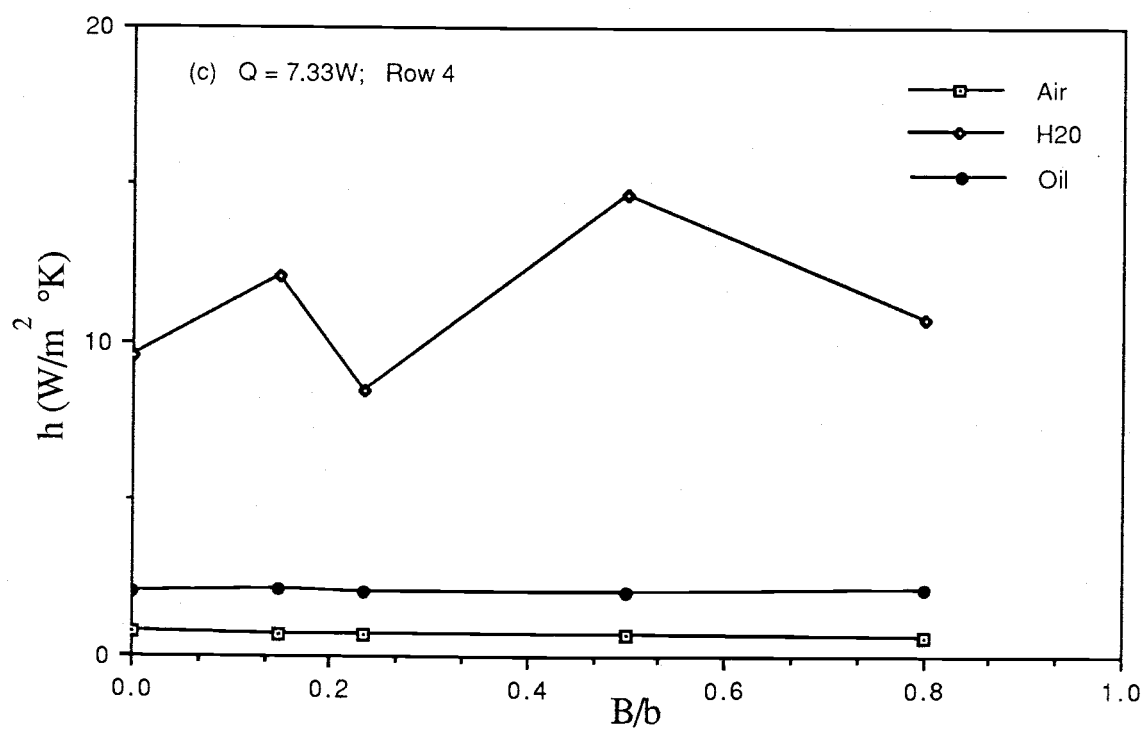


Figure 5.9 Comparison of h versus B/b for Various Fluids

without shrouding can be interpreted by Figures 5.1 to 5.3. The heat transfer decreases rapidly as the natural convection flow passes over the first three rows of the elements. As the natural convection flow further advances downstream, the heat transfer coefficient increases gradually from the third row to the fourth row, then decrease from the fourth to the subsequent rows. The cold fluid is induced upward into the channel due to the uniform heating of the discrete heat sources. The greater convection heat transfer coefficient results near the lower portion of the channel because of lower temperature differences between the chamber temperature and the first three rows of heating surface temperatures. The flow reversal in the channel outlet causes the inflection point of the curve at the 4th row. The flow reversal phenomenon was observed in the flow visualization experiment. For oil as the working fluid, a heat transfer variation similar to the water case was observed. With air as the working fluid, a variation in the heat transfer coefficient similar to the water case was calculated, but with a slight increase in h from the 5th to the 6th row. For the vertical channel with $b/H = 0.104$, the heat transfer coefficient remains unchanged from the 5th to the 6th row for higher heat fluxes with oil as the heat transfer medium.

A persual of the heat transfer data shows that the Prandtl number effect is significant. Figure 5.10 exemplifies the significant effects of Prandtl number variation - three sets of data with 192 points are compressed into three distinct regions for an array of protruding elements without shrouding. Specifically, the local Nusselt number for oil was the lowest when compared to the local Nusselt numbers of air and water at various $Ra_x \times Pr$. The local Nusselt number of air is generally higher than the local Nusselt number of water. For a given value of $Ra_x \times Pr$, Nusselt number increases with the decrease of Prandtl number.

For a vertical plate, correlations of Dotson [77] underpredicts the local air Nusselt number for Ra_x^* over 10^6 and fits well for Ra_x^* less than

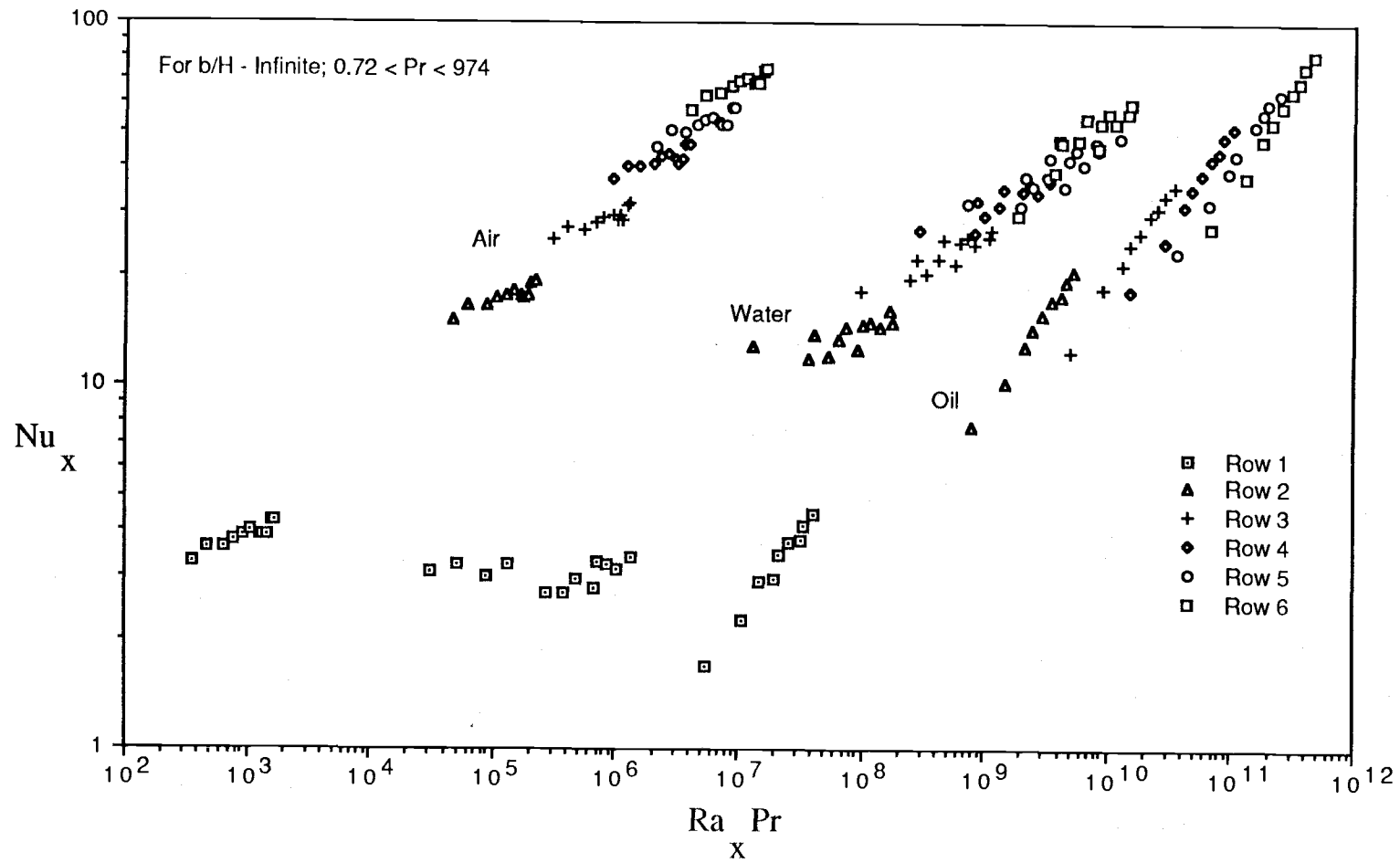


Figure 5.10 Comparison of Local Nu and $Ra \times Pr$ for Various Fluids

10^6 as shown in Figure 5.11. Comparison to the correlation of Vliet and Liu [76] was made with a plot of Nu_x versus Ra_x^* for water as shown in Figure 5.12. Their correlation overpredicts the present data for all the values of modified Rayleigh number, particularly in the lower range. For oil, the correlation of Fujii and Fujii [78] is in good agreement for Ra_x^* around 10^9 , overpredicts local Nusselt number with Ra_x^* below 10^8 , and underpredicts Nu_x slightly in the higher modified Rayleigh number range as shown in Figure 5.13.

Correlations of Churchill and Chu [57] were also used to compare with the data of Nu_x and Ra_x for the vertical plate case. The equation for air underestimates the Nu_x in Figure 5.14 and the equation for water in Figure 5.15 overestimates the Nu_x for all the values of Ra_x . The equation for oil fits the Nu_x closely for Rayleigh number greater than 10^8 and overpredicts the data in the lower range of Ra ($< 10^7$) as shown in Figure 5.16.

For vertical channel data, comparisons of the results with equations recommended by Fujii and Fujii [78], are shown in Figures 5.17 to 5.19. As can be seen in Figure 5.17, the equation of Fujii and Fujii underpredicts the values of Nusselt number at all values of Elenbaas number $(b/H) Ra_b^*$ for air. However, the equations of Fujii and Fujii fit the data for water and oil, particularly in the higher range of $(b/H) Ra_b^*$ but overpredicts slightly in the lower range of $(b/H) Ra_b^*$ as depicted in Figures 5.18 and 5.19. The majority of data fit equations of Fujii and Fujii unsatisfactorily. This is not surprising because the present study dealt with protruding discrete heating surfaces instead of a continuous heating surface on one of the channel walls.

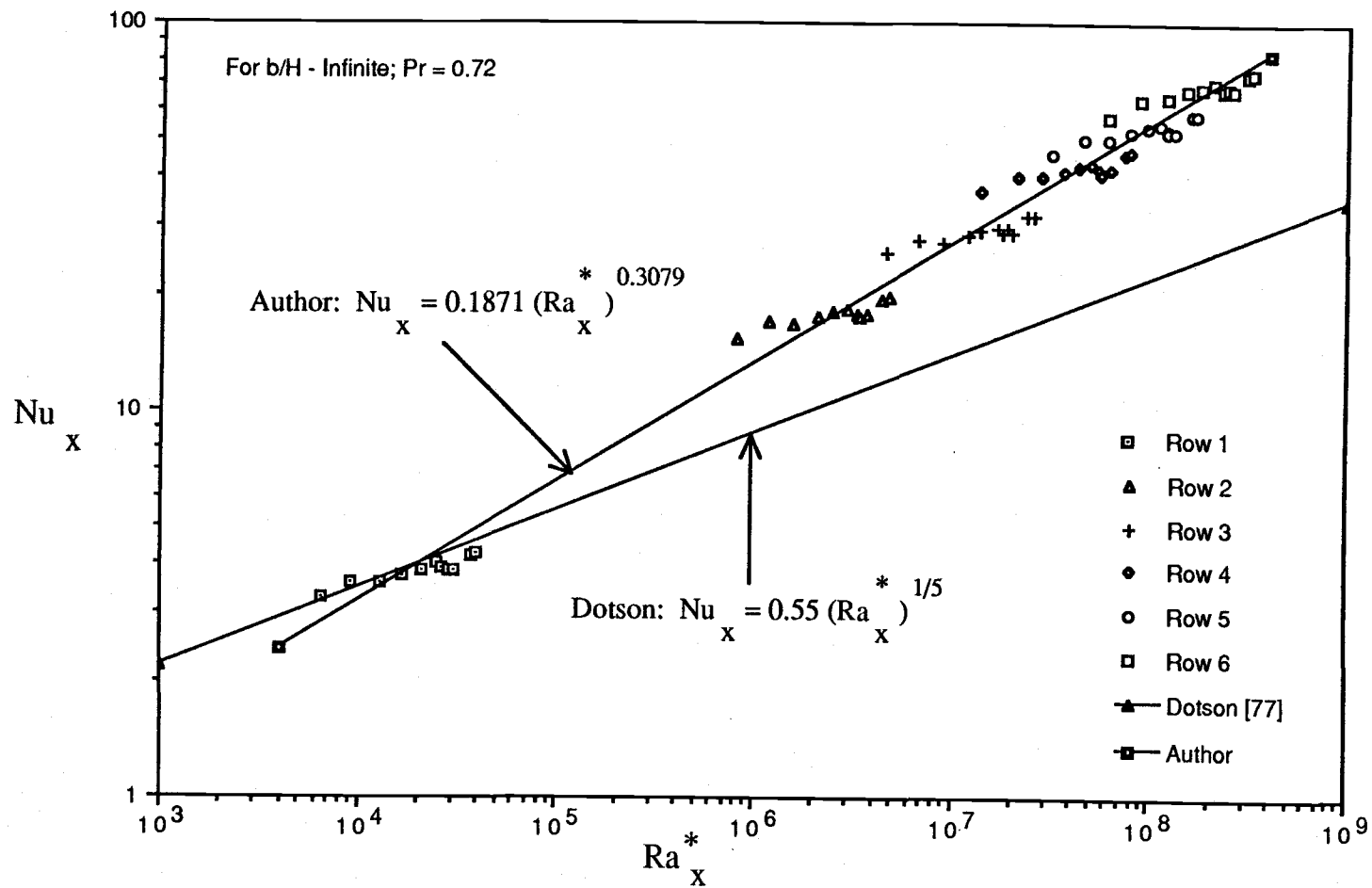


Figure 5.11 Comparison of Air Data with Dotson [77] for Protruding Arrays without Shrouding

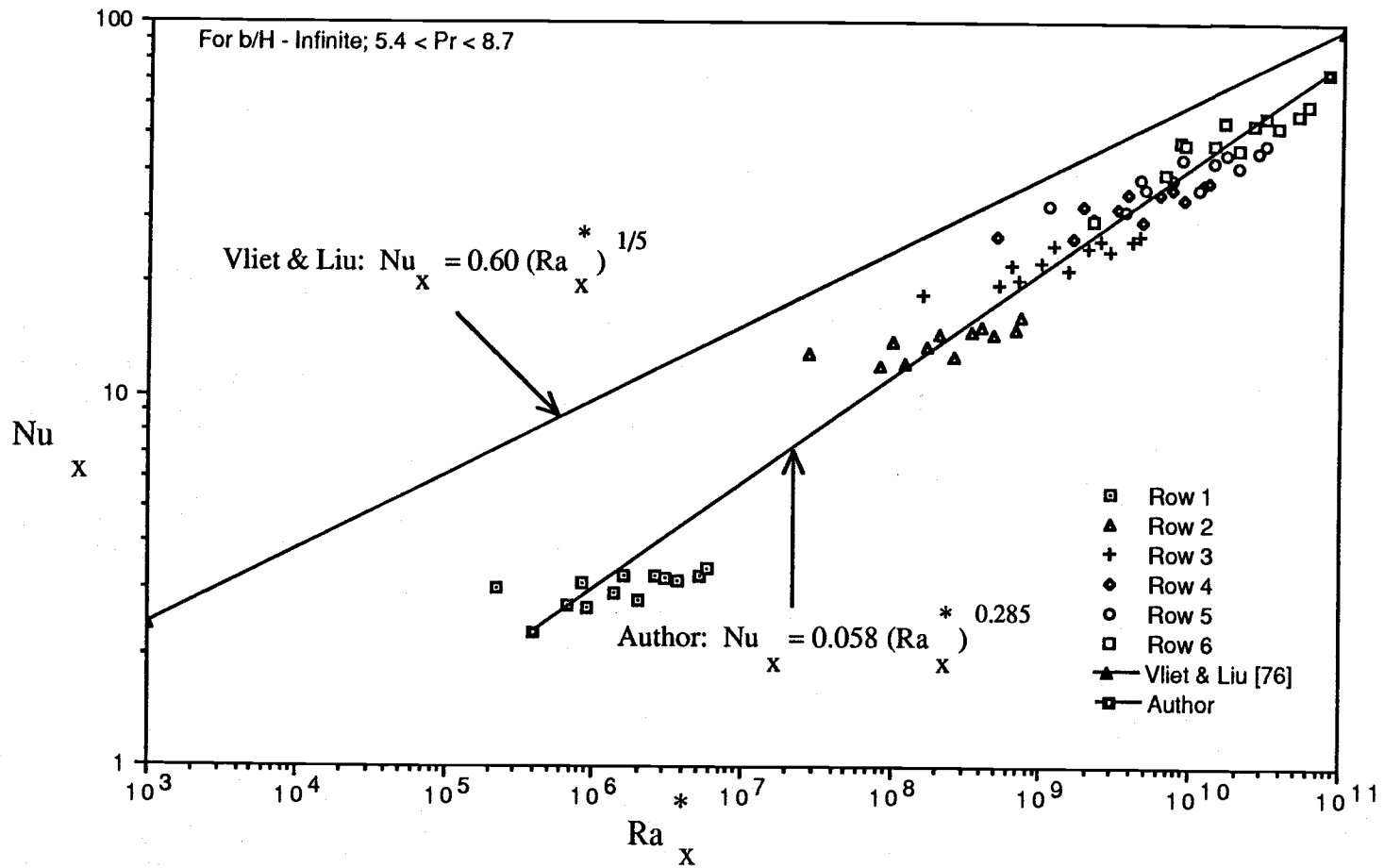


Figure 5.12 Comparison of Water Data with Vliet & Liu [76] for Protruding Arrays without Shrouding

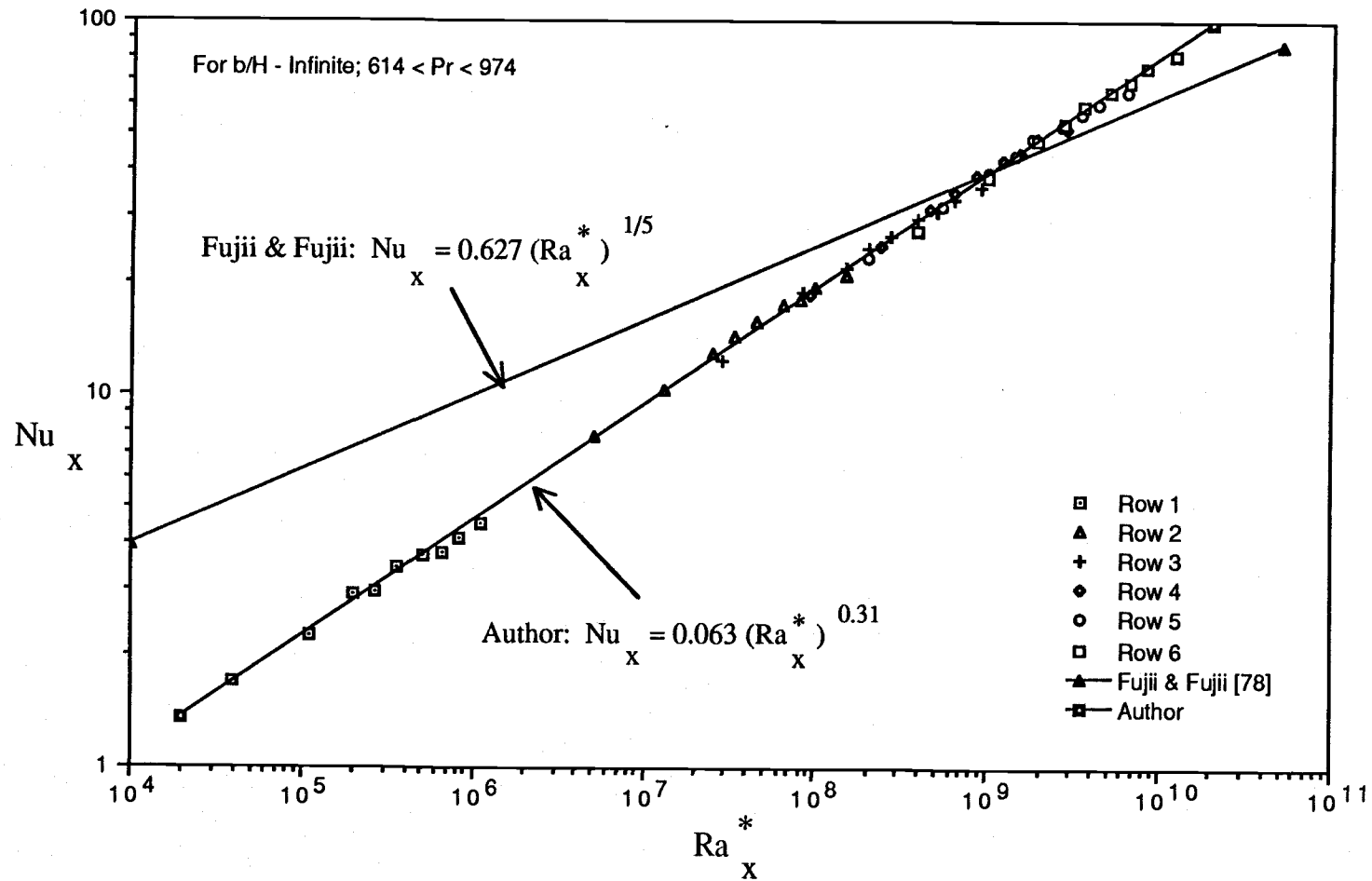


Figure 5.13 Comparison of Oil Data with Fujii & Fujii [78] for Protruding Arrays without Shrouding

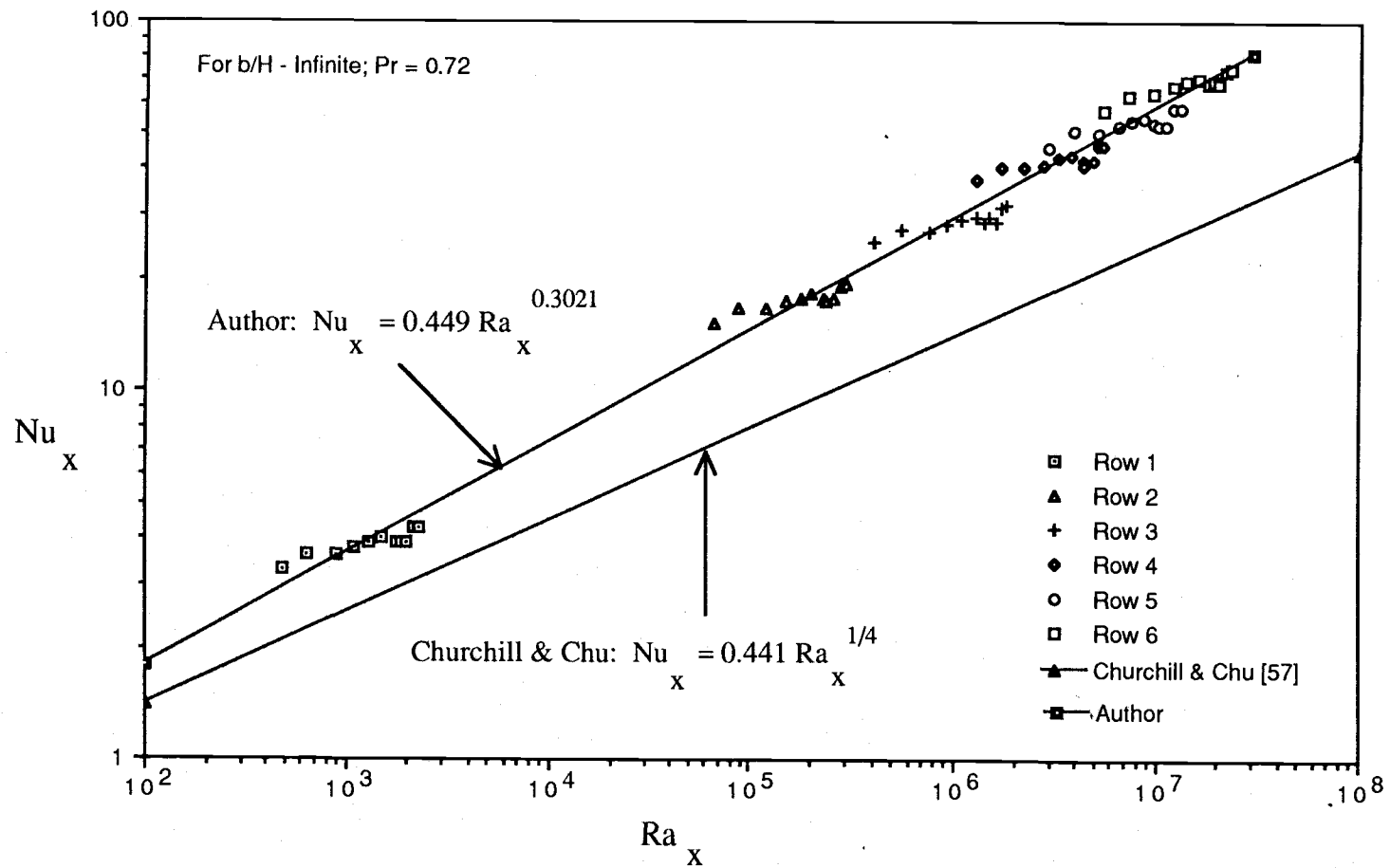


Figure 5.14 Comparison of Air Data with Churchill & Chu [57] for Protruding Arrays without Shrouding

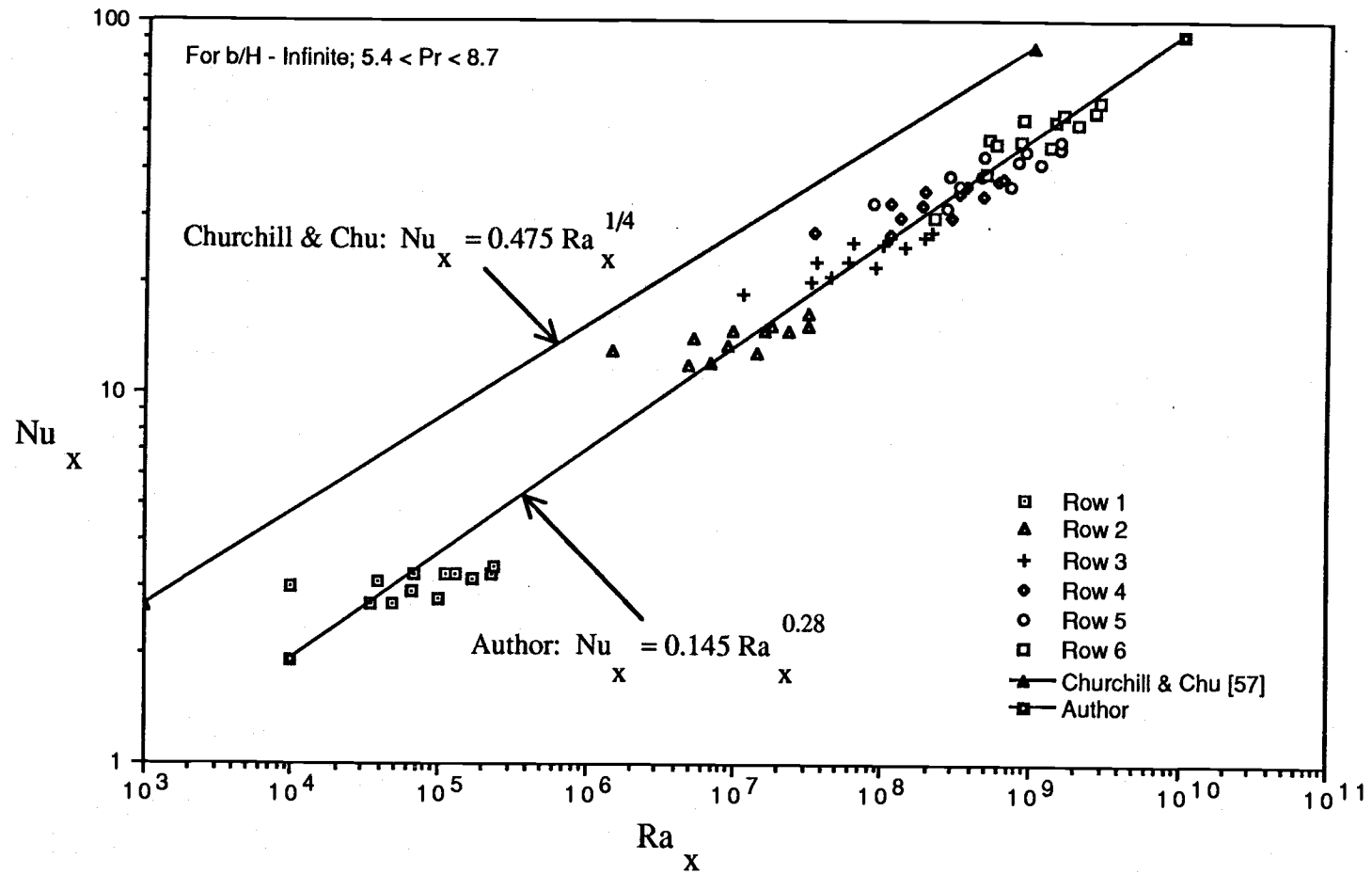


Figure 5.15 Comparison of Water Data with [57] for Protruding Arrays without Shrouding

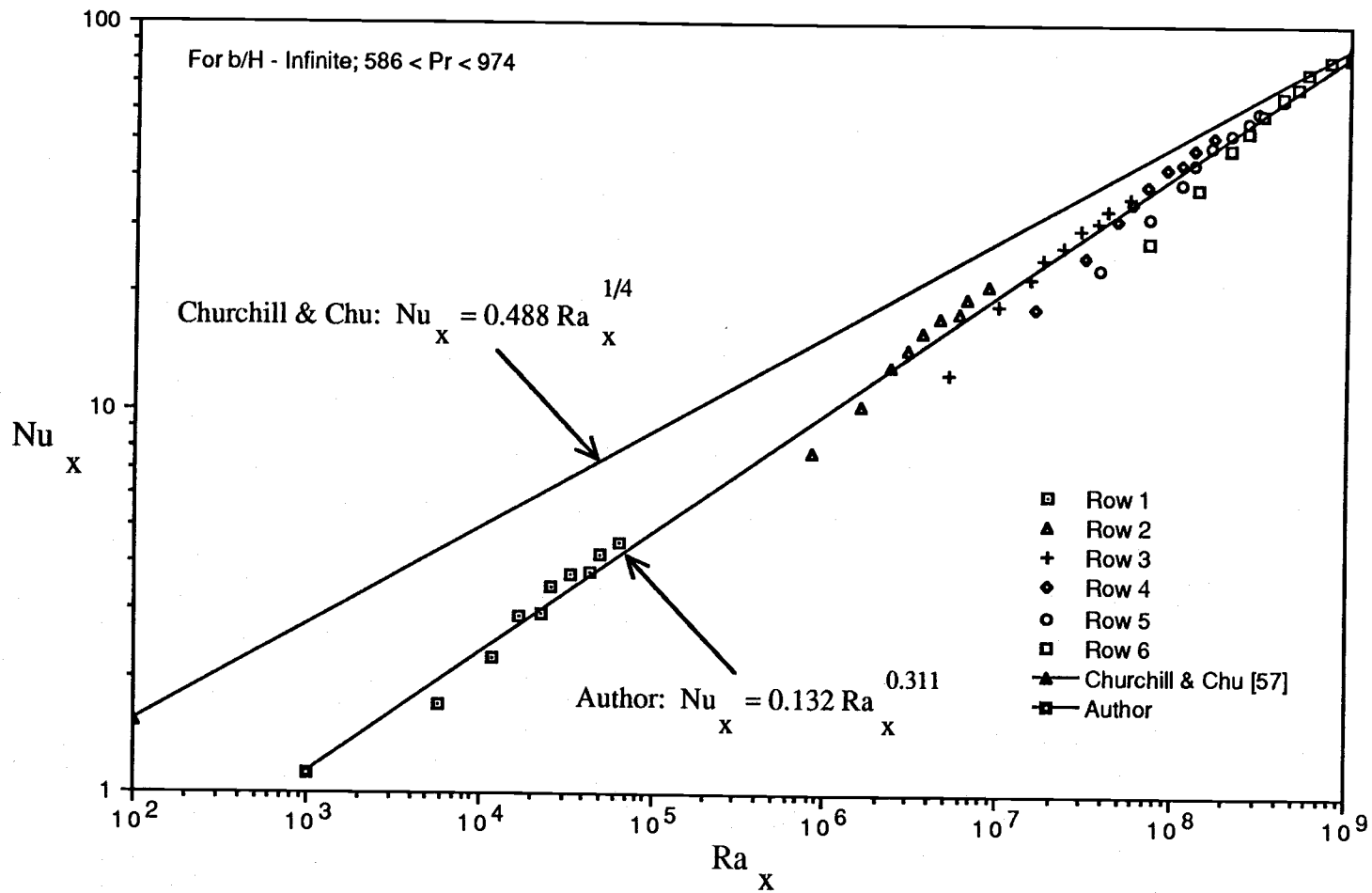


Figure 5.16 Comparison of Oil Data with [57] for Protruding Arrays without Shrouding

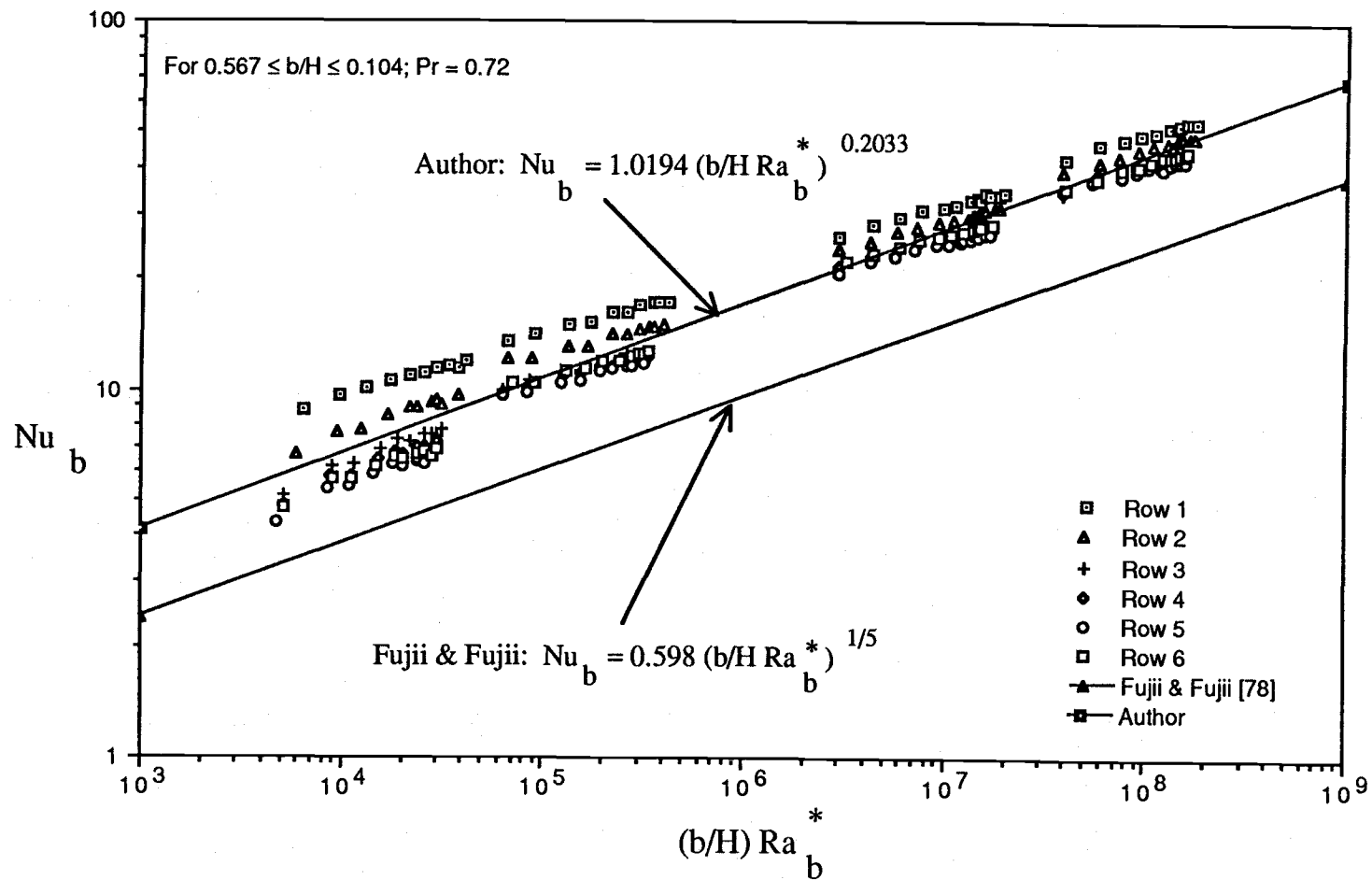


Figure 5.17 Comparison of Air Data with Fujii & Fujii [78] for Protruding Arrays with Shrouding

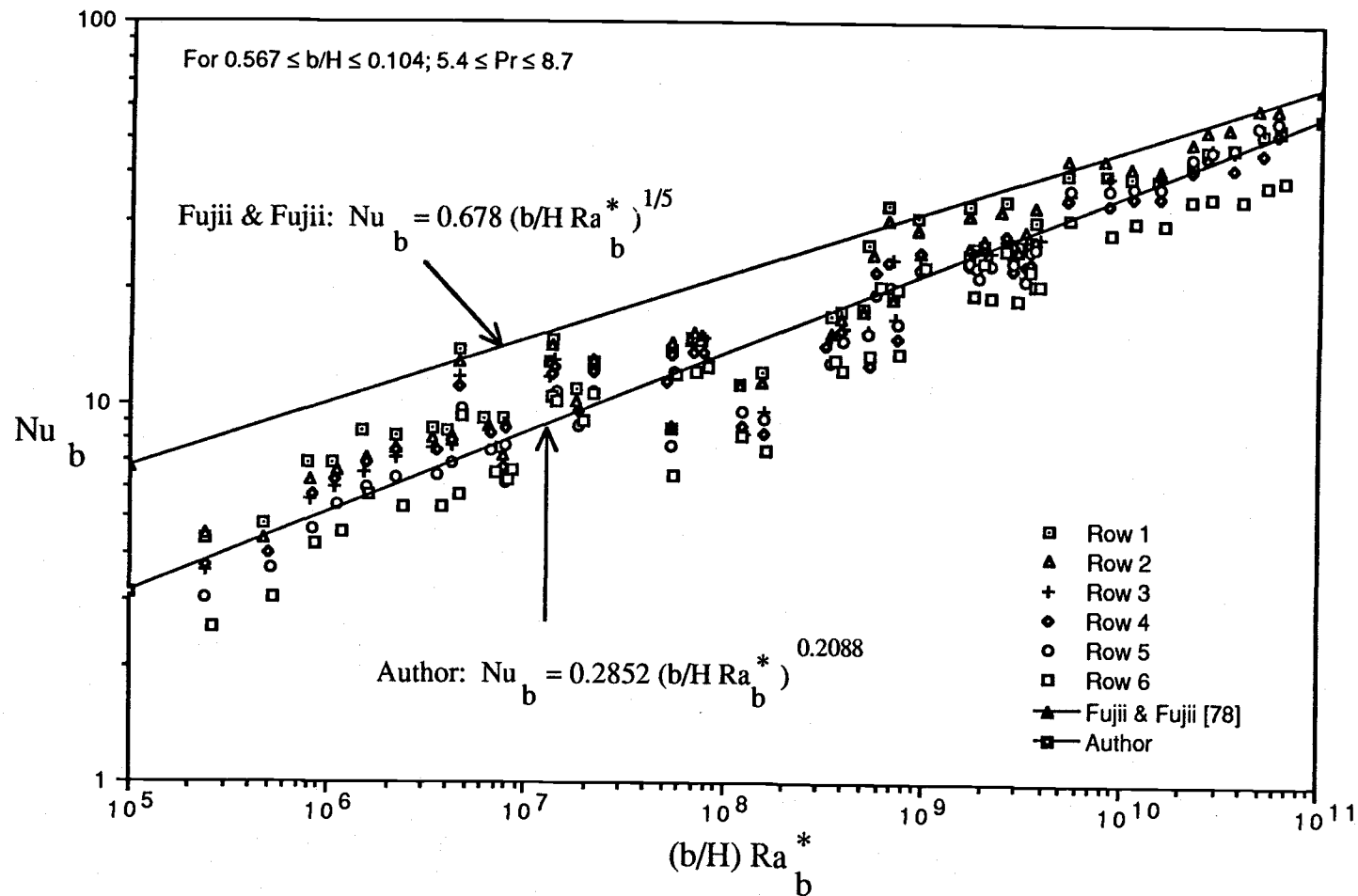


Figure 5.18 Comparison of Water Data with Fujii & Fujii [78] for Protruding Arrays with Shrouding

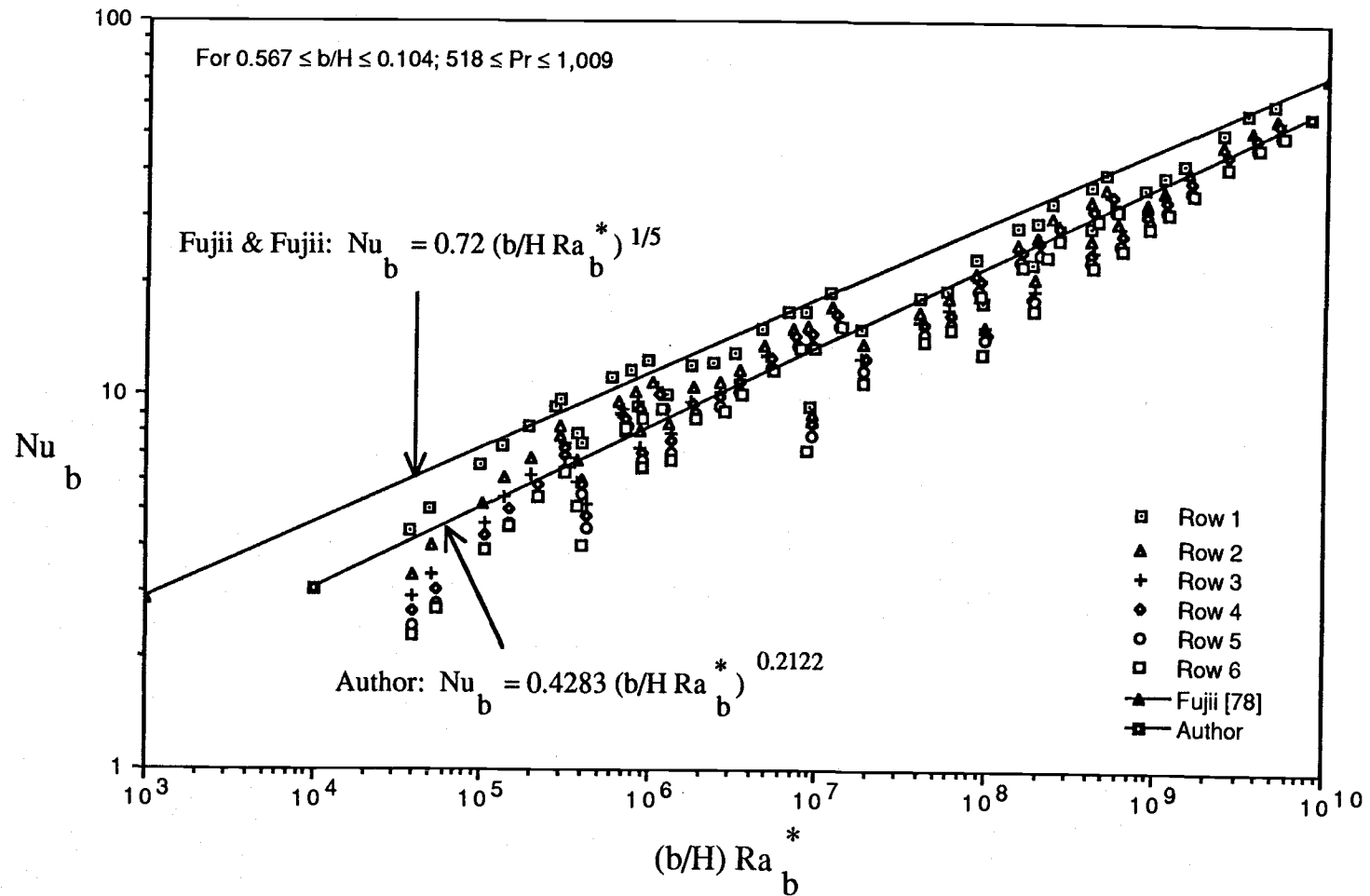


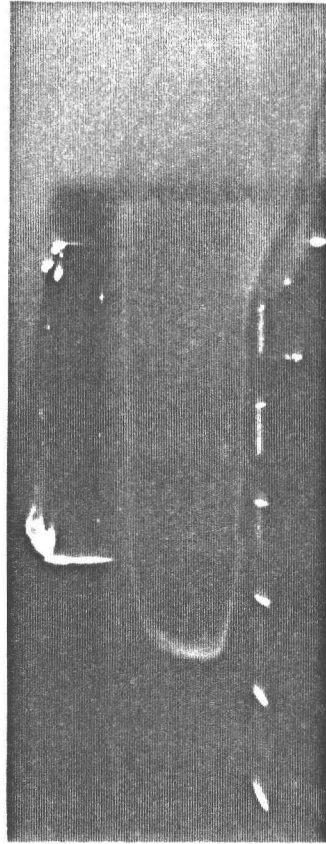
Figure 5.19 Comparison of Oil Data with Fujii & Fujii [78] for Protruding Arrays with Shrouding

5.6 Flow Visualization in Vertical Channel

Comparisons of flow patterns in vertical channels with the same heat flux condition are depicted in Figure 5.20. Figure 5.21 shows the typical flow pattern in the vertical channel with protruding discrete heating. Three distinct flow regions were observed as described in the following:

1. A relatively high velocity of rising upward boundary layer flow closely followed the protruding discrete heated surfaces. The momentum boundary layer is thickening at the top as the rising flow advances and accelerates downstream.
2. A relatively slow reversed flow was drawn into the channel top. The penetration depth, d_p , of the reversal flow was closely linked to the magnitude of the heat flux, channel spacing, and working fluid properties. When air was used as the working fluid, it appears that the penetration depth was below the mid-height of the channel in contrast to the distilled water case which was above the mid-height point at the same heat flux condition. This may be attributed to the low viscosity of air. If the fluid dynamic viscosity is closely linked to the penetration depth of the reversed flow, then the following inequality relation exists for a given heating condition:

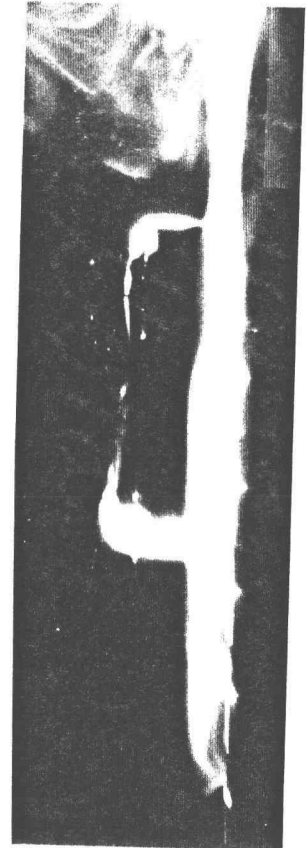
$$d_{p,\text{air}} > d_{p,\text{H}_2\text{O}} > d_{p,\text{oil}} \text{ because } Pr_{\text{air}} < Pr_{\text{H}_2\text{O}} < Pr_{\text{oil}}.$$
3. A stagnation flow region was located adjacent to the unheated wall in the lower portion of the channel. This stagnation region occupied slightly over (the ratio of the stagnation region to overall channel space) half the space of the channel for the widely spaced channel. The stagnation region decreases as the channel spacing decreases for a given boundary condition and working fluid.
4. A flow circulation cell was observed in the channel central region for water as the working fluid. However, no circulation cell



(a) Air; $b/H=0.357$
 $Ra_b^* = 3.5 \times 10^7$



(b) H₂O; $b/H=0.357$
 $Ra_b^* = 9.2 \times 10^8$



(c) H₂O; $b/H=0.167$
 $Ra_b^* = 4.6 \times 10^7$

Figure 5.20 Comparisons of Flow Patterns in Vertical Channels with the Same Heat Flux, $Q=5.86W$

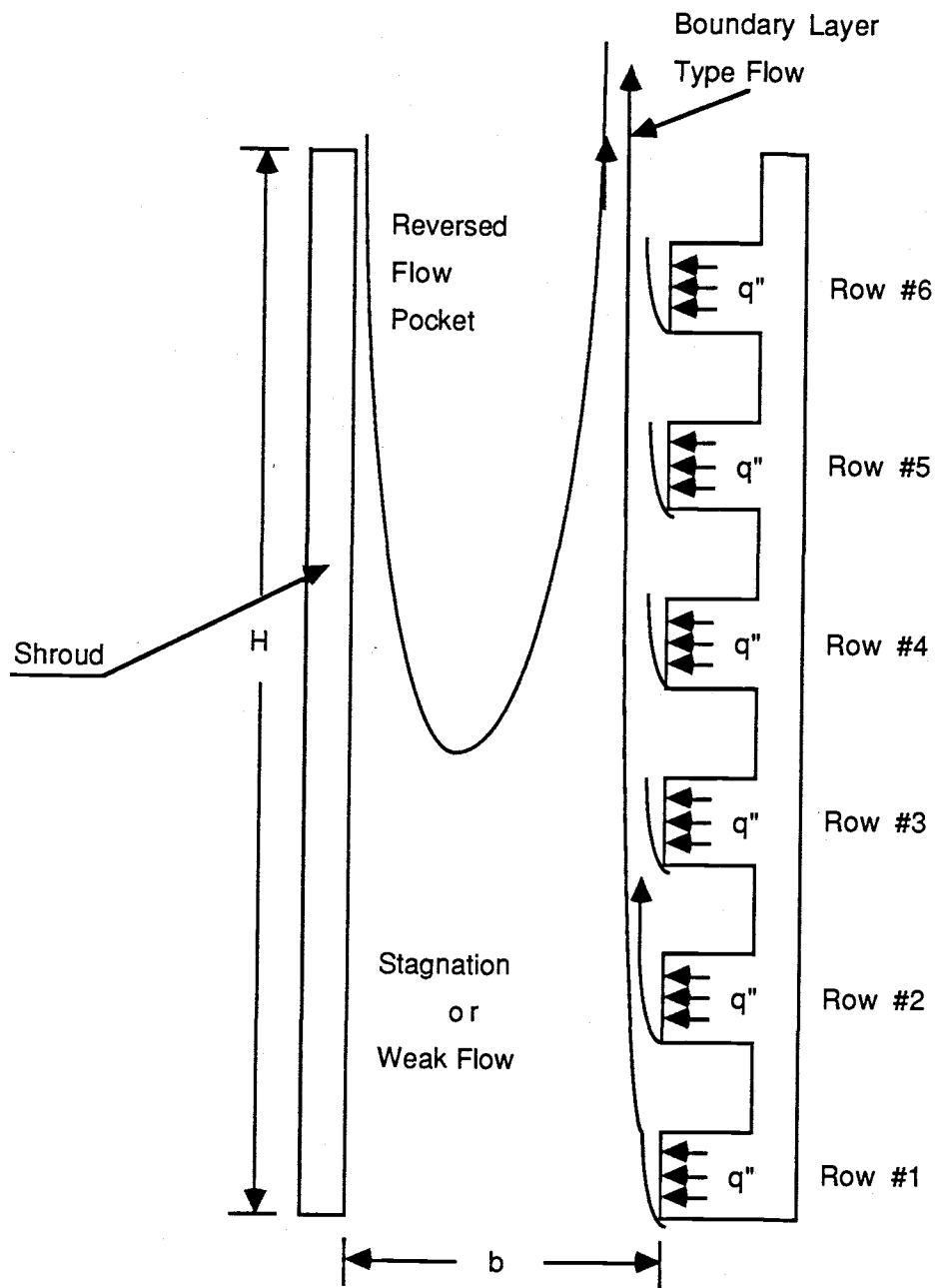


Figure 5.21 Typical Flow Pattern in Vertical Channel with Protruding Heated Arrays for $b/H = 0.567$ & 0.358

was observed in the channel for the air case. This is not to say that there would be no separation or circulation flow between each pair of protruding elements; No flow visualization was made in that particular region.

The flow reversal phenomenon satisfies the conservation principles of mass, momentum, and energy in the system. The flow was first drawn into the channel at the bottom. The buoyancy flow was slow in the lower portion of the channel. As the flow advances along the heated surfaces, it accelerates farther downstream. Because friction and pressure vary along the streamwise (low temperature difference) direction, the friction makes it difficult for more flow to be drawn in from the bottom. The typical velocity profile adjacent to the channel outlet may be anticipated as depicted in Figure 5.22.

To balance the mass in and mass out, the top cold fluid outside the channel provides a more advantageous environment to be drawn in from the channel top. This is due to a much larger temperature gradient along the traverse direction so as to satisfy the principle of mass conservation. The reversed flow phenomenon in a vertical channel was also observed by Azevedo and Sparrow et al. [52]. The present reversed flow occurrence in the vertical channel may be characterized by the criterion of Aung and Worku [82]. The criterion suggests that the flow reversal for the present experiment may be corresponded to $(Gr_b/Re_b)_{max} = 72$ and $(T_s - T_\infty)/(T_b - T_\infty) \cong 0$. However, no flow reversal would be present if a heated shrouding wall boundary condition is imposed. This is due to a relatively large flow being drawn into the channel from the bottom.

Vliet and Liu [76] found that the transition flow was in the Ra_x^* range from 3×10^{12} to 10^{14} in their experimental study of natural convection from a vertical plate with uniform heat flux condition. The local modified

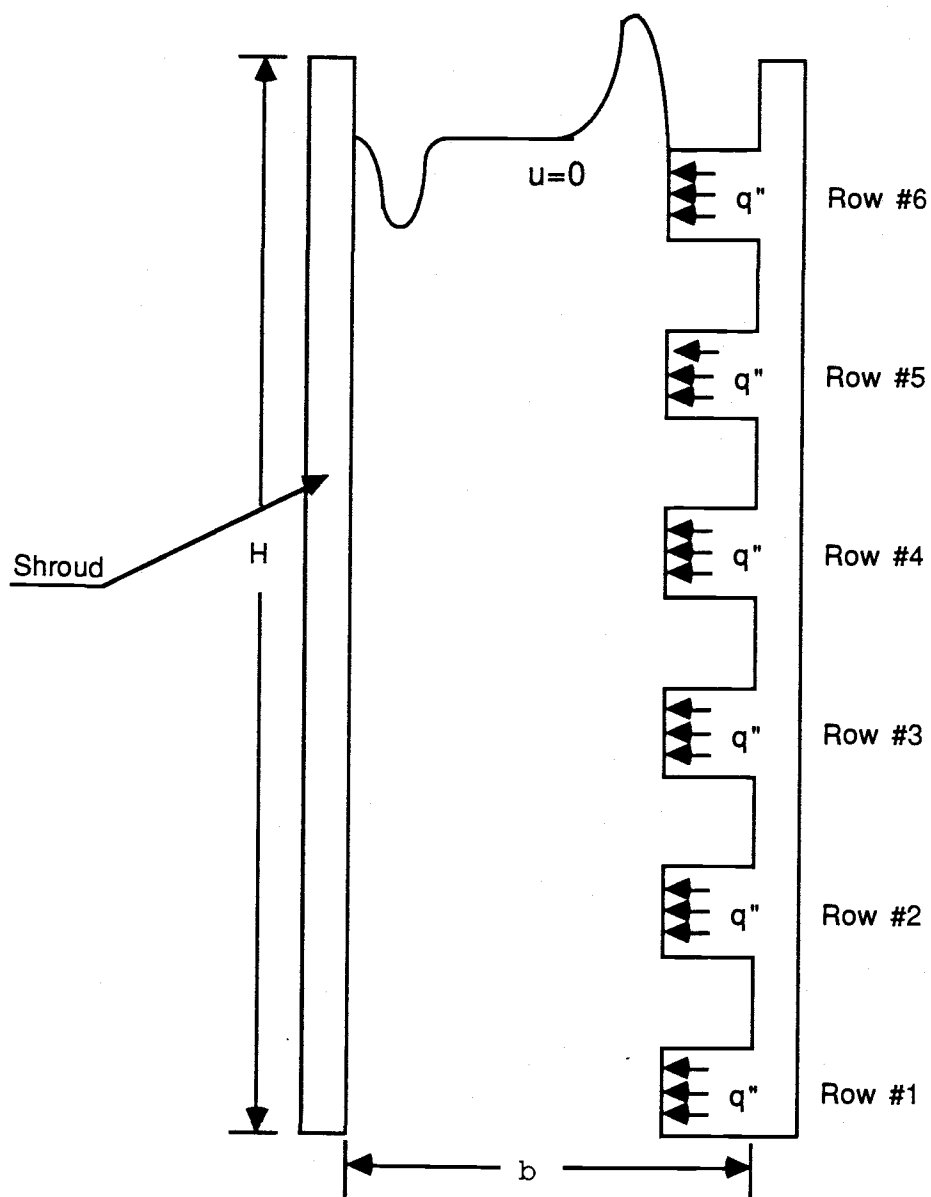


Figure 5.22 Anticipated Velocity profile adjacent to the Channel Outlet with Protruding Heated Arrays for $b/H = 0.567$ & 0.358

Rayleigh number in the present experiment was between 6.0×10^3 and 1.5×10^{11} . No eddies were observed to protrude through the interface of the ambient fluid. No turbulence was observed at this interface in the flow visualization experiments. This may infer that the natural convective flow in the study was still in the laminar flow regime even with heating from the protruding arrays.

To estimate the magnitude of the flow velocities among various fluids in a given condition, a simple scheme was developed as follows.

The convective heat transfer may be approximated by

$$Q = M C_p \Delta T_m$$

where M is the buoyancy induced mass flow rate and is defined as ρG . ΔT_m is the temperature difference between the mean fluid and the fluid ambient temperature, $\Delta T_m = 0.5 (T_h - T_c) = 0.5 \Delta T$. Rearranging the previous equation, the following relation can be derived

$$M = Q / (C_p \Delta T_m)$$

Referring to Figure G.1 and choosing $Q = 5 \text{ W}$, gives $\Delta T_m \cong 1.5 \text{ }^\circ\text{K}$ for the water case, $\Delta T_m \cong 10 \text{ }^\circ\text{K}$ for the oil case, $\Delta T_m \cong 25 \text{ }^\circ\text{K}$ for the air case.

Noting that

$$C_{p\text{H}_2\text{O}} \cong 4, C_{p\text{oil}} \cong 2, \text{ and } C_{p\text{air}} \cong 1 \text{ kJ}/(\text{kg} \cdot ^\circ\text{K}).$$

And since $M_{\text{H}_2\text{O}} = Q/6 > M_{\text{oil}} = Q/20 > M_{\text{air}} = Q/25 \text{ kg/sec}$,

then, $M_{\text{H}_2\text{O}} = 0.833 > M_{\text{oil}} = 0.25 > M_{\text{air}} = 0.2 \text{ kg/sec}$.

Substituting $\rho_{\text{H}_2\text{O}} \cong 1000$, $\rho_{\text{oil}} \cong 800$, $\rho_{\text{air}} \cong 1.25 \text{ kg/m}^3$ into the foregoing relationship, the volumetric flow rates are calculated as:

$$G_{\text{H}_2\text{O}} \cong 0.00833 \text{ m}^3/\text{sec},$$

$$G_{\text{oil}} \cong 0.0003125 \text{ m}^3/\text{sec},$$

$$G_{\text{air}} \cong 0.16 \text{ m}^3/\text{sec}.$$

Similar analysis can also be performed for other values of heat flux . The findings suggest that

$$M_{\text{H}_2\text{O}} > M_{\text{oil}} > M_{\text{air}}, \text{ or}$$

$$G_{\text{oil}} < G_{\text{H}_2\text{O}} < G_{\text{air}}, \text{ or}$$

$$u_{\text{oil}} < u_{\text{H}_2\text{O}} < u_{\text{air}}$$

for a given uniform heat flux condition.

Considering a fully developed laminar flow field in a long channel, the fluid friction coefficient is derived by Ortega and Moffat [56] as

$$C_f = 24 / \text{Re}_D$$

where Re_D denotes for Reynolds number based on the hydrodynamic diameter of the channel. For a long channel with protruding discrete heating and fully developed flow region, a similar expression may be in the form of

$$C_f = C / \text{Re}_D$$

where C is an arbitrary constant. Noting that $\mu_{\text{oil}} > \mu_{\text{H}_2\text{O}} > \mu_{\text{air}}$ and $G_{\text{air}} > G_{\text{H}_2\text{O}} > G_{\text{oil}}$, thus, the inequality relation of the fluid friction coefficient can be written as $C_{f,\text{oil}} > C_{f,\text{H}_2\text{O}} > C_{f,\text{air}}$.

5.7 Empirical Equation

As derived in Chapter 3, the independent dimensionless parameters are the Rayleigh number and the geometric ratio. The dependent dimensionless parameter, Nusselt number, was calculated in the following relations to fit the heat transfer data by use of a least-squares method of curve fitting:

$$\text{Nu}_x = C_1 \text{Ra}_x^{C_2} \quad (5.1)$$

$$\text{Nu}_x = C_1 \text{Ra}_x^* C_2 \quad (5.2)$$

$$\text{Nu}_B = C_1 \text{Ra}_B^* C_2 \quad (5.3)$$

$$Nu_b = C_1 (b/H Ra_b^*) C_2 \quad (5.4)$$

$$Nu_b = C_1 (Ra_b^*) C_2 (b/H) C_3 \quad (5.5)$$

Equation (5.1) is used to correlate heat transfer data for the vertical plate case only. Equations (5.4) and (5.5) are employed to correlate heat transfer data for the vertical channel case only. Equations (5.2) and (5.3) are used for vertical plate and channel cases. Note that x in Equations (5.1) and (5.2) represent the center positions for protruding heated elements. The ranges of correlating parameters appear in Table 5.1. Tables 5.2, 5.3 and 5.4 list the calculated constants, average deviation, maximum deviation, and % of the data within % of the equation for various correlations and geometric arrangements. These were evaluated by a correlation program listed in Appendix I.

The best fit equations for the vertical plate case with various fluids are:

$$Nu_B = 1.6884 (Ra_B^*)^{0.1223} \quad \text{for } Pr \cong 0.72$$

$$Nu_x = 1.6884 (Ra_x^*)^{0.1279} \quad \text{for } 5 < Pr < 8.7$$

$$Nu_B = 0.0783 (Ra_B^*)^{0.3035} \quad \text{for } 518 < Pr < 974$$

with 6%, 12.5% and 6% average deviations and 15%, 42% and 17% maximum deviations, respectively.

The best correlation for all fluids combined is

$$Nu_B = 7.5021 (Ra_B^*)^{-0.1930} \quad \text{for } 0.72 < Pr < 974$$

with a 18% average deviation and 80% of the data within 25% of equation.

The correlations using a single parameter for various channels with different fluids are

$$Nu_b = 1.0194 (b/H Ra_b^*)^{0.2033} \quad \text{for } Pr \cong 0.72$$

with a 10% average deviation and a 32% maximum deviation.

$$Nu_b = 0.2852 (b/H Ra_b^*)^{0.2088} \quad \text{for } 5 < Pr < 8.7$$

Table 5.1 Range of Correlating Parameter

Correlating Parameter	Minimum	Maximum
Nux	1.7	81.23
Nub	1.37	60.01
Rax	5800	3.8 E+09
Rax*	6000	1.5 E+11
Rab*	3.8 E+05	1.2 E+11
RaB*	1.6 E+05	3.8 E+08
b/H	0.104	0.567
x	0.79 cm (5/16")	18.26 cm (7 3/16")

Table 5.2 Correlation for Vertical Plate Case

Equation Form	b/H	Empirical Constants		AD %	MD %	% of Data within % of Equation	
		C1	C2				
Air							
5.1	Infinite	0.4490	0.3021	7.6	17.25	100	20
5.2		0.1871	0.3079	8.96	19.95	100	20
5.3		1.6884	0.1223	5.99	14.66	100	15
Distilled Water							
5.1	Infinite	0.1446	0.2799	12.49	41.74	82	20
5.2		0.0579	0.2847	14.57	47.11	86	25
5.3		10.5988	-0.0398	17.39	111.81	74	25
Chevron 68 Machine Oil							
5.1	Infinite	0.1317	0.3109	8.22	33.34	93	20
5.2		0.0630	0.3102	2.58	73.49	100	10
5.3		0.0783	0.3035	6.17	16.69	100	20
All Fluids Combined							
5.1	Infinite	0.7952	0.2105	51.71	231.19	57	50
5.2		0.5085	0.2105	54.58	272.7	83	50
5.3		7.5021	-0.1930	17.94	128.09	80	25

Table 5.3 Correlation for Vertical Channel Case

Equation Form	b/H	Empirical Constants			AD %	MD %	% of Data within % of Equation	
		C1	C2	C3				
Air								
5.4	0.567	2.2303	0.1605		6.54	14.99	100	15
	0.358	2.4174	0.1499		6.87	15.37	100	20
	0.167	1.7985	0.1590		10.37	21.92	100	25
	0.104	0.6319	0.2496		15.93	36.02	85	25
	All	1.0194	0.2033		9.78	31.73	95	25
5.5	All	1.1941	0.1791	0.3060	9.71	34.73	94	25
Distilled Water								
5.4	0.567	0.4814	0.1880		11.42	47.52	87	25
	0.358	0.0460	0.2932		15.13	55.93	77	25
	0.167	0.9858	0.1448		15.31	58.66	77	25
	0.104	0.0495	0.3322		18.88	70.87	73	25
	All	0.2852	0.2088		18.85	134.9	76	25
5.5	All	0.0465	0.2829	-0.1610	16.93	103.0	77	20
Chevron 68 Machine Oil								
5.4	0.567	0.0484	0.3146		7.14	15.52	100	20
	0.358	0.0446	0.3330		8.25	28.54	98	25
	0.167	0.1005	0.3130		10.35	42.89	96	25
	0.104	0.0631	0.3706		14.28	41.19	83	25
	All	0.4283	0.2122		16.45	78.14	80	25
5.5	All	0.0281	0.3337	-0.3325	10.24	52.13	93	25
All Fluids Combined								
5.4	All	1.3181	0.1490		43.28	442.5	84	50
5.5	All	4.9884	0.1480	0.7657	27.77	352.8	62	25

Table 5.4 Correlation for Protruding Array Plate with Shrouding

Equation Form	b/H	Empirical Constants		AD %	MD %	% of Data within % of Equation	
		C1	C2	C3			
Air							
5.2	Infinite	0.1871	0.3079	8.96	19.95	100	20
	0.567	0.1719	0.3081	6.26	16.02	100	20
	0.358	0.1795	0.3055	7.59	21.8	100	20
	0.167	0.2279	0.2924	7.78	20.65	100	20
	0.104	0.2990	0.2715	5.15	13.5	100	15
	All	0.2048	0.2982	8.3	26.41	99	25
Distilled Water							
5.2	Infinite	0.0579	0.2847	14.57	47.11	86	25
	0.567	0.0394	0.3003	12.97	38.83	87	25
	0.358	0.0362	0.3004	13.73	39.95	84	25
	0.167	0.0514	0.2934	19.12	43.99	76	25
	0.104	0.0379	0.3008	16	67.68	89	25
	All	0.0423	0.2969	15.68	76.91	80	25
Chevron 68 Machine Oil							
5.2	Infinite	0.0630	0.3102	2.58	73.49	100	10
	0.567	0.0647	0.3080	2.69	12.36	100	15
	0.358	0.0628	0.3095	5.05	27.24	98	25
	0.167	0.0801	0.2971	4.97	32.05	97	25
	0.104	0.0877	0.2915	9.77	43.76	89	25
	All	0.0714	0.3029	5.45	46.44	97	25
All Fluids Combined							
5.2	All	0.4492	0.2081	54.65	575.6	71	50

with a 19% average deviation and 76% of the data within 25% of the equation.

$$\text{Nu}_b = 0.3917(b/H \text{ Ra}_b^*)^{0.3337} \quad \text{for } 614 < \text{Pr} < 1,009$$

with a 16.5% average deviation and a 80% of the data within 25% of the equation.

The equations using two correlation parameters for the vertical channels with various channel spacings are

$$\text{Nu}_b = 1.1941(b/H)^{0.306}(\text{Ra}_b^*)^{0.1791} \quad \text{for } \text{Pr} \cong 0.72$$

with a 10% average deviation and a 34% maximum deviation.

$$\text{Nu}_b = 0.0465(b/H)^{-0.161}(\text{Ra}_b^*)^{0.2033} \quad \text{for } 5 < \text{Pr} < 8.7$$

with a 17% average deviation and 77% of data within 25% of equation.

$$\text{Nu}_b = 0.04936(b/H)^{-0.3325}(\text{Ra}_b^*)^{0.3337} \quad \text{for } 518 < \text{Pr} < 1,009$$

with a 10% average deviation and 93% of data within 25% of equation.

For all fluids combined, the correlation equation using a single correlation parameter for the vertical channels is

$$\text{Nu}_b = 1.3181(b/H \text{ Ra}_b^*)^{0.149} \quad \text{for } 0.72 < \text{Pr} < 1,009$$

with a 43% average deviation and having 84% of the data within 25% of the equation.

The empirical equation using two correlation parameters for the channels is

$$\text{Nu}_b = 4.9884(b/H)^{0.7657}(\text{Ra}_b^*)^{0.148} \quad \text{for } 0.72 < \text{Pr} < 1,009$$

with a 28% average deviation and having 62% of the data within 25% of the equation.

For $b/H = 0.104$ to ∞ , the equations using a single correlation parameter are

$$\text{Nu}_x = 0.2048(\text{Ra}_x^*)^{0.2982} \quad \text{for } \text{Pr} \cong 0.72$$

with an 8% average deviation, a 26.41% maximum deviation, and having 99% of the data within 25% of the equation.

$$\text{Nu}_x = 0.0423(\text{Ra}_x^*)^{0.2969} \quad \text{for } 5 < \text{Pr} < 8.7$$

with a 16% average deviation and 80% of the data within 25% of the equation.

$$\text{Nu}_x = 0.0714(\text{Ra}_x^*)^{0.3029} \quad \text{for } 518 < \text{Pr} < 1,009$$

with 5.5% average deviation and 97% of the data within 25% of the equation. For all fluids combined and $b/H = 0.104$ to ∞ , the single parameter equation is

$$\text{Nu}_x = 0.4492(\text{Ra}_x^*)^{0.2081}$$

with a 55% average deviation and 71% of the data within 25% of the equation.

By perusing Tables 5.2 to 5.4, the correlation constant, C_2 , for the dimensionless parameter of Ra is not the familiar 1/5th power for correlating reduced heat transfer data. This is not surprising, since the heated boundary wall consists of six protruding discrete heated surfaces in lieu of a continuous heating surface. Nevertheless, the constant C_2 is 0.2081 for the last empirical equation with overall data combined and is close to the 1/5th power.

For the protruding array plate case without a shrouding wall, Figures 5.11 to 16 show how the empirical correlations fit the experimental data. For the shrouded case, the empirical correlations were developed and plotted as shown in Figures 5.17 to 5.19 for the three different fluids.

CHAPTER 6

CONCLUSIONS AND RECOMMENDATIONS

6.1 Conclusions

This investigation has presented the results of an experimental study of natural convection heat transfer from an array of protruding heat sources on a vertical plate with and without a shrouding wall. The boundary conditions were all uniform with equal heat flux for the six protruding elements. The three different fluid baths, namely, are air, distilled water, and Chevron multi-machine oil 68 were employed to determine the effects of fluid properties on heat transfer. The dimensionless parameters were achieved in the following ranges:

$$\begin{aligned} 0.72 < Pr &< 1,009 \\ 1.6 \times 10^5 < Ra_B^* &< 3.8 \times 10^8 \\ 6.0 \times 10^3 < Ra_x^* &< 1.5 \times 10^{11} \\ 0.104 < b/H &< \infty \end{aligned}$$

A number of major conclusions from the study can be drawn in brief fashion:

1. Temperature difference (ΔT) between the heated surface and cold chamber temperature increases linearly as the heat flux (Q) is increased to each protruding element for air, water, and oil. The only exception was that ΔT increased in a nonlinear trend at the lower range of Q for oil case.
2. The slope (m) of the line of a Q versus ΔT plot increases with the increase in fluid thermal conductivity (k_f), or thermal diffusivity (α_f), or with the decrease in fluid thermal expansion, (β_f); i.e.,

$$M_{H_2O} > M_{oil} > M_{air} \text{ or } G_{air} > G_{H_2O} > G_{oil}$$

because

$$k_{\text{H}_2\text{O}} > k_{\text{oil}} > k_{\text{air}}, \beta_{\text{H}_2\text{O}} < \beta_{\text{oil}} < \beta_{\text{air}}, \text{ and}$$

$$C_{p\text{H}_2\text{O}} > C_{p\text{oil}} > C_{p\text{air}}.$$

3. The slopes (m) of the lines of the Q versus ΔT plots for three types of fluids used are

$$\pi/2 < m_{\text{H}_2\text{O}} < \pi/4, m_{\text{oil}} \cong \pi/4, \text{ and } \pi/4 < m_{\text{air}} < 0.$$

These depict that $\Delta T_{\text{air}} > \Delta T_{\text{oil}} > \Delta T_{\text{H}_2\text{O}}$ for a given Q. In other words, the protruding surface temperature is the lowest in water bath, the second lowest in oil, and the highest in the ambient air for a given discrete uniform heating.

4. The 1st row protruding array exhibits the lowest surface temperature and the best cooling effect due to its location at the plate leading edge. Generally, the 5th and 6th row protruding arrays have relatively higher surface temperatures than other element because of the boundary layer thickening and preheating effect from the rising warm fluids.
5. The heat transfer coefficient decreases rapidly as the buoyancy-driven flow passes over the first three rows of the elements. As the rising warm flow further advances downstream, the heat transfer coefficient increases gradually from the third row to the fourth row, then decreases from the fourth to the last row. This typical variation in heat transfer coefficient for the discrete heated surfaces is valid for all fluids.
6. A fully developed temperature profile seemed to be present for the 4th and 5th row near the trailing edge in the vertical channels with $b/H = 0.104$ and 0.167 .
7. Maximum heat transfer coefficient or minimum protruding array surface temperature is attainable in the vertical channel with $b/H = 0.104$.
8. For a given modified Rayleigh number, the Nusselt number of oil is

highest with comparison to the Nusselt numbers of air and water. At a fixed Ra_x^* the inequality relation of $Nu_{x,oil} > Nu_{x,air} > Nu_{x,H_2O}$ was prevalent for all data.

9. The present natural convection processes are in the laminar flow regime even with protruding array heating. Three distinct flow regions were observed in the channels:

- (i) a relatively high velocity of rising upward boundary layer flow which follows the heated surfaces.
- (ii) a relatively slow reversed flow was drawn into the channel top.
- (iii) a stagnation or very weak flow region was located adjacent to the unheated wall in the lower portion of the channel.

Flow reversal phenomenon was not present for $b/H = 0.167$ and 0.104 due to the increased heat transfer between the opposing wall and the discrete heated surfaces. A flow circulation cell was observed in the channel central region for water as the working fluid.

10. The best correlation for the vertical plate with all fluids combined is

$$Nu_B = 7.5021 (Ra_B^*)^{-0.1930} \quad \text{for } 0.72 < Pr < 974$$

with a 18% average deviation.

The best empirical equation for the vertical channels with all fluids combined is

$$Nu_B = 4.9884 (b/H)^{0.7657} (Ra_B^*)^{0.1480} \quad \text{for } 0.72 < Pr < 1,009$$

with a 28% average deviation.

6.2 Recommendations

Future work which would extend the results reported here without major modification of the test apparatus are recommended as follows:

1. Vary the channel spacing-to-height ratio (b/H) less than 0.104 to determine a possible optimum channel spacing in conjunction with present data.
2. Employ a clear viscous fluid, for example, glycerin for flow visualization to detect flow pattern modification with Prandtl number ($\sim 10^4$) effects. Enhance light intensity to allow flow observation between each pair of protruding elements.
3. Vary the position of the plate such that the stagnation point at the leading edge will not coincide with the stagnation point of the first row element. This may alter the onset of thermal and hydrodynamic boundary layers thereby resulting in possibly another set of flow patterns.
4. Vary the protruding array height-to-width ratio (s/B) other than 1.
5. Determine the effect of cooling water temperature variation on the natural convection processes from the array of protruding heated elements.
6. Perform flow velocity measurements near the channel inlet. These would facilitate the development of analytical or numerical solutions.

BIBLIOGRAPHY

1. Bejan, Adrian, "Convection Heat Transfer," John Wiley & Sons, Inc., New York, 1984.
2. Arpaci, Vedat S. and Poul S. Larsen, "Convection Heat Transfer," Prentice-Hall, Inc., New Jersey, 1984.
3. Jaluria, Y, "Natural Convection," Pergamon Press Inc. New York, 1980.
4. Kakac, S. R. K. Shah, and W. Aung, (Editors) "Handbooks of Single Phase Convective Heat Transfer," John Wiley & Sons, Inc., New York, June 1987.
5. Gebhart, B., Y. Jaluria, R.L. Mahajan, and B. Sammakia, "Buoyancy-Induced Flows and Transport," Hemisphere Publishing Corporation, New York, 1988.
6. Sparrow, E. M. and J. L. Gregg, "Similar Solutions for Free Convection From a Nonisothermal Vertical Plate," Transactions of the ASME, Journal of Heat Transfer, Vol. 80, pp. 379-386, 1958.
7. Yang, Kwang-Tzu, "Possible Similarity Solutions for Laminar Free Convection on Vertical Plates and Cylinders," Transactions of the ASME, Journal of Applied Mechanics, Vol. 27, pp. 230-236, June 1960.
8. Minkowycz, W.J. and E.M. Sparrow, "Local Nonsimilarity Solutions for Natural Convection on a Vertical Cylinder," Transactions of the ASME, Journal of Heat Transfer, pp. 178-183, May 1974.
9. Kays, William M. and Michael E. Crawford, "Convection Heat and Mass Transfer," 2nd Edition, McGraw-Hill, Inc., New York, 1980.
10. White, Frank M., "Viscous Fluid Flow," McGraw-Hill, Inc., New York, 1974.
11. Dresner, Lawrence, "Similarity Solutions of Nonlinear Partial Differential Equations," Pitman Advanced Publishing Program, Massachusetts, 1983.

12. Ostrach, S., "An Analysis of Laminar Free-Convection Flow and Heat Transfer about a Flat Plate Parallel to the Direction of the Generating Body Force," NACA Technical Note 2635, 1952.
13. Sparrow, E. M., "Laminar Free Convection on a Vertical Plate Prescribed Nonuniform Wall Heat Flux or Prescribed Nonuniform Wall Temperature," NACA Technical Note 3508, July 1955.
14. Sparrow, E. M. and J. L. Gregg, "Laminar Free Convection from a Vertical Plate With Uniform Surface Heat Flux," Transactions of the ASME, Journal of Heat Transfer, Vol. 78, pp. 435-440, February, 1956.
15. Sparrow, E. M. and J. L. Gregg, "The Variable Fluid-Property Problem in Free Convection," Transactions of the ASME, Vol. 80, pp. 879-886, May, 1958.
16. Yang, Kwang-Tzu and Edward W. Jerger, "First-Order Perturbation of Laminar Free Convection Boundary Layers on a Vertical Plate," Transactions of the ASME, Journal of Heat Transfer, Vol. 86, pp. 107-115, February 1964.
17. Sparrow, E. M. and R. B. Husar, "Free Convection from a Plane Vertical Surface With a Non-Horizontal Leading Edge," International Journal of Heat and Mass Transfer, Vol. 12, pp. 365-369, 1969.
18. Hwang, U.P., "Effect of Flow Direction on Mixed Convection Heat Transfer from a Vertical Flat Plate and a Plate with Square Protuberances," Letters in Heat and Mass Transfer, Vol. 6, pp. 459-468, 1979.
19. Jaluria, Y., "Buoyancy-Induced Flow due to Isolated Thermal Sources on a Vertical Surface," Transactions of the ASME, Journal of Heat Transfer, Vol. 104, pp. 223-227, May 1982.
20. Jaluria, Y., "Natural Convection Flow due to Line Thermal Sources on a Vertical Adiabatic Surface" Proceedings of the 7th International Heat Transfer Conference, Munchen, Germany, Vol. 2, pp. 147-152, 1982.
21. Jaluria, Y., "Interaction of Natural Convection Wakes Arising from Thermal Sources on a Vertical Surface," Transactions of the ASME, Journal of Heat Transfer, Vol. 107, pp. 883-892, November 1985.

22. Roache, Patrick J., "Computational Fluid Dynamics," Revised Printing, Hermosa Publishers, New Mexico, 1982.
23. Kishinami, K. and N. Sekei, "Natural Convective Heat Transfer on an Unheated Vertical Plate Attached to an Upstream Isothermal Plate," Transactions of the ASME, Journal of Heat Transfer, Vol. 105, pp. 759-766, November 1983.
24. Elenbaas, W., "Heat Dissipation of Parallel Plates by Free Convection," Physica IX, no. 1, pp. 1-28, January 1942.
25. Ostrach, Simon, "Combined Natural- and Forced-Convection Laminar Flow Heat Transfer of Fluids with and without Heat Sources in Channels with Linearly Varying Wall Temperatures," NACA TN 3141, April 1954.
26. Ostrach, Simon, "Unstable Convection in Vertical Channels with Heating from Below, Including Effects of Heat Sources and Frictional Heating," Technical Note 3458, July 1955.
27. Ostrach, Simon, "Laminar Natural Convection Flow and Heat Transfer of Fluids with and without Heat Sources in Channels with Constant Wall Temperatures," NACA TN 2863, 1952.
28. Tao, L. N., "On Combined Free and Forced Convection in Channels," Transactions of the ASME, Journal of Heat Transfer, Vol. 82, pp. 233-238, August 1960.
29. Bodoia, J. R. and J. F. Osterle, "The Development of Free Convection between Heated Vertical Plates," Transactions of the ASME, Journal of Heat Transfer, Vol. 84, February 1962.
30. Agrawal, H. C., "A Variational Method for Combined Free and Forced Convection in Channels," International Journal of Heat and Mass Transfer, Vol. 5, pp. 439-444, 1962.
31. Aung, W., "Fully Developed Laminar Free Convection between Vertical Plates Heated Asymmetrically," International Journal of Heat and Mass Transfer, Vol. 15, pp. 1577-1580, 1972.

32. Aung, W., L. S. Fletcher, and V. Sernas, "Developing Laminar Free Convection between Vertical Flat Plates with Asymmetric Heating," *International Journal of Heat and Mass Transfer*, Vol. 15, pp. 2293-2308, 1972.
33. Aung, W., T. J. Kessler, and K. I. Beitin, "Free Convection Cooling of Electronic Systems," *IEEE Transactions on Parts, Hybrids, and Packaging*, Vol. PHP-9, No. 2, June 1973.
34. Aung, W. and B. Chimah, "Laminar Heat Exchange in Vertical Channels-Application to Cooling of Electronic Systems," from "Low Reynolds Number Flow Heat Exchangers," Hemisphere Publishing Corporation, Washington, D. C., pp. 395-413, 1983.
35. Aung, Win and Worku, G., "Developing Flow and Flow Reversal in a Vertical Channel with Asymmetric Wall Temperatures," *Transactions of the ASME, Journal of Heat Transfer*, Vol. 108, pp. 299-304, May 1986.
36. Miyatake, O. and T. Fujii, "Free Convective Heat Transfer between Vertical Parallel Plates - One Plate Isothermally Heated and the Other Thermally Insulated," *Heat Transfer - Japanese Research*, Vol. 1, No. 3, pp. 30-38, July 1972.
37. Miyatake, O., T. Fujii, and H. Tanaka, "Natural Convective Heat Transfer between Vertical Parallel Plates - One Plate with a Uniform Heat Flux and the Other Thermally Insulated," *Heat Transfer - Japanese Research*, Vol. 2, No. 1, pp. 25-32, January 1973.
38. Miyatake, O. and T. Fujii, "Natural Convection Heat Transfer between Vertical Parallel Plates at Unequal Uniform Temperatures," *Heat Transfer - Japanese Research*, Vol. 2, No. 4, pp. 79-88, October 1973.
39. Miyatake, O. and T. Fujii, "Natural Convection Heat Transfer between Vertical Parallel Plates with Unequal Heat Fluxes," *Heat Transfer - Japanese Research*, Vol. 3, No. 3, pp. 29-33, July 1974.
40. Siegel, R. and R. H. Norris, "Tests of Free Convection in a Partially Enclosed Space between Two Heated Vertical Plates," *Transactions of the ASME*, Vol. 79, pp. 663-673, April 1957.
41. Sparrow, E. M. and P. A. Bahrami, "Experiments on Natural Convection from Vertical Parallel Plates with Either Open or Closed Edges," *Journal of Heat Transfer*, Vol. 102, pp. 221-227, May 1980.

42. Sparrow E. M., S. Shah, and C. Prakash, "Natural Convection in a Vertical Channel: I. Interacting Convection and Radiation. II. The Vertical Plate with and without Shrouding," Numerical Heat Transfer, Vol. 3, pp. 297-314, 1980.
43. Patankar, Suhas V., "Numerical Heat Transfer and Fluid Flow," Hemisphere Publishing Corporation, Washington, D. C., 1980.
44. Sparrow E. M. and C. Prakash, "Enhancement of Natural Convection Heat Transfer by a Staggered Array of Discrete Vertical Plates," Transactions of the ASME, Journal of Heat Transfer, Vol. 102, pp. 215-220, May 1980.
45. Prakash C. and E. M. Sparrow, "Natural Convection Heat Transfer Performance Evaluations for Discrete- (In-Line or Staggered) and Continuous-Plate Arrays," Numerical Heat Transfer, Vol. 3, pp. 89-105, 1980.
46. Sobel, N., F. Landis, and W. K. Mueller, "Natural Convection Heat Transfer in Short Vertical Channels including the Effects of Stagger," Proceedings of the Third International Heat Transfer Conference, Vol. II, pp. 121-125, 1966.
47. Lauber, T. S. and A. U. Welch, "Natural Convection Heat Transfer between Vertical Flat Plates with Uniform Heat Flux," Proceedings of the Third International Heat Transfer Conference, Vol. II, pp. 126-131, 1966.
48. Levy, E. K., "Optimum Plate Spacing for Laminar Natural Convection Heat Transfer from Parallel Vertical Isothermal Flat Plates," Transactions of the ASME, Journal of Heat Transfer, Vol. 93, pp. 463-465, November 1971.
49. Wirtz, R. A. and Stutzman, R. J., "Experiments on Free Convection between Vertical Plates with Symmetric Heating," Transactions of the ASME, Journal of Heat Transfer, Vol. 104, pp. 501-507, August 1982.
50. Lehmann, G. L. and R. A. Wirtz, "Convection From Surface Mounted Repeating Ribs in a Channel Flow," The ASME, 84-WA/HT-88, 1984.
51. Burch, T., T. Rhodes and S. Acharya, "Laminar Natural Convection between Finitely Conducting Vertical Plates," International Journal of Heat and Mass Transfer, Vol. 28, No. 6, pp. 1173-1186, 1985.

52. Azevedo, L. F. A. and E. M. Sparrow, "Natural Convection in Open-Ended Inclined Channels," Transactions of the ASME, Journal of Heat Transfer, Vol. 107, pp. 893-901, November 1985.
53. Chu, H. H.-S., S. W. Churchill, and C. V. S. Patterson, "The Effect of Heater Size, Location, Aspect Ratio, and Boundary Conditions on Two-Dimensional, Laminar, Natural Convection in Rectangular Channels," Transactions of the ASME, Journal of Heat Transfer, Vol. 98, No. 2, pp. 194-201, May 1976.
54. Turner, B. L. and R. D. Flack, "The Experimental Measurement of Natural Convective Heat Transfer in Rectangular Enclosures with Concentrated Energy Sources," Transactions of the ASME, Journal of Heat Transfer, Vol. 102, No. 2, pp. 236-241, May 1980.
55. Flack, R. D. and B. L. Turner, "Heat Transfer Correlations for Use in Naturally Cooled Enclosures with High-Power Integrated Circuits," IEEE Transactions on Components, Hybrids, and Manufacturing Technology, Vol. CHMT-3, No. 3, pp.449-452, September 1980.
56. Ortega, A. and R.J. Moffat, "Heat Transfer from an Array of Simulated Electronic Components: Experimental Results for Free Convection with and without a Shrouding Wall," Heat Transfer in Electronic Equipment, ASME HTD-Vol. 48, pp. 5-15, August 4-7, 1985.
57. Churchill, S. W. and H. H. S. Chu, "Correlating Equations for Laminar and Turbulent Free Convection from a Vertical Plate," International Journal of Heat and Mass Transfer, Vol. 18, pp. 1323-1329, 1975.
58. Yan, W. M. and T. F. Lin, "Natural Convection Heat Transfer in Vertical Open Channel Flows with Discrete Heating," International Communications in Heat and Mass Transfer, Vol. 14, pp.187-200, 1987.
59. "Heat Transfer in Miniaturized Electronic Equipment," Bureau of Ship, Navy Department, Washington, D. C., NAVSHIPS 900,189, February 1955.
60. Antonetti, V. W. and R. E. Simons, "Bibliography of Heat Transfer in Electronic Equipment," IEEE Transactions on Components, Hybrids, and Manufacturing Technology, Vol. CHMT-8, No. 2, pp. 289-295, June 1985.

61. Seely, J. H. and R. C. Chu, "Heat Transfer in Microelectronic Equipment," Marcel Dekker, Inc., New York, 1972.
62. Steinberg, Dave S., "Cooling Techniques for Electronic Equipment," John Wiley & Sons, New York, 1980.
63. Kraus, Allan D. and A. Bar-Cohen, "Thermal Analysis and Control of Electronic Equipment," Hemisphere Publishing Corporation, Washington, D. C. 1983.
64. Ellison, Gordon, "Thermal Computations for Electronic Equipment," Van Nostrand Reinhold Company, 1984.
65. "Heat Transfer in Electronic Equipment," ASME HTD-Vol. 20, Edited by Kelleher, M. D. and M. M. Yovanovich, 1981.
66. "Heat Transfer in Electronic Equipmen," ASME WAM, Edited by Oktay, S. and A. Bar-Cohen, 1983.
67. "Fundamentals of Natural Convection/Electronic Equipment Cooling," ASME HTD-Vol. 32, Edited by Witte, L. C. and L. S. Saxena, 1984.
68. "Heat Transfer in Electronic Equipment," ASME HTD-Vol. 48, Edited by Oktay, S. and R. J. Moffat, 1985.
69. "Heat Transfer in Electronic Equipment," ASME HTD-Vol. 57, Edited by Bar-Cohen, A., 1986.
70. "Temperature/Fluid Measurements in Electronic Equipment," ASME HTD-Vol. 89, Edited by Bartoszek, J., S. Furkay, S. Oktay, and R. Simons, 1987.
71. "LSI Package and Module Thermal Control," Session 3, 2nd Annual International Electronics Packaging Conference, San Diego, CA, November 15-17, 1982.
72. Merzkirch, Wolfgang, "Flow Visualization," Academic Press, Inc., New York, pp. 5-52, 1974.
73. Simpson, John E., "Effects of the Lower Boundary on the Field of a Gravity Current," Journal of Fluid Mechanics, Vol. 53, Part 4, pp. 759-768, 1972.

74. Liley, P. E., "Thermophysical Properties" appeared in the Chapter 22 of "Handbook of Single Phase Convective Heat Transfer," Editors Kakac, S., R. K. Shah, and W. Aung, John Wiley & Sons, Inc, New York, 1987.
75. "Chevron Multi-Machine Oil 68" 70.22A, PD5-10-14, August 1987 and Personal Communication with Croley, C. E. (Technical Answerman), April 1988.
76. Vliet, G. C. and C. K. Liu, "An Experimental Study of Turbulent Natural Convection Boundary Layers," Transactions of the ASME, Journal of Heat Transfer, Vol. 91, pp. 517-531, 1969.
77. Dotson, J. P., "Heat Transfer for a Vertical Plate by Free Convection," M.S. Thesis, Purdue University, 1954.
78. Fujii, T. and M. Fujii, "The Dependence of Local Nusselt Number on Prandtl Number in the Case of Free Convection Along a Vertical Surface with Uniform Heat Flux," International Journal of Heat and Mass Transfer, Vol.19, pp.121-122, 1976.
79. Kraus, Allan D., Richard C. Chu, and Avram Bar-Cohen, "Thermal Management of Microelectronics: Past, Present, and Future," Computers in Mechanical Engineering, pp. 69-79, October 1982.
80. Oktay, Sevgin, Robert Hannemann, and Avram Bar-Cohen, "High Heat from a Small Package," Mechanical Engineering, pp. 36-42, March 1986.
81. Simons, R. E., "Thermal Management of Electronic Packages," Solid State Technology, pp. 131-137, October 1983.
82. Aung, Win and G. Worku, "Theory of Fully Developed, Combined Convection Including Flow Reversal," Transactions of the ASME, Journal of Heat Transfer, Vol. 108, pp. 485-488, May 1986.
83. Eckert, E. R. G. and T. W. Jackson, "Analysis of Turbulent Free Convection Boundary Layer on Flat Plate," NACA TR 10105, pp. 255-261, 1950.
84. Bayley, F. J., "An Analysis of Turbulent Free-Convection Heat Transfer," Proceedings of the Institution of Mechanical Engineers, Vol. 149, No. 20, pp. 361-368, 1955.

85. Bar-Cohen, A. and W. M. Rohsenow, "Thermally Optimum Spacing of Vertical, Natural Convection Cooled, Parallel Plates," Heat Transfer in Electronic Equipment, ASME, WAM, pp. 11-18, 1981.
86. Cebeci, T., A. A. Khattab, and R. LaMont, "Combined Natural and Forced Convection in Vertical Ducts," Proceedings of the 7th International Heat Transfer Conference, Munchen, Germany, Vol. 3, pp. 419-424, 1982.
87. Yao, L. S., "Free and Forced Convection in the Entry Region of a Heated Vertical Channel," International Journal of Heat and Mass Transfer, Vol. 26, No. 1, pp. 65-72, 1983.
88. Sparrow, E. M., G. M. Chrysler, and L. F. Azevedo, "Observed Flow Reversals and Measured Predicted Nusselt Numbers for Natural Convection in a One-Sided Heated Vertical Channel," Transactions of the ASME, Journal of Heat Transfer, Vol. 106, pp. 325-332, May 1984.
89. Shah, Ramesh K., "Research Needs in Low Reynolds Number Flow Heat Exchangers," Hemisphere Publishing Corporation, Washington, D. C., pp. 983-999, 1983.
90. Larson, B. Milton and Luc Fries, "Natural Convection to Water from Arrays of Short Wall-Attached Cylinders," Experimental Thermal and Fluid Science, 1: 253-258, 1988
91. Warrington, R. O. and R. A. Weaver, "Natural Convection Heat Transfer between Arrays of Horizontal Cylinders and Their Enclosure," ASME, WAM, HTD-Vol. 39, pp. 99-102, 1984.
92. Mussulman, R. L., R. O. Warrington, and P. C. Lin, "Heat Transfer and Thermal Performance in Passive Solar System," D.O.E. Conference 830702-Exc., Chapter II, 1983.

APPENDICES

APPENDIX A

TEMPERATURE DATA ACQUISITION PROGRAM

```

200 ' PCLAB BASIC definition file (short names)
202 ' This file may be MERGED with a user program to define
204 ' routine offsets and establish the PCLAB segment.
206 '
208 XAV=3      : XAOT=6      : XSA=9      : XAS=12     : XBAD=15   : XTAD=18
210 XWAD=21   : XDV=24     : XDOT=27    : XSD=30     : XDS=33    : XBDD=36
212 XTDD=39   : XWDD=42    : XSCD=45    : XSSC=48    : XSCF=51   : XSCP=54
214 XEFI=57   : XEFO=60    : XIDV=63    : XODV=66    : XIDOT=69  : XODOT=72
216 XSECW=75  : XGEC=78    : XSB=81     : XSBA=84    : XSDC=87   : XSAR=90
218 XSAC=93   : XSDR=96    : XSLF=99    : XSTG=102   : XST=105   : XGDE=108
220 XRD=111   : XGDS=114   : XCWFC=117  : XCWFO=120  : XCWFI=123 : XSAD=126
222 XSDD=129  : XCAD=132   : XCDD=135   : XMV=138    : XMT=141   : XMC=144
224 XATV=147  : XUTD=150   : XDTV=153   : XDLY=156   : XSTB=159  : XWD=162
226 XGC=165   : XCEV=168   : XREV=171   : XGF=174    : XSC=177   : XINIT=180
228 XTERM=183 : XIXR=186   : XIXW=189   : XFDL=192   : XESC=195  : XDSC=198
230 '
232 DEF SEG=&H0 ' get the PCLAB segment
234 PCLSEG = PEEK ( &H4FE ) + 256*PEEK ( &H4FF )
236 DEF SEG=PCLSEG ' REM address the PCLAB segment
238 ERROR.VALUE% = 0
240 CALL XSECW(ERROR.VALUE%)
242 '
1000 GAIN% = 8
1010 TYPE% = 116
1020 CJCHAN% = 0
1030 OPTION BASE 1
1040 DIM TEMP(3,7)
1041 OPEN "TEMP.DAT" FOR APPEND AS #1
1050 '
1060 CLS
1070 ON TIMER(60) GOSUB 1120
1080 TIMER ON
1090 GOTO 1090
1100 '
1120 LOCATE 2,1
1130 '
1140 '
1150   FOR BOARD% = 1 TO 3
1160     CALL XSB(BOARD%)
1170     FOR CHAN% = 1 TO 7
1180       CJTOTAL = 0
1190       TOTAL = 0
1200       FOR I = 1 TO 16
1210         CALL XAV(CJCHAN%, GAIN%, CJADATA%)
1220         CJTOTAL = CJADATA% + CJTOTAL
1230         CALL XAV(CHAN%, GAIN%, ADATA%)
1240         TOTAL = ADATA% + TOTAL
1250       NEXT I
1260       CJADATA% = CINT(CJTOTAL / 16)
1270       ADATA% = CINT(TOTAL / 16)
1280       CJTEMP = (((CJADATA% * .04) / 4096) - .02) * 2000
1290       CALL XDTV(TYPE%, CJTEMP, CJVOLTS)
1300       VOLTS = (((ADATA% * .04) / 4096) - .02) + CJVOLTS
1310       CALL XUTD(TYPE%, VOLTS, TEMPS)
1320       TEMP(BOARD%,CHAN%) = TEMPS
1330     NEXT CHAN%
1340   NEXT BOARD%
1350   PRINT "TIME: ";TIME$ "      DATE: ";DATE$
1355 PRINT "      *** VERTICAL PLATE      WORKING FLUID: WATER ***"
1360 PRINT "I. HEAT SOURCE TEMPERATURE"
1370 PRINT "  ROW CENTER      RIGHT"

```

```

1380 PRINT " 6 ";
1390 PRINT USING "###.## ";TEMP(1,6);TEMP(2,6)
1400 PRINT " 5 ";
1410 PRINT USING "###.## ";TEMP(1,5);TEMP(2,5)
1420 PRINT " 4 ";
1430 PRINT USING "###.## ";TEMP(1,4);TEMP(2,4)
1440 PRINT " 3 ";
1450 PRINT USING "###.## ";TEMP(1,3);TEMP(2,3)
1460 PRINT " 2 ";
1470 PRINT USING "###.## ";TEMP(1,2);TEMP(2,2)
1480 PRINT " 1 ";
1490 PRINT USING "###.## ";TEMP(1,1);TEMP(2,1)
1500 PRINT
1501 PRINT " *** HOT WALL REAR FACE TEMPERATURE: ";
1502 PRINT USING "###.## ";TEMP(3,7)
1510 PRINT " *** SHROUDE TEMPERATURE: ";
1520 PRINT USING "###.## ";TEMP(1,7)
1521 PRINT " *** LID TEMPERATURE: ";
1522 PRINT USING "###.## ";TEMP(3,1)
1530 PRINT " CHANNEL INLET TEMPERATURE: ";
1540 PRINT USING "###.## ";TEMP(3,2)
1550 PRINT "CHANNEL OUTLET TEMPERATURE: ";
1560 PRINT USING "###.## ";TEMP(3,3)
1570 PRINT
1580 PRINT " COOLING WATER INLET TEMPERATURE: ";
1590 PRINT USING "###.## ";TEMP(3,4)
1600 PRINT "COOLING WATER OUTLET TEMPERATURE: ";
1610 PRINT USING "###.## ";TEMP(3,5)
1620 PRINT
1630 PRINT " AMBIENT TEMPERATURE      CHAMBER TEMPERATURE"
1640 PRINT USING "      ###.##      ";TEMP(3,6);TEMP(2,7)
1650 PRINT #1, "TIME: ";TIME$ " DATE: "DATE$
1655 PRINT #1, " *** VERTICAL PLATE      WORKING FLUID: WATER ***"
1660 PRINT #1, "I. HEAT SOURCE TEMPERATURE"
1670 PRINT #1, " ROW CENTER      RIGHT"
1680 PRINT #1, " 6 ";
1690 PRINT #1, USING "###.## ";TEMP(1,6);TEMP(2,6)
1700 PRINT #1, " 5 ";
1710 PRINT #1, USING "###.## ";TEMP(1,5);TEMP(2,5)
1720 PRINT #1, " 4 ";
1730 PRINT #1, USING "###.## ";TEMP(1,4);TEMP(2,4)
1740 PRINT #1, " 3 ";
1750 PRINT #1, USING "###.## ";TEMP(1,3);TEMP(2,3)
1760 PRINT #1, " 2 ";
1770 PRINT #1, USING "###.## ";TEMP(1,2);TEMP(2,2)
1780 PRINT #1, " 1 ";
1790 PRINT #1, USING "###.## ";TEMP(1,1);TEMP(2,1)
1800 PRINT #1,
1801 PRINT #1, " *** HOT WALL REAR FACE TEMPERATURE: ";
1802 PRINT #1, USING "###.## ";TEMP(3,7)
1810 PRINT #1, " *** SHROUDE TEMPERATURE: ";
1820 PRINT #1, USING "###.## ";TEMP(1,7)
1821 PRINT #1, " *** LID TEMPERATURE: ";
1822 PRINT #1, USING "###.## ";TEMP(3,1)
1830 PRINT #1, " CHANNEL INLET TEMPERATURE: ";
1840 PRINT #1, USING "###.## ";TEMP(3,2)
1850 PRINT #1, "CHANNEL OUTLET TEMPERATURE: ";
1860 PRINT #1, USING "###.## ";TEMP(3,3)
1870 PRINT #1,
1880 PRINT #1, " COOLING WATER INLET TEMPERATURE: ";
1890 PRINT #1, USING "###.## ";TEMP(3,4)
1900 PRINT #1, "COOLING WATER OUTLET TEMPERATURE: ";
1910 PRINT #1, USING "###.## ";TEMP(3,5)
1920 PRINT #1,
1930 PRINT #1, " AMBIENT TEMPERATURE      CHAMBER TEMPERATURE"
1940 PRINT #1, USING "      ###.##      ";TEMP(3,6);TEMP(2,7)
1950 RETURN
1970 STOP
1980 END

```

APPENDIX B

RADIATION CORRECTION

Radiation heat loss may be significant from a vertical plate and from the vertical channels when air is used as the working fluid in the present experiment. The magnitude of the radiation heat loss depends on the specific heated surface boundary conditions, channel spacing, and surface condition. In order to evaluate the heat transfer coefficient for natural convection in air, radiation heat loss must first be determined and then its contribution should be subtracted from the input of each protruding heat source.

A vertical channel with six protruding arrays as shown in Figure B.1, is established for the basis of the formulation of the radiation problem. b is a channel spacing, H is a channel height, s is the spacing between each pair of protruding arrays, and B is the side length of each protruding heat source. Numbers 1 to 6 represent the 1st to 6th row of protruding heated surfaces. Number 7 is for the shroud which is the surface opposite to the discrete surfaces. Numbers 8 and 9 indicate the channel outlet and inlet. Numbers 10 to 15 represent the adiabatic surfaces between protruding surfaces.

The configuration factors are formulated with the crossed string method of Hottel [B.1]. The resultant formulation of configuration factors between surfaces are written as:

$$F_{i7} = 0.5 \left\{ \left[\sqrt{[R_2 - 2(i-1)]^2 + R_1^2} + \sqrt{(2i-1)^2 + R_1^2} \right] - \left[\sqrt{2(i-1)^2 + R_1^2} + \sqrt{[R_2 - (2i-1)]^2 + R_1^2} \right] \right\} \quad (B.1)$$

$$F_{i8} = 0.5 \left\{ \left[(2i-1) + \sqrt{[R_2 - 2(i-1)]^2 + R_1^2} \right] - \left[2(i-1) + \sqrt{[R_2 - (2i-1)]^2 + R_1^2} \right] \right\} \quad (B.2)$$

$$F_{i9} = 0.5 \left\{ \left[(2i-1) + \sqrt{2(i-1)^2 + R_1^2} \right] - \left[2(i-1) + \sqrt{(2i-1)^2 + R_1^2} \right] \right\} \quad (B.3)$$

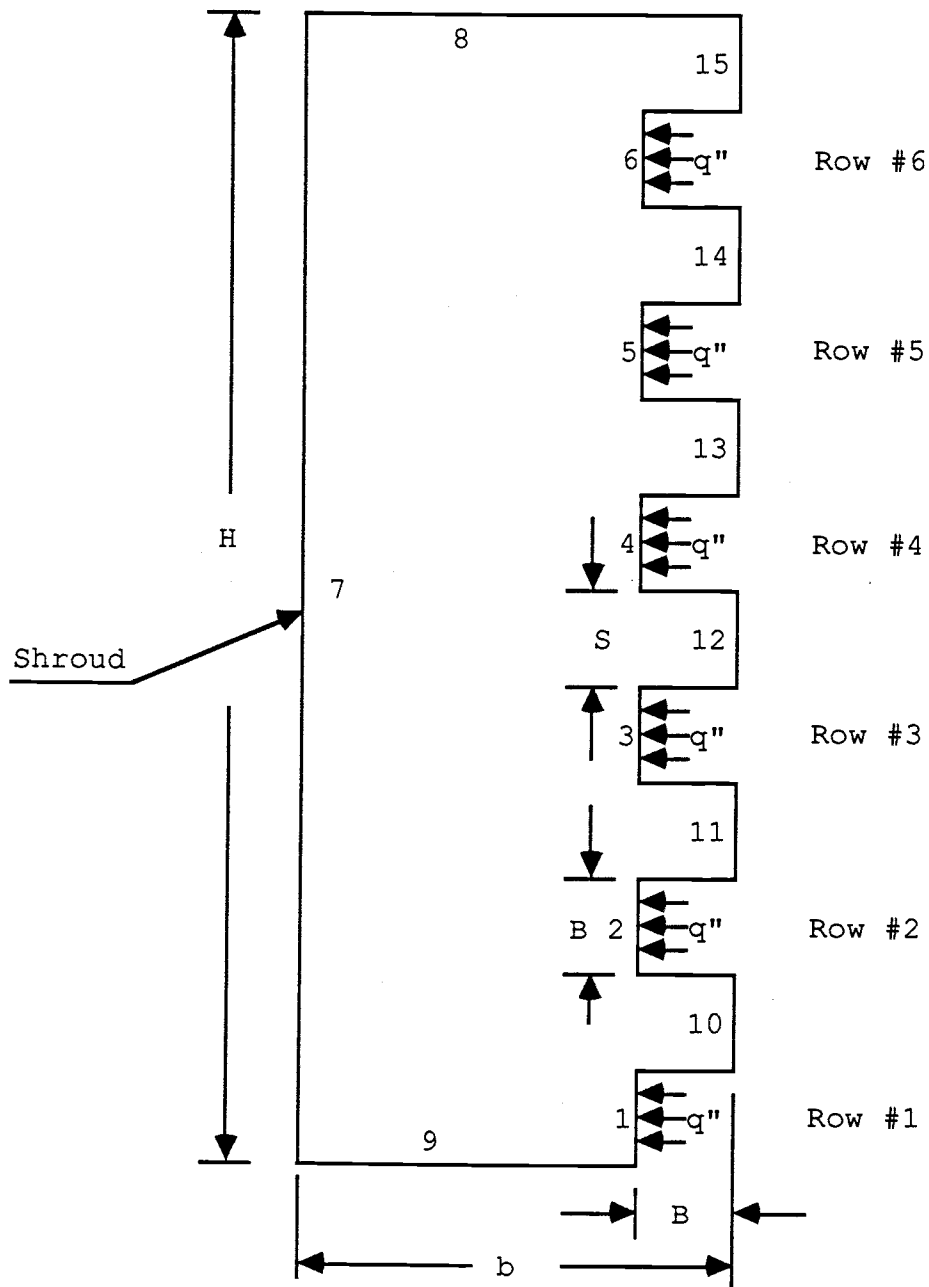


Figure B.1 Schematic of 2-D Vertical Channel with Protruding Discrete Heat Sources for Radiation Correction

where $R_1 = s/B$, $R_2 = H/B$, and $R_3 = s/H$. The reciprocity of the configuration factors yield the following relationships:

$$F_{7i} = R_6 F_{i7} \quad (B.4)$$

$$F_{8i} = R_5 F_{i8} \quad (B.5)$$

$$F_{9i} = R_5 F_{i9} \quad (B.6)$$

where $i = 1$ to 9 , $R_4 = 1/R_3$, $R_5 = 1/R_1$, and $R_6 = 1/R_2$. It is noted that $F_{ii} = 0$ because surface i can not see itself. Therefore

$$F_{7i} = 0.5 \left\{ \left[\sqrt{(2jR_6)^2 - R_3^2} + \sqrt{[1 - (2j-1)R_6]^2 + R_3^2} \right] - \left[\sqrt{(1-2jR_6)^2 + R_3^2} + \sqrt{(2j-1)^2 R_6^2} \right] \right\} \quad (B.7)$$

$$F_{8i} = 0.5 \left\{ \left[R_4 - (2j-1)R_5 + \sqrt{(R_4 - 2jR_5)^2 + 1} \right] - \left[\sqrt{[R_4 + (2j-1)R_5]^2 + 1} + (R_4 - 2jR_5) \right] \right\} \quad (B.8)$$

$$F_{9i} = 0.5 \left\{ \left[2jR_5 + \sqrt{(2j-1)^2 R_5^2 + 1} \right] - \left[\sqrt{(2jR_5)^2 + 1} + (2j-1)R_5 \right] \right\} \quad (B.9)$$

where $j = i - 9$ and $i = 10$ to 15 . Applying relationship of reciprocity gives

$$F_{i7} = R_2 F_{7i} \quad (B.10)$$

$$F_{i8} = R_1 F_{8i} \quad (B.11)$$

$$F_{i9} = R_1 F_{9i} \quad (B.12)$$

where $i = 10$ to 15 .

The configuration factors for all the surfaces are calculated with the aforementioned equations, and they must satisfy the equation below:

$$\sum_{j=1}^{N=15} F_{kj} = 1 \quad (B.13)$$

where $i = 1$ to 15 and $j = 1$ to 15 . $F_{ij} = 0$, when $i = j$. Also $F_{ij} = 0$, when $i \neq 7$ to 9 and $j \neq 7$ to 9 .

To account for the radiation exchange, the radiation model of a diffuse-gray enclosure summarized by Siegel and Howell [B.1] is employed. This model is also applicable for the vertical plate case when b , channel spacing is relatively large. The representation equation is listed below:

$$\sum_{j=1}^{N=15} \left(\frac{\delta_{kj}}{\epsilon_j} - F_{kj} \frac{1 - \epsilon_j}{\epsilon_j} \right) \frac{Q_j}{A_j} = \sum_{j=1}^{N=15} (\delta_{kj} - F_{kj}) \sigma T_j^4 \quad (B.14)$$

Corresponding to each surface k takes on one of the values $1, 2, \dots, N$. δ_{kj} is the Kronecker delta defined as

$$\delta_{kj} = \begin{cases} 1 & \text{when } k=j \\ 0 & \text{when } k \neq j \end{cases} \quad (B.15)$$

The surface temperatures of 1 to 7 are specified according to the temperature measurement of each experimental run. Adiabatic surfaces 8 and 9 are assigned for the case of the vertical plate or specified surface temperatures of 8 and 9 are assigned for the case of the vertical channel. Surfaces 10 to 15 are assumed to be adiabatic surfaces.

The emissivity of polished aluminum surfaces 1 to 6 are assumed to be 0.2 . The plexiglas surface painted with flat black are assumed to be 0.9 for surfaces 7 to 15 . The foregoing assumptions for surface emissivity have

been proven reasonably accurate according to the results of numerous iterations of the computer program.

AIR RADIATION CORRECTION			pa7.dat	SPACING: 10 IN
AIR RADIATION CORRECTION			pa7.dat	SPACING: 10 IN
Q(1)= 108.0242	E(1)= .9	
Q(2)= 121.5392	E(2)= .9	
Q(3)= 135.8242	E(3)= .9	without Shrouding
Q(4)= 133.424	E(4)= .9	
Q(5)= 139.7386	E(5)= .9	
Q(6)= 137.0581	E(6)= .9	
Q(7)= 160.2625	E(7)= .9	
Q(8)= -57.13143	E(8)= .9	
Q(9)= -114.0463	E(9)= .9	
T(10)= 28.31418	E(10)= .9	
T(11)= 29.28882	E(11)= .9	
T(12)= 29.90488	E(12)= .9	
T(13)= 30.12155	E(13)= .9	
T(14)= 29.95053	E(14)= .9	
T(15)= 29.45163	E(15)= .9	
QRAD	QTOT	%		
0.43558	3.93807	11.06076		
0.49008	3.99490	12.26755		
0.54768	3.96305	13.81958		
0.53800	3.98047	13.51597		
0.56346	3.97782	14.16507		
0.55265	4.02624	13.72627		
QRAD(7,8,9)	QRAD(1-6)			
-3.288079	3.127446			

B.1 Siegel, Robert and John R. Howell, "Thermal Radiation Heat Transfer,"

2nd Edition, McGraw-Hill Book Company, New York, pp.203-204, 1981.


```

10 ' VIEW FACTORS CALCULATIONS
11 DIM F(15,15), C(15,15), R(15), Q(15), E(15), T(15), QA(5), QR(9)
12 N=15 : NA=9 : NP=5
15 FOR IN=1 TO N
16 FOR JN=1 TO N
17 F(IN,JN)=0
18 NEXT
19 NEXT
20 INPUT " WHAT TEMPERATURE FILE? ". FILE$
21 OPEN "I". #2, FILE$
22 INPUT #2, ID, S, IDF
23 IF S=4! THEN S=10!
24 H=7.5 : B=.625
25 PRINT " ***** CHANNEL SPACING: ";S " INCHES *****"
26 PRINT " "
27 PRINT " THE VIEW FACTORS ARE: "
28 PRINT " "
30 R1=S/B : R2=H/B : R3=S/H : R4=1/R3 : R5=1/R1 : R6=1/R2
35 PRINT "      I      F(I,7)      F(I,8)      F(I,9)      F(7,I)      F(8,I)
F(9,I)";
36 PRINT " "
40 FOR I=1 TO NP
50 J2=2*(I-1) : JJ=J2*J2 : J3=2*I-1 : J1=J3*J3
60 R=R2-J2 : RR=R*R : SB=R1*R1
70 CR1=SQR(RR+SB) : CR2=SQR(JJ+SB)
80 UC1=SQR(JJ+SB) : UC2=SQR((R2-J3)*(R2-J3)+SB)
90 F(I,7)=.5*(CR1+CR2-UC1-UC2)
91 F(7,I)=F(I,7)/R2
100 F(I,9)=.5*(J3+SQR(JJ+SB)-J2-SQR(JJ+SB))
101 F(9,I)=F(I,9)/R1 : F(8,I)=F(I,8)/R1
110 F(I,8)=.5*(J3-J2+UC2-CR1)
120 F(8,I)=F(I,7)/R1
130 NEXT
140 F(8,7)=.5*(1+R4-SQR(1+R4*R4))
150 F(9,7)=F(8,7)
160 F(7,8)=F(8,7)*R3
170 F(7,7)=0 : F(8,8)=0 : F(9,9)=0
180 F(8,9)=.5*(2*SQR(1+R4*R4)-2*R4)
190 F(9,8)=F(8,9) : F(7,9)=F(9,7)*R3
200 FOR I=10 TO 15
210 J=I-9
220 CJ=2*J : CC=CJ*CJ : C1=CJ-1 : C2=C1*C1
225 BS=R5*R5 : D=CJ*R5 : E=C1*R5
230 CR=SQR(C2+BS+1)
240 UC=SQR(CC+BS+1)
250 F(9,I)=.5*(D+CR-UC-E)
255 E7=R4-E : EE=E7+E7
260 CR7=SQR((R4-D)*(R4-D)+1)
270 UC7=SQR(EE+1)
280 F(8,I)=.5*(E7+CR7-UC7-R4+D)
290 E8=CJ*R6 : D8=C1*R6 : DD=R3*R3 : GG=E8+E8 : GD=D8+D8
300 CR8=SQR(GG+DD) : CR6=SQR((1-D8)*(1-D8)+DD)
310 UC8=SQR((1-E8)*(1-E8)+DD) : UC6=SQR(GD+DD)
320 F(7,I)=.5*(CR8+CR6-UC8-UC6)
330 F(I,9)=R1*F(9,I)
340 F(I,8)=R1*F(8,I)
350 F(I,7)=R2*F(7,I)
360 NEXT
400 FOR I= 1 TO NA
410 PRINT USING " ###.##### "; I;F(I,7);F(I,8);F(I,9);F(7,I);F(8,I);F(9,I)
420 NEXT
424 PRINT " "
425 PRINT "      I      F(I,10)      F(I,11)      F(I,12)      F(I,13)      F(I,14)
F(I,15)";
426 PRINT " "
430 FOR I= 7 TO 9
440 PRINT USING " ###.##### "; I;F(I,10);F(I,11);F(I,12);F(I,13);F(I,14);F(I,15)

```

```

450 NEXT
455 PRINT " "
460 PRINT "      I      F(10.I)   F(11.I)   F(12.I)   F(13.I)   F(14.I)
F(15.I)";
470 PRINT " "
480 FOR I= 7 TO NA
490 PRINT USING " ###.#### " ; I;F(10.I);F(11.I);F(12.I);F(13.I);F(14.I);F(15.I)

495 NEXT
496 PRINT " "
498 PRINT " AIR RADIATION CORRECTION          "; FILE$. "SPACING:";S."IN";
499 PRINT " "
500 LPRINT "      ***** CHANNEL SPACING: ";S " INCHES *****"
510 LPRINT " "
520 LPRINT " THE VIEW FACTORS ARE: "
530 LPRINT " "
540 LPRINT "      I      F(I,7)   F(I,8)   F(I,9)   F(7,I)   F(8,I)
F(9,I)";
550 LPRINT " "
555 FOR I= 1 TO NA
560 LPRINT USING " ###.#### " ; I;F(I,7);F(I,8);F(I,9);F(7,I);F(8,I);F(9,I)
565 NEXT
570 LPRINT " "
580 LPRINT "      I      F(I,10)   F(I,11)   F(I,12)   F(I,13)   F(I,14)
F(I,15)";
590 LPRINT " "
600 FOR I= 7 TO 9
610 LPRINT USING " ###.#### " ; I;F(I,10);F(I,11);F(I,12);F(I,13);F(I,14);F(I,15)
)
620 NEXT
630 LPRINT " "
640 LPRINT "      I      F(10.I)   F(11.I)   F(12.I)   F(13.I)   F(14.I)
F(15.I)";
650 LPRINT " "
660 FOR I= 7 TO NA
670 LPRINT USING " ###.#### " ; I;F(10.I);F(11.I);F(12.I);F(13.I);F(14.I);F(15.I)
)
680 NEXT
682 LPRINT " "
685 LPRINT " AIR RADIATION CORRECTION          "; FILE$. "SPACING:";S."IN";
686 LPRINT " "
688 INPUT #2, TH, TA, T(9), T(8), T(7)
690 FOR I = 1 TO NP
700 INPUT #2, AMP, VOLT
702 QA(I)=AMP*VOLT
705 INPUT #2, T(I)
706 NEXT
710 FOR M= 1 TO N
720 SIGMA=5.729E-08
740 GOSUB 800
750 IF M>NA THEN T(M)=SQRT(SQRT(Q(M)))-273.15 : PRINT "T(";M.")=";T(M),"E(";M.")="
;E(M) ELSE PRINT "Q(";M.")=";Q(M),"E(";M.")=";E(M)
755 IF M>NA THEN T(M)=SQRT(SQRT(Q(M)))-273.15 : LPRINT "T(";M.")=";T(M),"E(";M.")="
;E(M) ELSE LPRINT "Q(";M.")=";Q(M),"E(";M.")=";E(M)
760 NEXT
762 PRINT "      QRAD      QTOT      %      "
765 LPRINT "      QRAD      QTOT      %      "
770 OPEN "QRAD.DAT" FOR APPEND AS #1
775 QIN=0 : QOUT=0
780 FOR J = 1 TO NP
781 QR(J)=Q(J)*10*(5/8)*(0.0254+.0254)
782 PERCENT=QR(J)/QA(J)*100
783 PRINT USING " ###.#### ";QR(J), QA(J), PERCENT
784 LPRINT USING " ###.#### ";QR(J), QA(J), PERCENT
785 PRINT #1, USING " #####.#### " ; QR(J)
786 QOUT=QOUT+QR(J)
787 NEXT

```

```

788 LPRINT " "
789 FOR J = 7 TO NA
790 QR(J)=Q(J)*S*10*(.0254*.0254)
791 IF J = 7 THEN QR(J)=Q(J)*H*10*(.0254*.0254)
792 QIN=QIN+QR(J)
793 NEXT
794 PRINT "QRAD(7.8.9)   QRAD(1-6)
795 LPRINT "QRAD(7.8.9)   QRAD(1-6)
796 PRINT QIN. QOUT
797 LPRINT QIN. QOUT
798 END
800 FOR K=1 TO N
805 SUMR=0
820 IF K > NA THEN Q(K)=0
830 FOR J= 1 TO N
835 IF J > 6 THEN E(J)=.9 ELSE E(J)=.2
840 IF J=K THEN KO=1 : C(K,J)=KD/E(J) : F(J,J)=0 ELSE KD=0 : C(K,J)=-F(K,J)*(1-E
(J))/E(J)
845 IF J > NA THEN C(K,J)=- (KD-F(K,J))*SIGMA
850 IF J > NA THEN RK=0 : GOTO 870 ELSE 860
860 RK=(KD-F(K,J))*SIGMA*(T(J)+273.15)^4
870 SUMR=SUMR+RK
920 NEXT
925 R(K)=SUMR
930 NEXT
950 FOR I = 1 TO N-1
960 FOR J = I+1 TO N
970 BB=-C(J,I)/C(I,I)
980 FOR K = I+1 TO N
990 C(J,K)=C(J,K)+C(I,K)*BB
1000 NEXT
1010 R(J)=R(J)+BB*R(I)
1020 NEXT
1025 NEXT
1030 Q(N)=R(N)/C(N,N)
1040 FOR I=N-1 TO 1 STEP -1
1050 Q(I)=R(I)
1060 FOR J= I+1 TO N
1070 Q(I)=Q(I)-C(I,J)*Q(J)
1080 NEXT
1090 Q(I)=Q(I)/C(I,I)
1100 NEXT
1110 RETURN

```

APPENDIX C

AVERAGE HEAT FLUX

For the present experiment, the average heat flux over the entire hot plate with protruding discrete heating can be computed by integrating the local heat flux from the stagnation point to the plate height (H) with respect to x .

$$\begin{aligned}\bar{q}'' &= \frac{1}{H} \int_0^H q_i'' dx \\ &= \frac{1}{H} \left(\int_0^B q_1'' dx + \int_B^{2B} q_2'' dx + \int_{2B}^{3B} q_3'' dx + \int_{3B}^{4B} q_4'' dx + \int_{4B}^{5B} q_5'' dx + \int_{5B}^H q_6'' dx \right)\end{aligned}\quad (C.1)$$

Where H is the plate or channel height and B is the protruding block height. Considering a uniform heat flux boundary condition for each protruding element, i.e., $q_i'' = q''$, equation (C.1) simplifies to

$$\bar{q}'' = \frac{n(B)}{n(B + s)} q'' = \frac{q''}{(1 + s/B)} \quad (C.2)$$

where n is the number of discrete heated elements and s is the spacing between each pair of protruding heated elements. For the present experiment $n=6$ and $s/B=1$, which gives the following relation:

$$\bar{q}'' = 0.5 q'' \quad (C.3)$$

APPENDIX D

HEAT TRANSFER DATA REDUCTION PROGRAM

```

PROGRAM MAIN
C-
C-   FLUID PROPERTIES:
C-       U(ID): DYNAMIC VISCOSITY (LBM/FT/SEC)
C-       CP(ID): SPECIFIC HEAT (BTU/LBM/F)
C-       RHO(ID): DENSITY (LBM/FT**3)
C-       COND(ID): THERMAL CONDUCTIVITY (BTU/HR/FT/F)
C-       BETA(ID): THERMAL EXPANSION COEFFICIENT (1/R)
C-       ID: FLUID IDENTIFICATION
C-           1 FOR AIR
C-           2 FOR WATER
C-           3 FOR OIL
C-
C-   IFNAME: INPUT DATA FILE NAME
C-   OFNAME: OUTPUT DATA FILE NAME
C-
CHARACTER*64 IFNAME,IFNAM,OFNAME,OFNAM1,OFNAM2,OFNAM3,OFNAM4
CHARACTER*64 OFNAM5,IFNAM1,OFNAM6,OFNAM7,OFNAM8
DIMENSION U(3),CP(3),RHO(3),COND(3),BETA(3),T(35),TIO(2)
C-
C-   DIMENSIONLESS PARAMETERS:
C-       ZNU(NR,NP): NUSSELT NUMBER;  $H \cdot L / K$ 
C-       RA(NR,NP): RAYLEIGH NUMBER;  $Pr \cdot Gr$ 
C-       PR(NR,NP): PRANDTL NUMBER;  $U \cdot CP / COND$ 
C-       GR(NR,NP): GRASHOF NUMBER;  $g \cdot BETA \cdot RHO \cdot L^3 \cdot DT / U^2$ 
C-       GRM(NR,NP): MODIFIED GRASHOF NUMBER;  $Q / AREA / COND \cdot Gr \cdot L$ 
C-       RAM(NR,NP): MODIFIED RAYLEIGH NUMBER;  $Pr \cdot GrM$ 
C-
C-   NR: NUMBER OF ROW
C-   NP: NUMBER OF DATA POINTS
C-   H: HEAT TRANSFER COEFFICIENT OBTAINED BY EXPERIMENTS
C-       (BTU/HR*FT**2/F)
C-
DIMENSION H(6,22),ZNU(6,22),PR(6,22),SHRAM(6,22),THETA(6,22)
DIMENSION RAM(6,22),HTCONV(6,22),GR(6,22),RMB(6,22),YBAR(6,22)
DIMENSION ZXIB(6,22),ZXIB(6,22),ZS(6,22),RPR(6,22),TTB(6,22)
DIMENSION TBLK(6,22),DELTEMP(6,22),Q1(6,22),QB(6,22),QVAR(6,22)
DIMENSION RMS(6,22),GRM(6,22),SHGRM(6,22),QC(6,22)
C-
C-   HEIGHT: CHANNEL HEIGHT, 7.5 IN.
C-   AREA: PROTRUDED HEATING SURFACE AREA, 0.0042 FT*FT
C-   HE: HEIGHT OF THE PROTRUDED ELEMENT (FT)
C-   N: NUMBER OF ROW OF THE PROTRUDED ELEMENT; 6 ROWS TOTAL
C-
C-   OPEN THE FILE: *.SOL AS THE OUTPUT SOLUTION DATA FILE
C-
OPEN(7,FILE=' ',STATUS='NEW')
WRITE(*,777)
WRITE(7,777)
777  FORMAT(' PLEASE ENTER FILE FOR REDUCING HEAT TRANSFER DATA: ')
READ(*,222) IFNAM1
OPEN(21,FILE=IFNAM1)
READ(21,776) NP, NR
776  FORMAT(2I2)
C-
HEIGHT=7.50
AREA=(10.0-1.0/32.0)*0.625/144.0
HE=0.625/12.0
BL=HE
C-
C-   Q: POWER INPUT TO THE PROTRUDED ELEMENT OR HEAT FLUX (BTU/HR)
C-   POWER: POWER INPUT (WATT)
C-   CURNT: CURRENT PASSED THRU THE HEATED RESISTANT WIRE (AMPERE)
C-   VOLT: VOLTAGE ACROSSED THE ONE OHM RESISTOR (VOLT)
C-   OHM: ONE OHM RESISTOR'S RESISTANCE (OHM)
C-   EMF: VOLTAGE DROP BETWEEN THE HEATED ELEMENT (VOLT)

```

```

C-      NP:  NUMBER OF THE DATA POINTS
C-
      DO 80 INP=1, NP
C-
C-      OPEN THE FILE:  IN.DAT AS AN EXISTING INPUT DATA FILE
C-
      READ(21,222) IFNAME
222  FORMAT(A)
      OPEN(6,FILE=IFNAME)
      WRITE(*,111) IFNAME
      WRITE(7,111) IFNAME
111  FORMAT(10X,'      ENTER INPUT DATA FILE NAME: ',A)
C-
C-      TI:  CHANNEL AVERAGE INLET TEMPERATURE (C)
C-      TO:  CHANNEL AVERAGE OUTLET TEMPERATURE (C)
C-
      READ(6,41) ID, SPACING, IDT
41  FORMAT(I2,F6.3,I2)
      S=SPACING+0.625
C-
      IF (ID-2) 1,2,3
1  WRITE(*,10)
   WRITE(7,10)
10  FORMAT(10X,'      *** THE WORKING FLUID IS AIR ***')
   GO TO 31
2  WRITE(*,11)
   WRITE(7,11)
11  FORMAT(10X,'      *** THE WORKING FLUID IS WATER ***')
   GO TO 31
3  WRITE(*,12)
   WRITE(7,12)
12  FORMAT(10X,'      *** THE WORKING FLUID IS OIL ***')
31  CONTINUE
      IF(SPACING .GT. 3.70) THEN
        WRITE(*,45)
        WRITE(7,45)
45  FORMAT(' *VERTICAL PLATE WITH PROTRUDED DISCRETE HEAT SOURCES*')
      ELSE
        WRITE(*,42) S
        WRITE(7,42) S
42  FORMAT(10X,'      ***** CHANNEL SPACING: ',F5.3,' IN. *****')
      END IF
C-
C-      ND:  NUMBER OF NODAL POINTS FOR CHANNEL INLET/OUTLET
C-
      IF(IDT.EQ.1) THEN
        DO 90 LO=1,2
          IF(SPACING .GT. 3.70) SPACING=3.50
          GAP=SPACING
          ND=GAP*8+1
          IF(SPACING.EQ.0.156) ND=3
C-
C-      LO:  LO=1 FOR CHANNEL OUTLET; LO=2 FOR CHANNEL INLET
C-
          IF(LO.EQ.1) ND=ND+6
C-
C-      INPUT CHANNEL INLET/OUTLET TEMPERATURE DISTRIBUTION
C-
          DO 100 J=1, ND
            READ(6,43) T(J)
43  FORMAT(F6.2)
100  CONTINUE
C-
C-      SUBROUTINE CHNLTM IS USED TO CLCULATE THE AVERAGE OF CHANNEL
C-      INLET/OUTLET TEMPERATURE
C-
          CALL CHNLTM(ND,T,TAUG)
          TIO(LO)=TAUG
90  CONTINUE
      TI=TIO(2)
      TO=TIO(1)
C-

```

```

C-
C-   CALCULATE THE BULK FLUID TEMPERATURE (F)
C-
TAVG=(TI+TO)/2.0
TR=TAVG*1.80+32.0
IF(SPACING .GT. 3.50) THEN
  WRITE(*,46) TI, TO
  WRITE(7,46) TI, TO
46  FORMAT(' INFLOW TEMP:',F6.2,'C', '   OUTFLOW TEMP:',F6.2,'C')
  ELSE
    WRITE(*,44) TI, TO
    WRITE(7,44) TI, TO
  44  FORMAT(' CHANNEL INLET:',F6.2,'C', '   CHANNEL OUTLET:',F6.2,'C')
  END IF
  ELSE
    END IF
C-
C-   INITIALIZATION
C-
QTOT=0
C-
C-   TBR:  HOT WALL REAR FACE TEMPERATURE (C)
C-   TA:  AMBIENT TEMPERATURE (C)
C-
READ(6,24) TBR, TA, TENC
24  FORMAT(1X,3F6.2)
WRITE(*,20) TBR, TA, TENC
WRITE(7,20) TBR, TA, TENC
20  FORMAT(' *HOTREAR',F6.2,' C *AMBIENT:',F6.2,' C *ENC:',F6.2,' C')
IF(ID.EQ.1) THEN
  READ(21,222) IFNAM
  OPEN(5,FILE=IFNAM)
  WRITE(*,101) IFNAM
  WRITE(7,101) IFNAM
101  FORMAT(' PLEASE ENTER AIR RADIATION CORRECTION: ',A)
  ELSE
    END IF
  WRITE(*,15)
  WRITE(7,15)
15  FORMAT(' ROW#  TB(C) CURRENT(A) VOLTAGE  Q(BTU/HR) QCOND  QCONV
*   QRAD')
C-
DO 50 INR= 1, NR
  READ(6,22) V, EMF
  22  FORMAT(F6.3,F7.3)
C-
C-   TBC:  PROTRUDED HEATING SURFACE CENTER TEMPERATURE (C)
C-   TBS:  PROTRUDED HEATING SURFACE SIDE TEMPERATURE (C)
C-
  READ(6,23) TB
  23  FORMAT(F6.2)
C-
  TTB(INR,INP)=TB
  TBLK(INR,INP)=TB
  TM=(TB+TENC)/2.0
C-
C-   DTLS (K):  TEMPERATURE DIFFERENCE BETWEEN THE FRONT & REAR FACES
C-               OF THE HOT WALL
C-   DTRM (K):  TEMPERATURE DIFFERENCE BETWEEN THE BLOCK & AMBIENT
C-
  DTLS=(TB-TBR)*1.8
  DTRM=(TB-TA)*1.8
  IF (ID.EQ.1) THEN
    READ(5,210) QRAD
    210  FORMAT(F10.4)
    IF(QRAD.LT.0) QRAD=0
    ELSE
      QRAD=0
    END IF
    QRAD=QRAD*3.413
C-

```

```

CALL POWER(U,EMF,CURNT,QTOT,Q,DTLS,DTRM,QCOND,QCONV,QRAD,AREA)
C-
QB(INR,INP)=Q
Q1(INR,INP)=Q
C-   CONVERT TO SI UNITS FOR QC (W) FOR PLOTTING
      QC(INR,INP)=Q/3.413
C-
      WRITE(*,16) INR, TB, CURNT, EMF, Q, QCOND, QCONV, QRAD
      WRITE(7,16) INR, TB, CURNT, EMF, Q, QCOND, QCONV, QRAD
16   FORMAT(2X,I2,3X,F6.2,F9.4)
C-
C-   HTCONV: CONVECTION CONTRIBUTION
C-
      HTCONV(INR,INP)=QCONV
C-
C-   CALCULATE TEMPERATURE DIFFERENCE BETWEEN THE BLOCK HEATED SURFACE
C-   AND THE BULK FLUID TEMPERATURE (F)
C-
      DELTEMP(INR,INP)=TB-TENC
      DT=DELTEMP(INR,INP)*1.80
C-
C-
C-   FLUID PROPERTIES EVALUATED AT FLUID MEAN TEMPERATURE (C)
C-
      CALL PROPTY(TB,U,CP,COND,RHO,BETA,ID)
      PRO=U(ID)*CP(ID)/COND(ID)*3600
      CALL PRMETER(HTCONV,AREA,BL,TM,DT,INR,INP,H,ZNU,PR,GR,GRM,RAM,ID)
      IF(SPACING .GT. 3.700) THEN
        XIB=(INR-1)*2.0+0.5
        ZXIB(INR,INP)=ZNU(INR,INP)*XIB/2
        GXIB(INR,INP)=GR(INR,INP)*XIB*XIB*XIB
        RMXB(INR,INP)=GXIB(INR,INP)*PR(INR,INP)
        ZS(INR,INP)=ZNU(INR,INP)/2
        GRM(INR,INP)=GRM(INR,INP)/2
        RAM(INR,INP)=RAM(INR,INP)/2
      ELSE
        B=(S/12.0)/BL
        ZS(INR,INP)=ZNU(INR,INP)*B/2
        SHGRM(INR,INP)=S/HEIGHT*GRM(INR,INP)*B*B*B*B/2
        RMS(INR,INP)=RAM(INR,INP)*B*B*B*B/2
        SHRAM(INR,INP)=S/HEIGHT*RMS(INR,INP)
      END IF
      RPR(INR,INP)=PR(INR,INP)/PRO
50   CONTINUE
      CALL SORT(TTB,TBLK,TENC,THETA,YBAR,INP)
      CALL SORTQ(Q1,QB,QVAR,INP)
      WRITE(*,113)
      WRITE(7,113)
      WRITE(*,177) (QVAR(INR,INP), INR=1,NR)
      WRITE(7,177) (QVAR(INR,INP), INR=1,NR)
      WRITE(*,113)
      WRITE(7,113)
      DO 578 II = 1, NR
C-   CONVERT TO SI UNITS FOR h (W/M**2 C) FOR PLOTTING
      H(II,INP)=H(II,INP)/5.677
578   CONTINUE
C-
80   CONTINUE
C-
177   FORMAT(' % VARIATION OF HEAT FLUX: ',6(F8.2))
C-

```



```

C-      READ(21,233) OFNAME
233      FORMAT(A)
C
C      OFNAME: HEAT TRANSFER DATA REDUCTION FILE READY FOR PLOTTING
      OPEN(8,FILE=OFNAME,STATUS='NEW')
      WRITE(*,333) OFNAME
      WRITE(7,333) OFNAME
333      FORMAT(' OUTPUT FILE NAME FOR DATA REDUCTION: ',A)
      IF(SPACING .GT. 3.625) THEN
        DO 72 N=1, NR
          WRITE(*,29) N
          WRITE(7,29) N
29          FORMAT(' ***** #',I1,' ROW PROTRUDED HEATING ELEMENT *****')
          WRITE(*,27)
          WRITE(7,27)
27          FORMAT(' #PT      h',5X,'NuXB',6X,'Pr',5X,'Pr/Pro',3X,'GrXB',5X,'RaMX
          *B')
          DO 62 I=1, NP
            WRITE(*,18) I,H(N,I),ZXIB(N,I),PR(N,I),RPR(N,I),6XIB(N,I),RMB(N,I)
            WRITE(7,18) I,H(N,I),ZXIB(N,I),PR(N,I),RPR(N,I),6XIB(N,I),RMB(N,I)
            WRITE(8,18) I,H(N,I),ZXIB(N,I),PR(N,I),RPR(N,I),6XIB(N,I),RMB(N,I)
62          CONTINUE
            WRITE(*,113)
            WRITE(7,113)
113          FORMAT(' ')
72          CONTINUE
            READ(21,233) OFNAM2
            OPEN(12,FILE=OFNAM2,STATUS='NEW')
            WRITE(*,122) OFNAM2
            WRITE(7,122) OFNAM2
122          FORMAT(' FILE NAME FOR DATA PLOTTING Grx & Rax vs Nu: ',A)
            DO 162 I=1, NP
              WRITE(12,38) (6XIB(N,I), RMB(N,I), ZXIB(N,I), N=1,NR)
162            CONTINUE
38            FORMAT(6(1X,E8.2,1X,E8.2,1X,F7.2))
            DO 571 N=1, NR
              WRITE(*,29) N
              WRITE(7,29) N
              WRITE(*,537)
              WRITE(7,537)
537            FORMAT(' #NPT      h',5X,'Nu      Pr',8X,' GrM      RaM ')
              DO 561 I=1, NP
                WRITE(*,28) I,H(N,I),ZS(N,I),PR(N,I),GRM(N,I),RAM(N,I)
                WRITE(7,28) I,H(N,I),ZS(N,I),PR(N,I),GRM(N,I),RAM(N,I)
                WRITE(8,28) I,H(N,I),ZS(N,I),PR(N,I),GRM(N,I),RAM(N,I)
28              FORMAT(1X,I2,2F8.2,1X,F9.3,2X,2E9.2)
561              CONTINUE
                WRITE(*,113)
                WRITE(7,113)
571              CONTINUE
                READ(21,233) OFNAM1
                OPEN(12,FILE=OFNAM1,STATUS='NEW')
                WRITE(*,102) OFNAM1
                WRITE(7,102) OFNAM1
102              FORMAT(' FILE NAME FOR DATA PLOTTING GrM & RaM vs Nu: ',A)
                DO 161 I=1, NP
                  WRITE(12,38) (GRM(N,I), RAM(N,I), ZS(N,I), N=1,NR)
161                CONTINUE
              ELSE
                DO 70 N=1, NR
                  WRITE(*,19) N
                  WRITE(7,19) N
19                FORMAT(' ***** #',I1,' ROW PROTRUDED HEATING ELEMENT *****')
                  WRITE(*,17)
                  WRITE(7,17)
17                FORMAT(' #PT      h',7X,'Nu',6X,'Pr',5X,'Pr/Pro',4X,'RaM',5X,'b/H*GrM
                  * b/HReM')

```

```

DO 60 I=1, NP
  WRITE(*,18) I, H(N,I), ZS(N,I), PR(N,I), RPR(N,I), RMS(N,I), SH6RM(N,I
*) , SHRAM(N,I)
  WRITE(7,18) I, H(N,I), ZS(N,I), PR(N,I), RPR(N,I), RMS(N,I), SH6RM(N,I
*) , SHRAM(N,I)
  WRITE(8,18) I, H(N,I), ZS(N,I), PR(N,I), RPR(N,I), RMS(N,I), SH6RM(N,I
*) , SHRAM(N,I)
18  FORMAT(1X,I2,2F8.2,1X,F9.3,F7.2,2X,3E9.2)
60  CONTINUE
    WRITE(*,113)
    WRITE(7,113)
70  CONTINUE
    READ(21,233) OFNAM4
    OPEN(14,FILE=OFNAM4,STATUS='NEW')
    WRITE(*,104) OFNAM4
    WRITE(7,104) OFNAM4
104  FORMAT(' FILE NAME FOR DATA PLOTTING b/H*6-Mb & RaMb vs Nub:
*,A)
    DO 64 I=1, NP
      WRITE(14,38) (SH6RM(N,I), SHRAM(N,I), ZS(N,I), N=1,NR)
64  CONTINUE
    END IF
    READ(21,233) OFNAM3
C
C    OFNAM3: DIMENSIONLESS TEMPERATURE VS DISTANCE DATA FOR PLOTTING
    OPEN(13,FILE=OFNAM3,STATUS='NEW')
    WRITE(*,553) OFNAM3
    WRITE(7,553) OFNAM3
553  FORMAT(' FILE FOR PLOTTING OF THETA vs x/H : ',A)
    READ(21,233) OFNAM5
C    OFNAM5: DATA FILE OF TB - TC (C) vs ROW# FOR PLOTTING
    OPEN(15,FILE=OFNAM5,STATUS='NEW')
    WRITE(*,665) OFNAM5
    WRITE(7,665) OFNAM5
665  FORMAT(' FILE FOR PLOTTING OF TB-TC vs ROW# : ',A)
    READ(21,233) OFNAM6
C    OFNAM6: DATA FILE OF h vs x/H FOR PLOTTING
    OPEN(16,FILE=OFNAM6,STATUS='NEW')
    WRITE(*,666) OFNAM6
    WRITE(7,666) OFNAM6
666  FORMAT(' FILE FOR PLOTTING OF h (W/M**2 C) vs x/H : ',A)
    READ(21,233) OFNAM7
C    OFNAM7: DATA FILE OF DT (C) vs Q (W) FOR PLOTTING
    OPEN(17,FILE=OFNAM7,STATUS='NEW')
    WRITE(*,667) OFNAM7
    WRITE(7,667) OFNAM7
667  FORMAT(' FILE FOR PLOTTING OF DT (C) vs Q (W) : ',A)
    READ(21,233) OFNAM8
C    OFNAM8: DATA FILE OF THETA vs Q (W) FOR PLOTTING
    OPEN(18,FILE=OFNAM8,STATUS='NEW')
    WRITE(*,668) OFNAM8
    WRITE(7,668) OFNAM8
668  FORMAT(' FILE FOR PLOTTING OF THETA vs Q (W) ',A)
    DO 355 I=1, NR
      WRITE(13,533) YBAR(I,1), (THETA(I,J), J=1, NP)
      WRITE(15,535) I, (DELTEMP(I,J), J=1,NP)
      WRITE(16,533) YBAR(I,1), (H(I,J), J=1, NP)
355  CONTINUE
    DO 357 J=1, NP
      WRITE(17,538) (DELTEMP(I,J), QC(I,J), I=1, NR)
      WRITE(18,538) (THETA(I,J), QC(I,J), I=1, NR)
357  CONTINUE
533  FORMAT(F6.3,20(F6.2))
535  FORMAT(I2,20(F6.2))
538  FORMAT(6(2F6.2))
END

```

```

C      THIS SUBROUTINE CALCULATES THE DIMENSIONLESS TEMPERATURE
C      VARIATION vs DISTANCE ALONG THE STREAMWISE DIRECTION
      SUBROUTINE SORT(T,TBLK,TC,THETA,YBAR,J)
      DIMENSION T(6,22), TBLK(6,22), THETA(6,22), YBAR(6,22)
      NR=6
      K=0
      JJ=0
3     DO 1 I=1, NR-1
      IF(K.GT. NR-1) GO TO 4
      IF(T(I,J)-T(I+1,J)) 2, 1, 1
2     D=T(I,J)
      T(I,J)=T(I+1,J)
      T(I+1,J)=D
      JJ=1
1     CONTINUE
      IF(JJ.EQ.1) GO TO 3
      TMAX=T(1,J)
4     DO 7 I=1, NR
      THETA(I,J)=(TBLK(I,J)-TC)/(TMAX-TC)
      YBAR(I,J)=(2*(I-1)+0.5)*0.625/7.5
7     CONTINUE
      RETURN
      END

C      THIS SUBROUTINE DETERMINES THE NONUNIFORMITY OF HEAT FLUX
C      FOR EACH PROTRUDING DISCRETE HEATING ELEMENT
C      SUBROUTINE SORTQ(Q,QB,QVAR,J)
      DIMENSION Q(6,22), QB(6,22), QVAR(6,22)
      NR=6
      K=0
      JJ=0
3     DO 1 I=1, NR-1
      IF(K.GT. NR-1) GO TO 4
      IF(Q(I,J)-Q(I+1,J)) 2, 1, 1
2     D=Q(I,J)
      Q(I,J)=Q(I+1,J)
      Q(I+1,J)=D
      JJ=1
1     CONTINUE
      IF(JJ.EQ.1) GO TO 3
      QMAX=Q(1,J)
4     DO 7 I=1, NR
      QVAR(I,J)=(QMAX-QB(I,J))/QMAX*100
7     CONTINUE
      RETURN
      END

C-   SUBROUTINE CHNLTM(ND,T,TAUG)
      DIMENSION T(35)
      TT=0
      TDIST=0
      IF(ND.EQ.3) THEN
        STEP=1.0/20.0
      ELSE
        STEP=1.0/8.0
      END IF
      DO 20 II=1, ND
        DIST=(II-1)*STEP
        TT=TT+T(II)*DIST
        TDIST=TDIST+DIST
20     CONTINUE
      TAUG1=TT/TDIST
      TT=0
      TDIST=0
      DO 40 II=ND, 1, -1
        DIST=(ND-II)*STEP
        TT=TT+T(II)*DIST
        TDIST=TDIST+DIST
40     CONTINUE
      TAUG2=TT/TDIST
      TAUG=(TAUG1+TAUG2)/2.0
      RETURN
      END

```

```

SUBROUTINE POWER(V,EMF,CURNT,QT,Q,DTLS,DTRM,QCND,QCNV,QRAD,AREA)
C
C  V:  VOLTAGE (V)
C  OHM: ONE OHM RESISTOR
C
      OHM=1.0
      CURNT=V/OHM
      POW=CURNT*EMF
      QT=QT+POW
C-
C-  CONVERT WATTAGE TO BTU/HR BY MULTIPLING 3.413
C-
      Q=POW*3.413
      QQ=QT*3.413
C-
C-  Q:  TOTAL POWER INPUT (BTU/HR)
C-  QCNV: TOTAL CONVECTION HEAT TRANSFER CONTRIBUTION (BTU/HR)
C-  QCND: TOTAL CONDUCTION HEAT LOSS (BTU/HR)
C-  QRD: TOTAL RADIATION HEAT LOSS (BTU/HR)
C-  HLOSS1: CONDUCTION HEAT LOSS THRU THE HOT WALL
C-  HLOSS2: CONDUCTION HEAT LOSS THRU THE WIRES
C-  HOTK: THERMAL CONDUCTIVITY OF THE HOT (PLOXIGLAS) WALL
C-  WIREKCP: THERMAL CONDUCTIVITY OF THE COPPER WRIES
C-  WIREKCN: THERMAL CONDUCTIVITY OF THE CONSTANTAN WRIES
      PI=3.141596
      HOTK=0.000121
C-  2*AREA: AVERAGE BACKPLANE SURFACE AREA
      HLOSS1=HOTK*DTLS*2*AREA/((1.-1./32.)/12.0)
      WIREKCP=223.0
      WIREKCN=13.1
      WIREK=WIREKCP+WIREKCN
      IF(DTRM .LT. 0) DTRM = 0
      HLOSS2=WIREK*DTRM*PI/4.*((.01*.01/6.)*2*3+(.04*.04/6.)*2)/144.
      QCND=HLOSS1+HLOSS2
      QCNV=Q-QCND-QRAD
      RETURN
      END
SUBROUTINE PRMETER(HTCONV,AREA,BL,TM,DT,N,NP,H,ZNU,PR,GR,GRM,RAM
*,ID)
      DIMENSION U(3),CP(3),COND(3),RHO(3),BETA(3),RAM(6,22),GR(6,22)
      DIMENSION H(6,22),ZNU(6,22),PR(6,22),HTCONV(6,22),GRM(6,22)
C-
C-  CALCULATE THE HEAT TRANSFER COEFFICIENT (BTU/HR/FT**2/F)
C-
      H(N,NP)=HTCONV(N,NP)/(AREA*DT)
C-
      CALL PROPTY(TM,U,CP,COND,RHO,BETA,ID)
C-
      CALCULATE CHANNEL HYDRODYNAMIC DIAMETER
C-
      CALCULATE NUSSELT NUMBER
C-
      ZNU(N,NP)=H(N,NP)*BL/COND(ID)
C-
      CALCULATE PRANDTL NUMEER
C-
      PR(N,NP)=U(ID)*CP(ID)/COND(ID)*3600
C-
      CALCULATE GRASHOF NUMBER
C-
      BL3=BL*BL*BL
      GRC=32.174*BETA(ID)*BL3*RHO(ID)*RHO(ID)/(U(ID)*U(ID))
      DTT=DT

```

```

C-
C-      BECAUSE THE UNIT OF THERMAL EXPANSION OF WATER IS (1/K)
C-
      IF(ID .EQ. 2) DTT=DTT/1.8
      GR(N,NP)=GRC*DTT
C-
C-      CALCULATE MODIFIED GRASHOF NUMBER
C-
      GRM(N,NP)=GRC*BL*HTCONV(N,NP)/AREA/COND(ID)
C-
C-      CALCULATE RAYLEIGH NUMBER
C-
      RA=PR(N,NP)*GR(N,NP)
C-
C-      CALCULATE MODIFIED RAYLEIGH NUMBER
      RAM(N,NP)=PR(N,NP)*GRM(N,NP)
      RETURN
      END
      SUBROUTINE PROPTY (T,U,CP,COND,RHO,BETA,ID)
C-
C-      -----
C-      THE THERMOPHYSICAL PROPERTIES OF AIR AND WATER ARE TABULATED
C-      FROM P.E. LILEY OF PURDUE UNIVERSITY
C-      -----
C-
C-      *****
C-      * AIR PROPERTIES ARE ACCURATE FOR TEMPERATURE 290 TO 390 K *
C-      *****
C-
      DIMENSION U(3),CP(3),RHO(3),BETA(3),COND(3)
C-
      TEMP=T*1.80+32.0+459.67
      TP=T+273.15
      T2=TP*TP
      T3=TP*T2
      T4=T2*T2
      T5=TP*T4
      T6=T3*T3
      T7=T4*T3
      IF (ID .EQ. 2) GO TO 2
      IF (ID .EQ. 3) GO TO 3
C-
C-      DYNAMIC VISCOSITY OF AIR (LBM/FT/SEC)
C-
      C0=3.190021D+00
      C1=-1.444086D-02
      C2=-2.167551D-05
      C3=4.746222D-07
      C4=-1.306392D-09
      C5=1.114788D-12
      USI=C0+C1*TP+C2*T2+C3*T3+C4*T4+C5*T5
      U(1)=USI*0.00001*2419.1/3600.0
C-
C-      SPECIFIC HEAT OF AIR (BTU/LBM/F)
C-
      C0=1.245847D+00
      C1=-2.076383D-03
      C2=5.771101D-06
      C3=-5.087554D-09
      CPSI=C0+C1*TP+C2*T2+C3*T3
      CP(1)=CPSI*0.23885
C-
C-      THERMAL CONDUCTIVITY OF AIR (BTU/HR/FT/F)
C-
      C0=2.257755D-02
      C1=-6.451070D-05
      C2=3.345389D-08
      C3=2.210519D-09
      C4=-6.737578D-12
      C5=5.878443D-15
      CONDSI=C0+C1*TP+C2*T2+C3*T3+C4*T4+C5*T5
      COND(1)=CONDSI*0.5782

```

```

C-
C-   DENSITY OF AIR AT ATMOSPHERIC PRESSURE (LBM/FT**3)
C-
      C0=3.948300D-02
      C1=2.486437D-03
      C2=1.007611D-06
      C3=-9.708828D-10
      SPVOLSI=C0+C1*TP+C2*T2+C3*T3
      RHO(1)=1.0/SPVOLSI*0.06243

C-
C-   THERMAL EXPANSION COEFFICIENT OF AIR (1/R)
C-
      BETA(1)=1.0/TEMP
      60 TO 4

C-
C-
C-   *****
C-   *   WATER PROPERTIES ARE ACCURATE FOR TEMPERATUE 280.2 TO 314 K *
C-   *****
C-
C-   DYNAMIC VISCOSITY OF WATER (LBM/FT/SEC)
C-
      2  CONTINUE
      C0=3.295241D+02
      C1=-1.385693D-00
      C2=1.873376D-03
      C3=-2.103273D-05
      C4=9.562115D-08
      C5=-1.524354D-10
      C6=2.105862D-13
      C7=-2.910178D-16
      U(2)=(C0+C1*TP+C2*T2+C3*T3+C4*T4+C5*T5+C6*T6+C7*T7)*2419.1/3600
      U(2)=U(2)/10000

C-
C-   SPECIFIC HEAT OF WATER (BTU/LBM/F)
C-
      C0=1.219052D+01
      C1=-7.068683D-02
      C2=2.052166D-04
      C3=-1.953862D-07
      CP(2)=(C0+C1*TP+C2*T2+C3*T3)*0.23885

C-
C-   THERMAL CONDUCTIVITY OF WATER (BTU/HR/FT/F)
C-
      C0=6.727199D-01
      C1=-1.899778D-03
      C2=2.947036D-06
      C3=-7.344579D-09
      C4=1.532032D-10
      C5=-3.175081D-13
      COND(2)=(C0+C1*TP+C2*T2+C3*T3+C4*T4+C5*T5)*0.5782

C-
C-   DENSITY OF WATER (LBM/FT**3)
C-
      C0=1.955742D+00
      C1=-8.556334D-03
      C2=2.437580D-05
      C3=-2.145198D-08
      SPVOLSI=C0+C1*TP+C2*T2+C3*T3
      RHO(2)=1.0/SPVOLSI*0.06243*1000

C-
C-   THERMAL EXPANSION COEFFICIENT OF WATER (1/K)
C-
      C0=-7.861458D+01
      C1=4.623678D-01
      C2=-6.294295D-04
      BETA(2)=(C0+C1*TP+C2*T2)*0.0001

      3  CONTINUE

```

```

C-
C- *****
C- * OIL PROPERTIES ARE ACCURATE FOR TEMPERATURE 37 TO 143 C *
C- * (100 TO 300 F) CHEVRON MULTI MACHINE OIL 68) *
C- *****
C-
C- THERMAL CONDUCTIVITY OF OIL (BTU/HR/FT/F)
C-
C- C0=7.872908D-02
C- C1=-4.607572D-05
C- C2=8.171009D-09
C- COND(3)=C0+C1*T+C2*T*T
C-
C- SPECIFIC HEAT OF OIL (BTU/LBM/F)
C-
C- C0=4.269602D-01
C- C1=1.088413D-03
C- C2=-4.066165D-07
C- CP(3)=C0+C1*T+C2*T*T
C-
C- DENSITY OF OIL (LBM/FT**3)
C-
C- CALCULATE OIL DENSITY (LBM/GAL)
C-
C- C0=7.3996260
C- C1=-6.913703D-03
C- C2=8.108694D-06
C- RHO(3)=(C0+C1*T+C2*T*T)*7.4805
C-
C- DYNAMIC VISCOSITY OF OIL (LBM/FT/SEC)
C-
C- C0=98.860
C- C1=-0.9150
C- V: KINEMATIC VISCOSITY (CM*CM/SEC)
C- V=(C0+C1*T)*0.01
C- VNU: KINEMATIC VISCOSITY (FT*FT/SEC)
C- VNU=V/((2.54*12.0)*(2.54*12.0))
C- U(3)=VNU*RHO(3)
C-
C- THERMAL EXPANSION COEFFICIENT OF OIL (1/F)
C-
C- BETA(3)=0.0004
C- GO TO 4
C- RETURN
4
END

```

APPENDIX E

UNCERTAINTY ANALYSIS

A method described by Holman [D.1] was used to perform the uncertainty analysis for the experiments. Consider the definition of the heat transfer coefficient, h , as

$$h = \frac{Q}{A(T_h - T_c)} = \frac{IV}{BL(T_h - T_c)} = \frac{V^2}{RBL(T_h - T_c)} \quad (E.1)$$

where the power input, Q equals the product of the measurement current (I) and voltage (V) or (V/R^2). The surface area, A , is the product of height (B) and length (L) of the protruding array. The temperature difference between the protruding array and the chamber surface is denoted as $T_h - T_c$. The estimation of uncertainty in the experimental results for h , the heat transfer coefficient, is listed by the following. The result, h , is first written as a function of the independent variables R, V, B, L, T_h, T_c . Hence,

$$h = h(R, V, B, L, T_h, T_c) \quad (E.2).$$

Then, taking the partial derivative of h with respect to each independent variable as

$$\begin{aligned} \frac{\partial h}{\partial R} &= \frac{-V^2}{R^2 BL(T_h - T_c)} \\ \frac{\partial h}{\partial V} &= \frac{2V}{RBL(T_h - T_c)} \\ \frac{\partial h}{\partial B} &= \frac{-V^2}{RB^2 L(T_h - T_c)} \end{aligned} \quad (E.3)$$

$$\frac{\partial h}{\partial L} = \frac{-V^2}{RBL^2(T_h - T_c)}$$

$$\frac{\partial h}{\partial T} = \frac{-V^2}{RBL(T_h - T_c)^2}$$

$$\frac{\partial h}{\partial T_w} = \frac{V^2}{RBL(T_h - T_c)^2}$$

Substituting the partial derivatives into the following equation

$$W_h = \left[\left(\frac{\partial h}{\partial R} W_1 \right)^2 + \left(\frac{\partial h}{\partial V} W_2 \right)^2 + \left(\frac{\partial h}{\partial B} W_3 \right)^2 + \left(\frac{\partial h}{\partial L} W_3 \right)^2 + \left(\frac{\partial h}{\partial T_h} W_4 \right)^2 + \left(\frac{\partial h}{\partial T_c} W_4 \right)^2 \right]^{1/2} \quad (E.4)$$

Then gives

$$W_h = \left[\frac{V^2}{RA(T_h - T_c)} \left(\frac{W_1^2}{R^2} + \frac{4W_2^2}{V^2} + \frac{W_3^2}{B^2} + \frac{W_3^2}{L^2} + \frac{2W_4^2}{(T_h - T_c)^2} \right) \right]^{1/2} \quad (E.5)$$

Simplifying gives

$$\frac{W_h}{h} = \left(\frac{W_1^2}{R^2} + \frac{4W_2^2}{V^2} + \frac{W_3^2}{B^2} + \frac{W_3^2}{L^2} + \frac{2W_4^2}{(T_h - T_c)^2} \right)^{1/2} \quad (E.6)$$

For the following conditions:

$$R = 1 \text{ ohm} \pm 5 \%$$

$$V = 20 \text{ V} \pm 0.01 \%$$

$$B = 5/8 \text{ in.} \pm 0.01 \%$$

$$L = 10 \text{ in.} \pm 0.01 \%$$

$$T_h - T_c = 50 \text{ }^\circ\text{F} \pm 0.50 \text{ }^\circ\text{F}$$

with the previous equation, then

$$\begin{aligned} \frac{W_h}{h} &= \left[\left(\frac{0.05}{1} \right)^2 + 4 \left(\frac{0.0001}{20} \right)^2 + \left(\frac{0.0001}{\frac{5}{8 \times 12}} \right)^2 + \left(\frac{0.0001}{\frac{10}{12}} \right)^2 + 2 \left(\frac{0.5}{50} \right)^2 \right]^{1/2} \\ &= (0.0025 + 1.0 \times 10^{-10} + 3.6864 \times 10^{-6} + 1.44 \times 10^{-8} + 0.0002)^{1/2} \\ &= (0.0027)^{1/2} \end{aligned}$$

Thus, the percent uncertainty in the heat transfer coefficient is about

$$\frac{W_h}{h} = 5 \%$$

D.1 Holman, Jack P., "Experimental Method for Engineers," 3rd Edition, McGraw-Hill Book Company, New York, pp. 44-47, 1978.

APPENDIX F

SAMPLE OF EXPERIMENTAL DATA LOG

*** CHANNEL SPACING 2.686 IN. WORKING FLUID: DISTILLED WATER ***
 TIME: 18:25:03 DATE: 11-12-1987

I. HEAT SOURCE TEMPERATURE

ROW	CENTER	RIGHT
5	45.25	44.35
5	41.18	41.62
4	40.95	39.35
3	40.02	40.05
2	38.92	37.10
1	39.58	37.79

30 W each

*** HOT WALL REAR FACE TEMPERATURE: 26.53
 *** SHROUDE TEMPERATURE: 45.25
 *** LID TEMPERATURE: 27.27
 CHANNEL INLET TEMPERATURE: 23.86
 CHANNEL OUTLET TEMPERATURE: 27.51

COOLING WATER INLET TEMPERATURE: 11.86
 COOLING WATER OUTLET TEMPERATURE: 12.62

AMBIENT TEMPERATURE CHAMBER TEMPERATURE
 22.36 17.73

TIME: 15:47:43 DATE: 03-20-1988

*** CHANNEL SPACING 0.781 IN. WORKING FLUID: AIR ***

I. HEAT SOURCE TEMPERATURE

ROW	CENTER	RIGHT
5	47.68	46.27
5	48.37	45.93
4	47.70	46.71
3	47.46	46.24
2	43.83	42.84
1	41.55	40.80

3 W each

*** HOT WALL REAR FACE TEMPERATURE: 25.86
 *** SHROUDE TEMPERATURE: 12.50
 *** LID TEMPERATURE: 20.47
 CHANNEL INLET TEMPERATURE: 11.19
 CHANNEL OUTLET TEMPERATURE: 16.32

COOLING WATER INLET TEMPERATURE: 10.48
 COOLING WATER OUTLET TEMPERATURE: 10.95

AMBIENT TEMPERATURE CHAMBER TEMPERATURE
 21.95 10.95

TIME: 09:28:11 DATE: 05-09-1988

*** CHANNEL SPACING 0.781 IN. WORKING FLUID: OIL ***

I. HEAT SOURCE TEMPERATURE

ROW	CENTER	RIGHT
5	27.39	26.46
5	26.65	25.74
4	26.17	25.00
3	25.93	25.00
2	24.96	25.74
1	23.74	22.83

2.5 W each

*** HOT WALL REAR FACE TEMPERATURE: 17.68
 *** SHROUDE TEMPERATURE: 14.94
 *** LID TEMPERATURE: 21.33
 CHANNEL INLET TEMPERATURE: 12.79
 CHANNEL OUTLET TEMPERATURE: 13.03

COOLING WATER INLET TEMPERATURE: 12.05
 COOLING WATER OUTLET TEMPERATURE: 12.55

AMBIENT TEMPERATURE CHAMBER TEMPERATURE
 21.83 12.55

APPENDIX G

RAW HEAT TRANSFER DATA ANALYSIS

It is appropriate to analyze the experimental heat transfer data which yields the basic information and its physical significance before grouping them into dimensionless parameters. The heat flux, Q , to each protruding element plotted as a function of temperature difference, ΔT , between each heated surface and the cold chamber temperature for various fluids is shown in Figures G.1 and G.2 (a)-(d). These graphs exhibit unreduced heat transfer data which appear compressed into three regions. For air and water as the working fluids, ΔT is proportionally increased as the increase in heat flux input, however, the ΔT of air is much greater than the ΔT of water for a given heat flux. For oil, ΔT increases in a nonlinear trend with small heat flux input and then increased proportionally with the increase in ΔT . These Figures also show that $\Delta T_{\text{air}} > \Delta T_{\text{oil}} > \Delta T_{\text{H}_2\text{O}}$ for a given heat flux Q . The plots of Q versus ΔT for various working fluids clearly indicate that the effects of fluid property variation on heat transfer and temperature distribution are very significant. For the air case, the slope of the line of Q versus ΔT is close to $\pi/18$. For oil case, the slope of the line is near $\pi/4$. For distilled water case, the slope of the line is close to $7\pi/18$.

Figures G.1 and G.2 (a)-(d) generally show that the upper protruding element surface temperature is higher than the lower protruding element surface temperature. This trend is contributed to the rising buoyancy flow as it convects on the upper element and the thermal spreading that manifests itself as the flow advances downstream. The temperature difference increases in the last two rows of protruding arrays is caused by the effect of thermal boundary layer thickening and the preheating effect from the rising

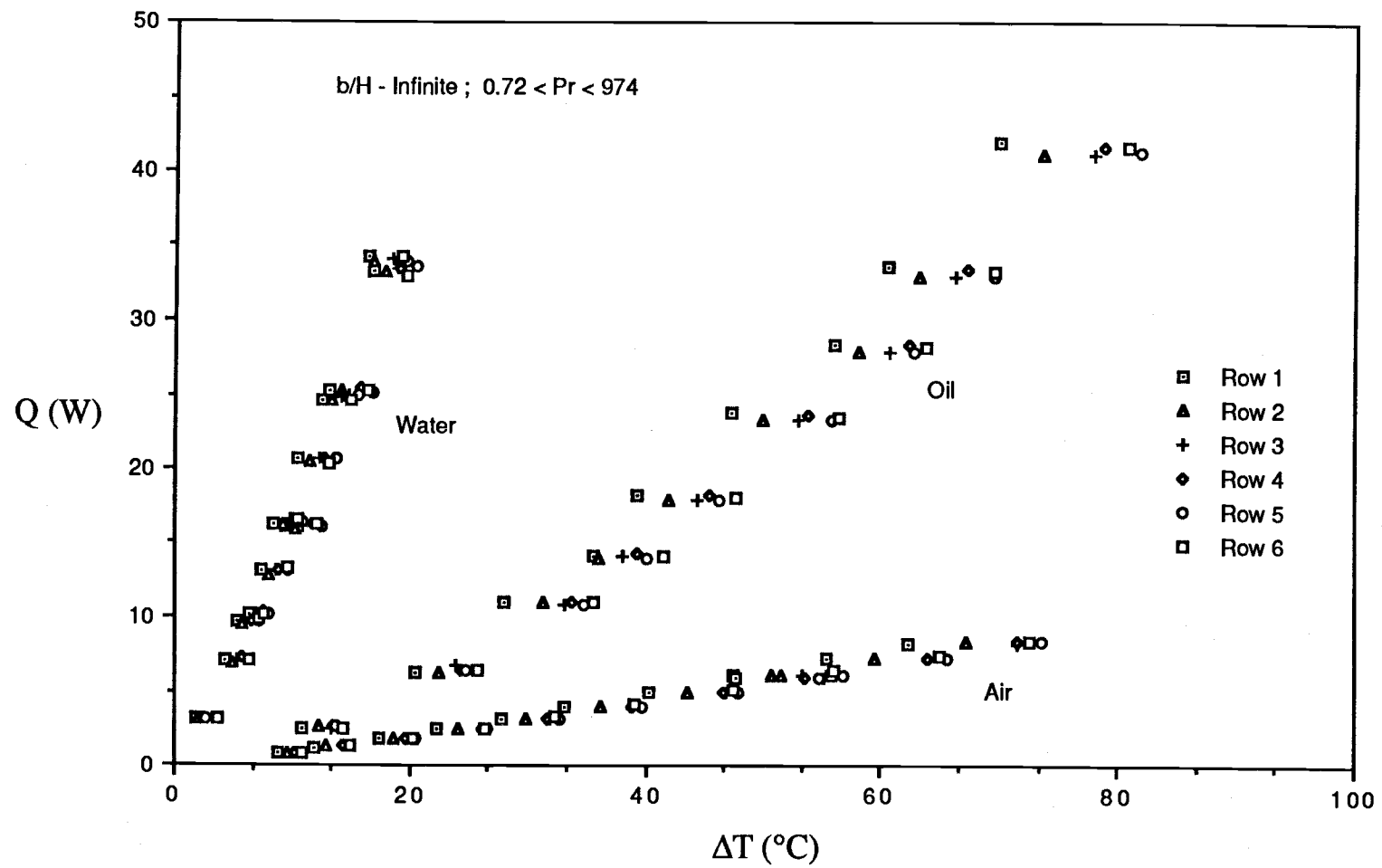


Figure G.1 Q and ΔT Variation on Protruding Arrays without Shrouding for Various Fluids

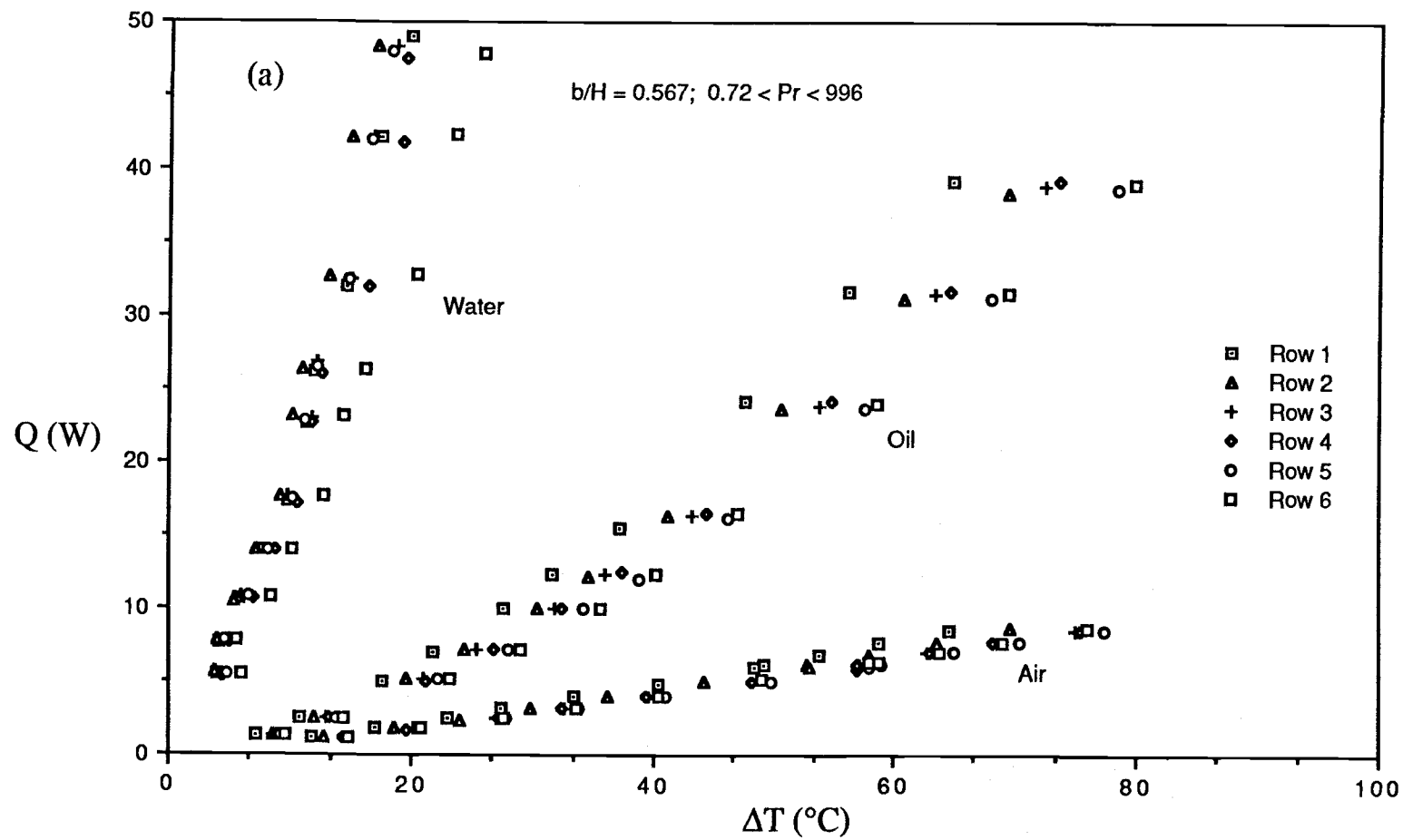


Figure G.2 Q and ΔT variation on Protruding Arrays with Shrouding for Various Fluids

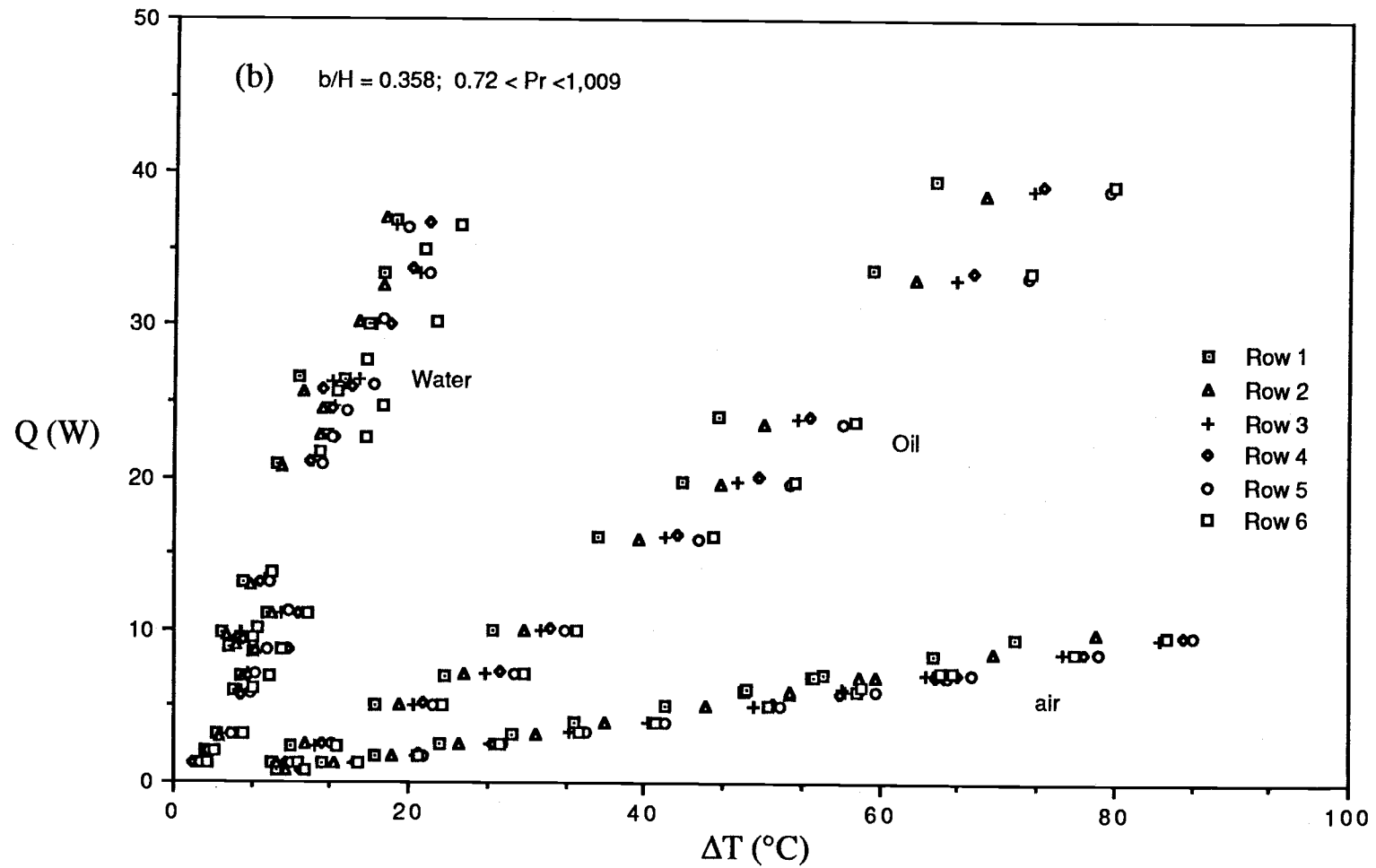


Figure G.2 Q and ΔT Variation on Protruding Arrays with Shrouding for Various Fluids

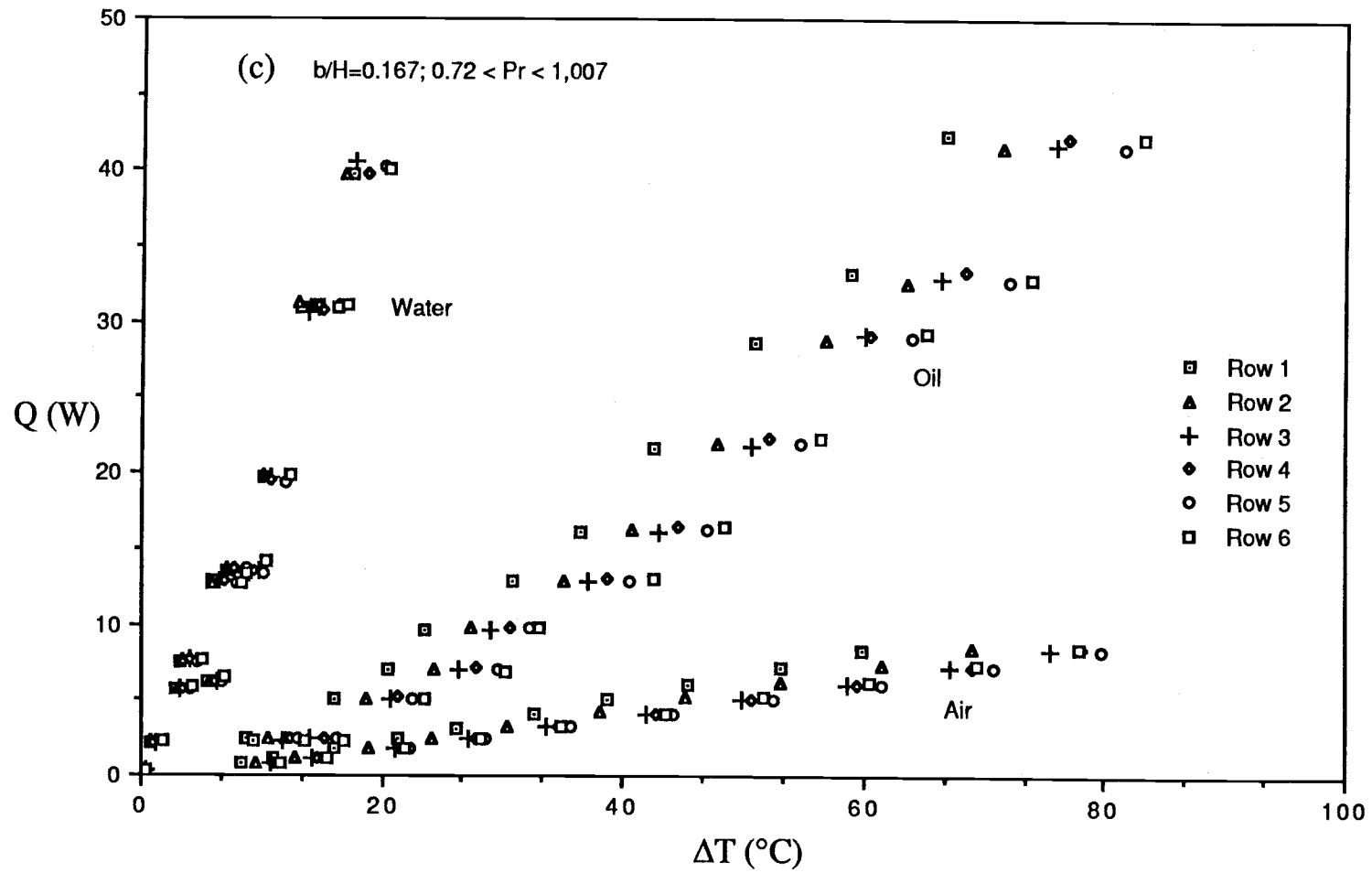


Figure G.2 Q and ΔT Variation on Protruding Arrays with Shrouding for Various Fluids

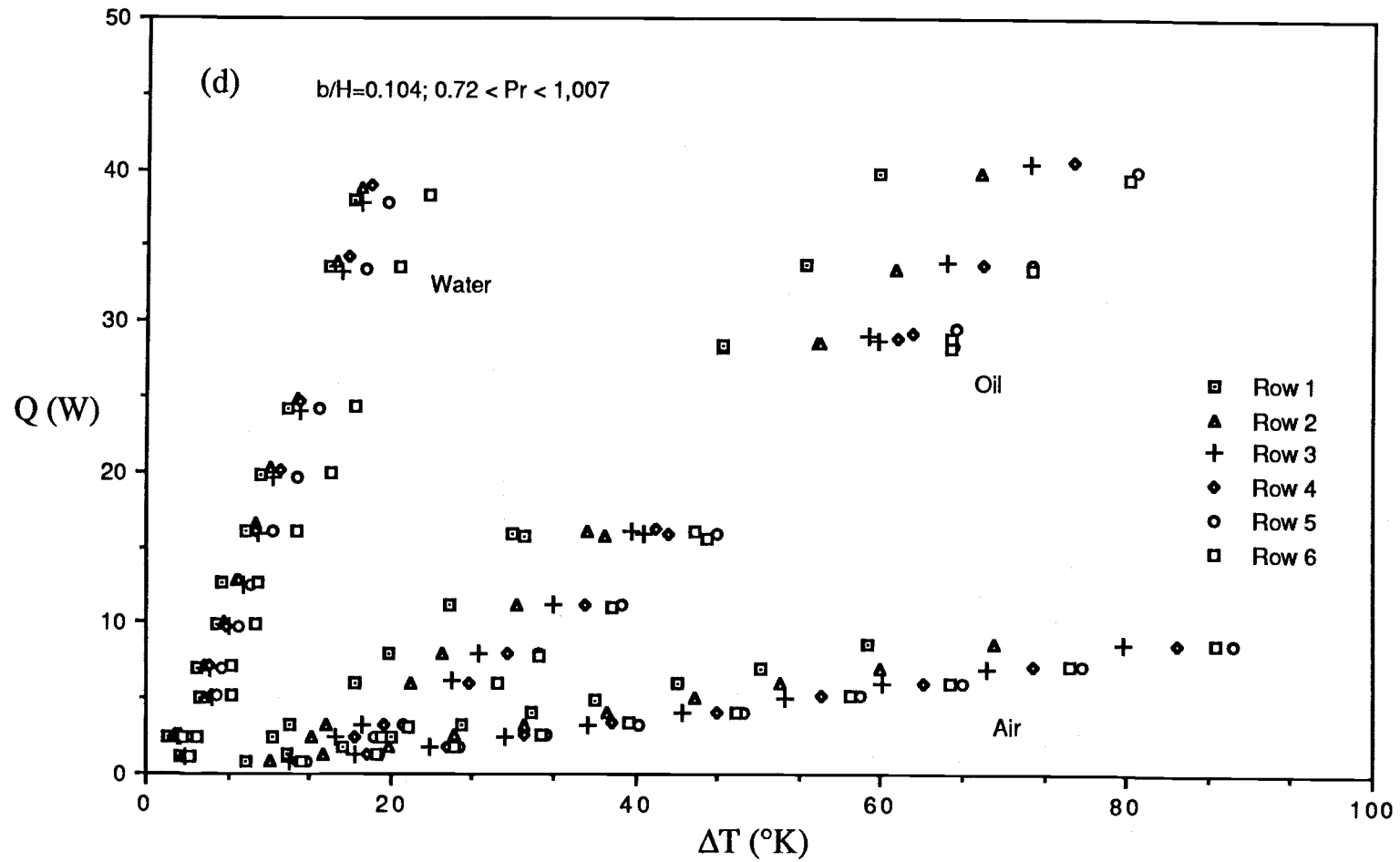


Figure G.2 Q and ΔT Variation on Protruding Arrays with Shrouding for Various fluids

fluid. This is to say that the higher temperature in the upper element resulted from the rising warm fluid. Plots of heat flux (Q) versus temperature difference (ΔT) with various values of b/H for row 1, row 4 and row 6 are shown in Figures G.3 (a)-(c). Figures G.3 (a)-(c) depict the heated discrete surface temperature, which generally decreases as the channel spacing decreases (except for the water in the smallest channel spacing case). The magnitude of the temperature difference, $T_h - T_c$ for the smallest channel spacing ($b/H = 0.104$) is the lowest compared with other channel spacings for a fixed heat flux, as shown in Figures G.3 (a) and (c). The interactions of shrouding and the heating surfaces and a relative rapid buoyancy flow may contribute to this trend resulting in a low $T_h - T_c$. For water data, the lowest ΔT occurs in a vertical channel with $b/H \approx 0.358$ in the lower range of Q ; however, as the Q reaches to the higher range, ΔT becomes the highest among other channel spacings as seen in Figure G.3(a).

A similar trend in the temperature distributions for the protruding arrays also holds true for the case of oil and distilled water working fluids. The interplay of working fluid properties contribute to a different magnitude of heated surface temperature at the same heat flux for three types of fluid used.

The slope(m) of the line of Q versus ΔT remains unchanged for $b/H = \infty$ and 0.567. This indicates that the heat transfer results for large channel spacing ($b/H = 0.567$) is not affected by the presence of an unheated shrouding wall. This is to say that the natural convection heat transfer rate for the large channel spacing is virtually the same as for the vertical plate case. As b/H decreases from 0.567 to 0.104, the slope, m , of the line of Q versus ΔT , increases slightly because of the decrease in ΔT . This suggests that the peak heat transfer coefficient or the lowest ΔT is reached for $b/H = 0.104$ in comparison to other values of b/H at the same boundary conditions.

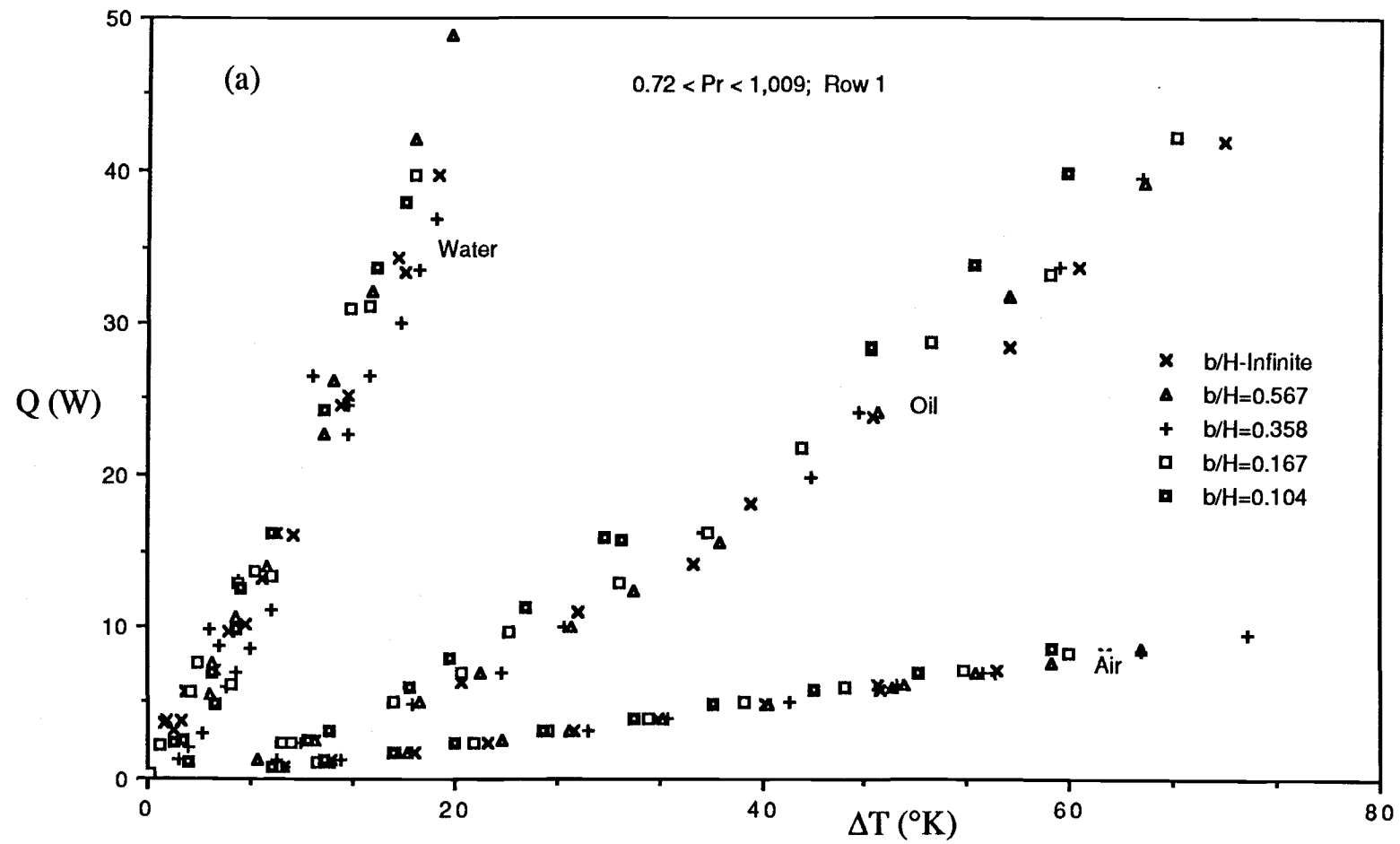


Figure G.3 Q and ΔT Variation on the 1st Row Protruding Array for Various b/H Values

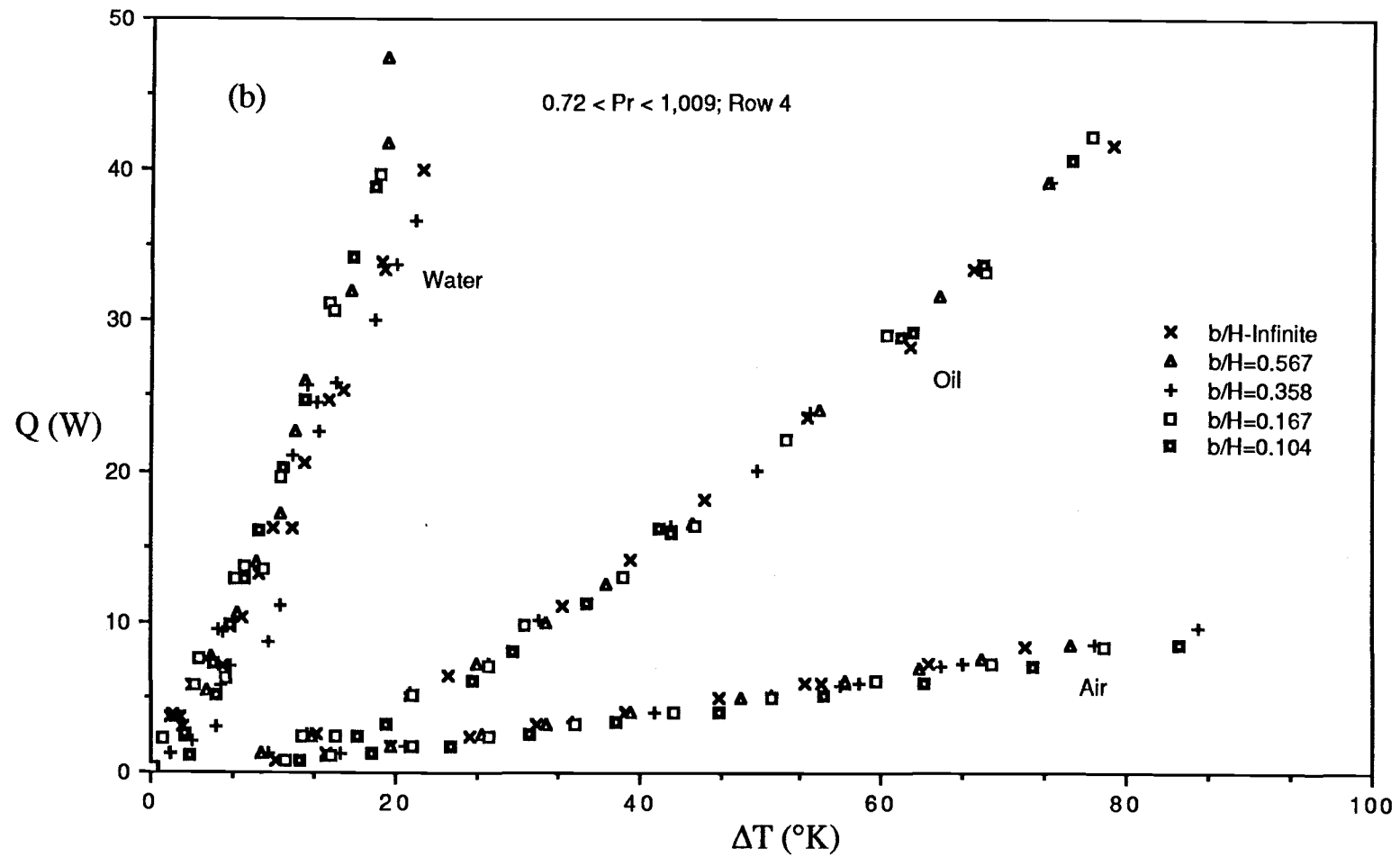


Figure G.3 Q and ΔT Variation on the 4th Row Protruding Array for various b/H Values

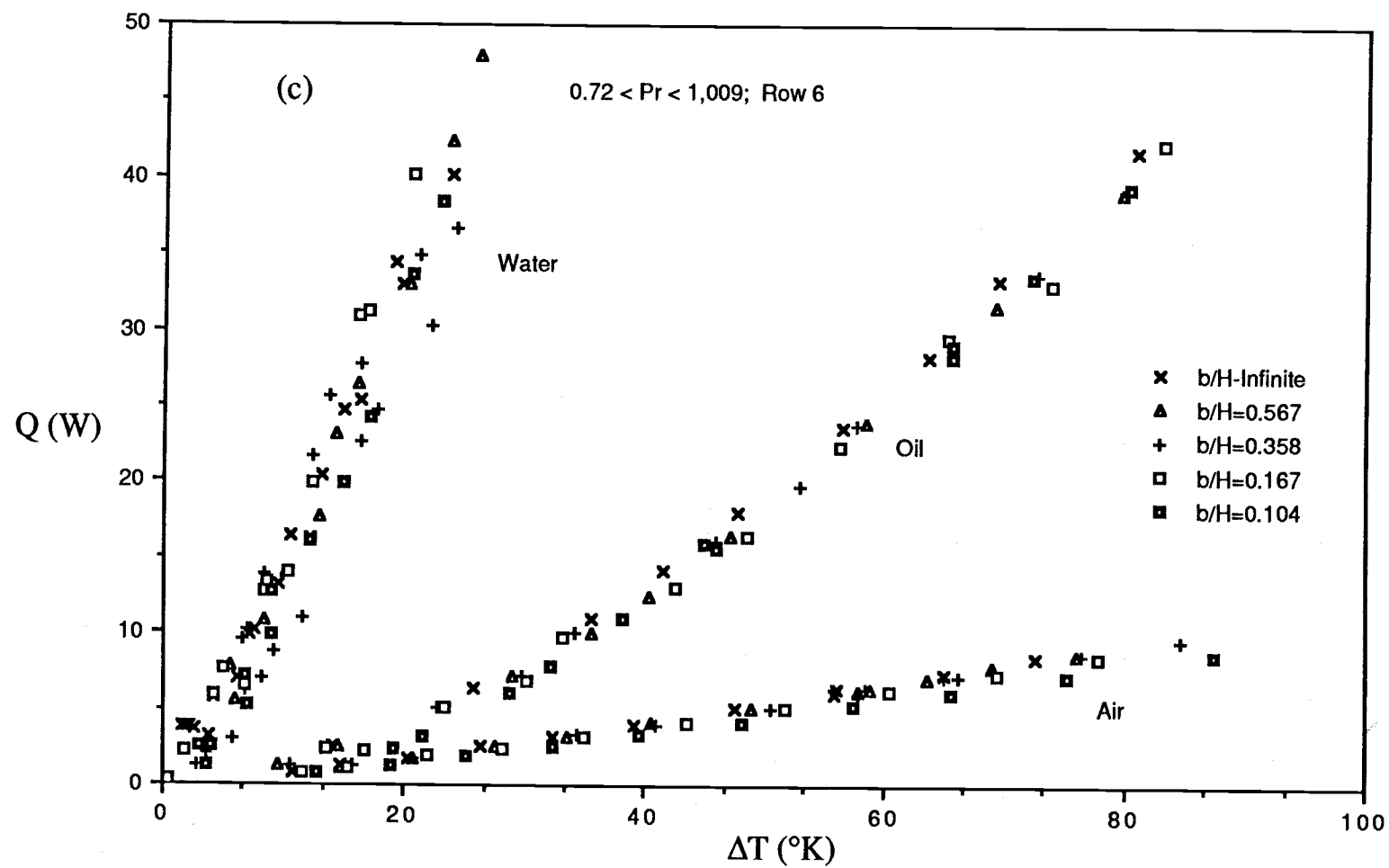


Figure G.3 Q and ΔT Variation on the 6th Row Protruding Array for Various b/H Values

In other words, the vertical channel with a small spacing is suitable to achieve minimum heated surface temperature and higher heat transfer rate.

APPENDIX H

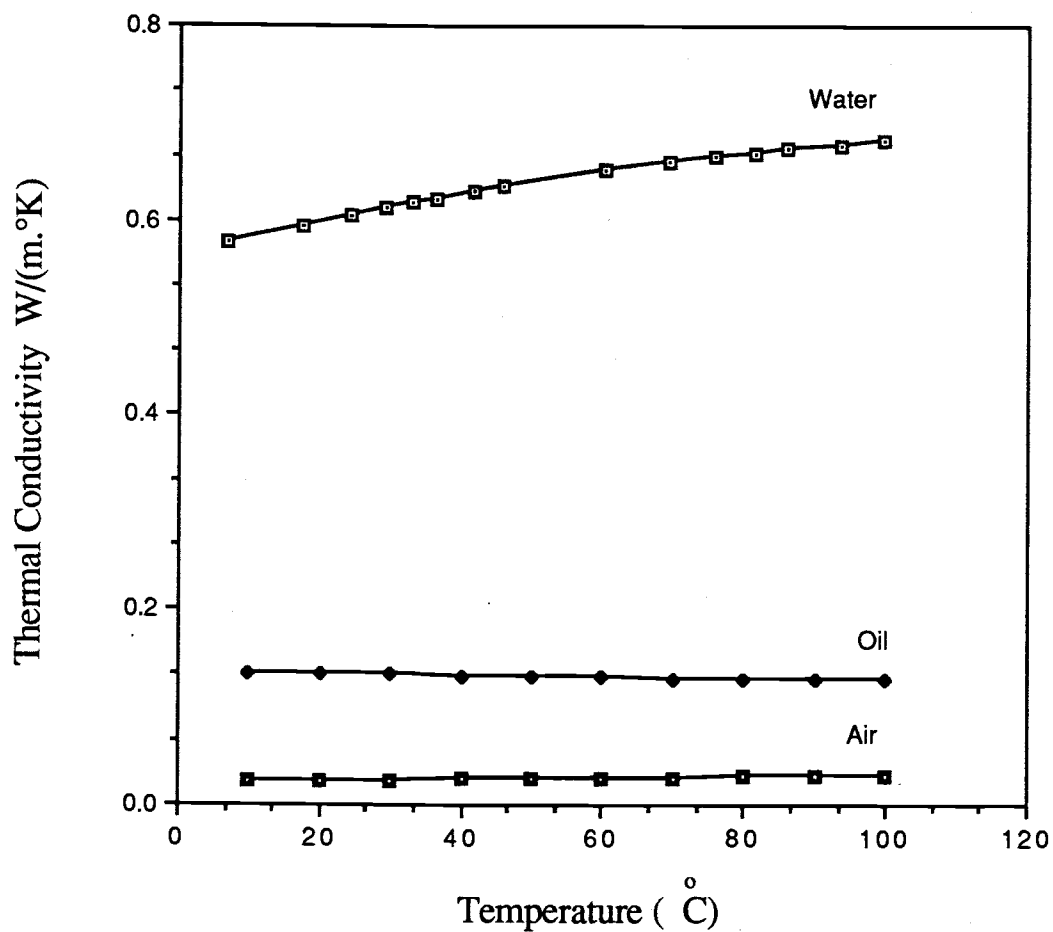
FLUID PROPERTY VARIATION WITH TEMPERATURE

Figure H (a) Thermal Conductivity-Temperature Variation

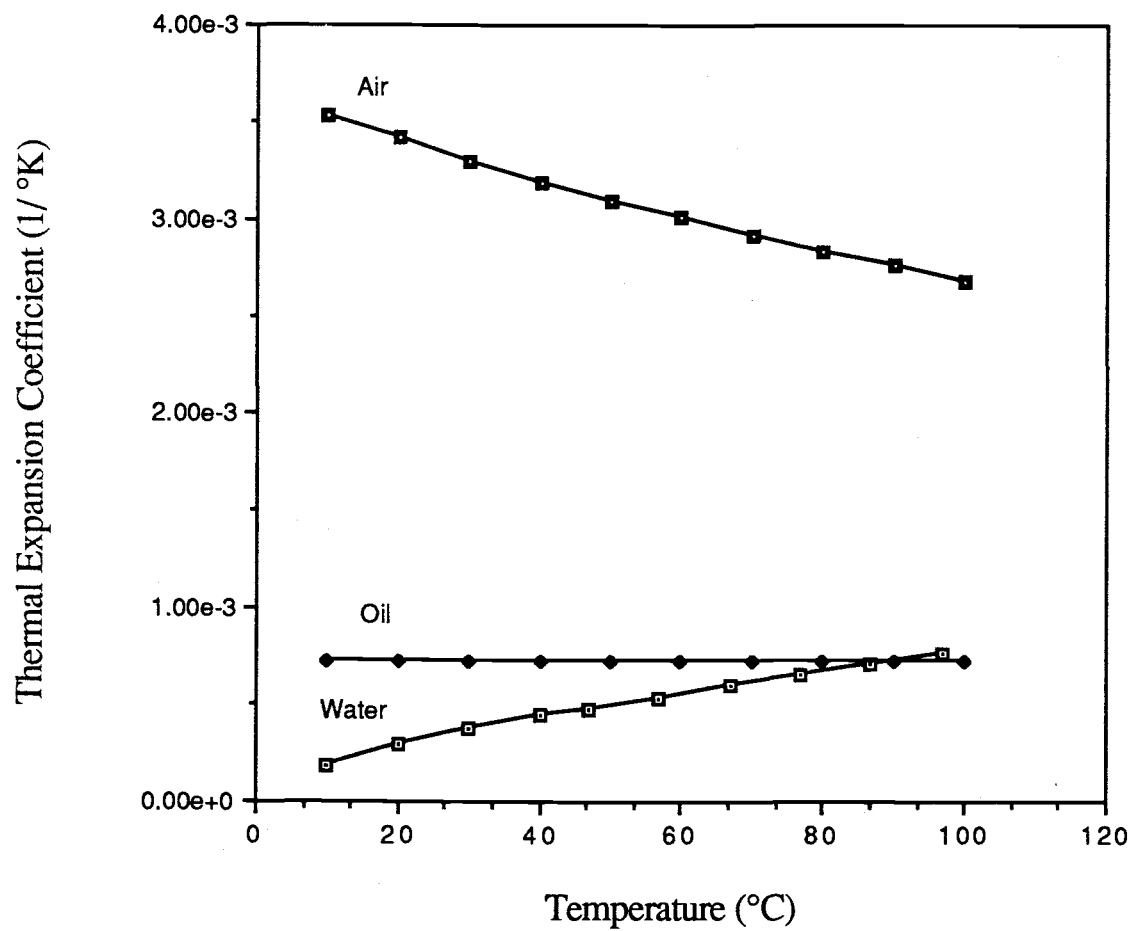


Figure H (b) Thermal Expansion Coefficient - Temperature Variation

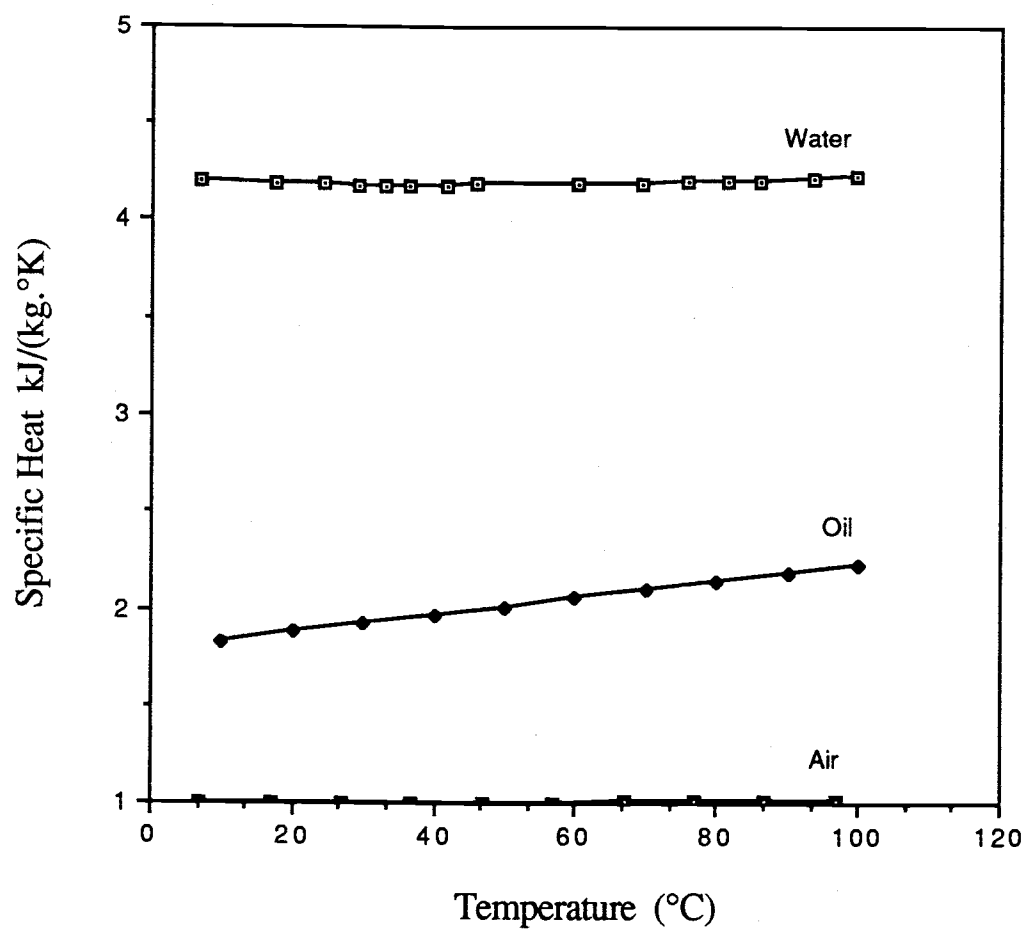


Figure H (c) Specific Heat-Temperature Variation

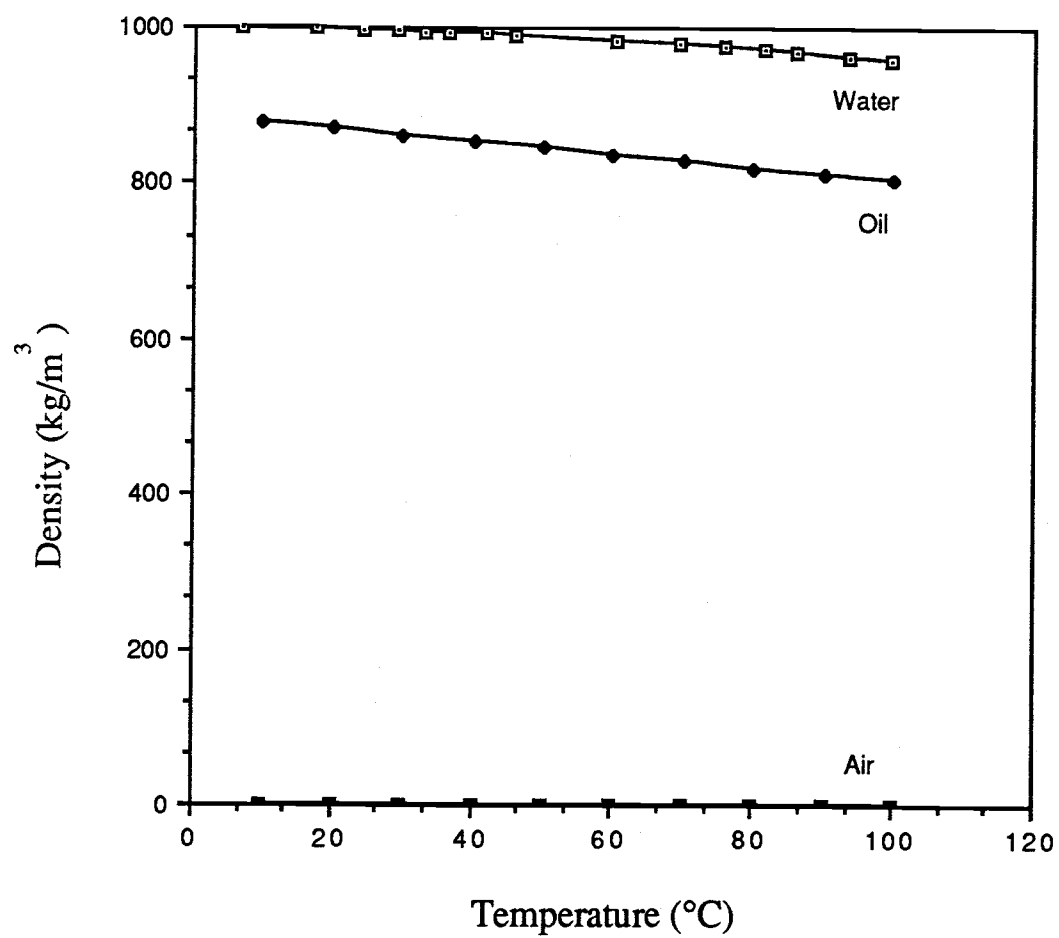


Figure H (d) Density-Temperature Variation

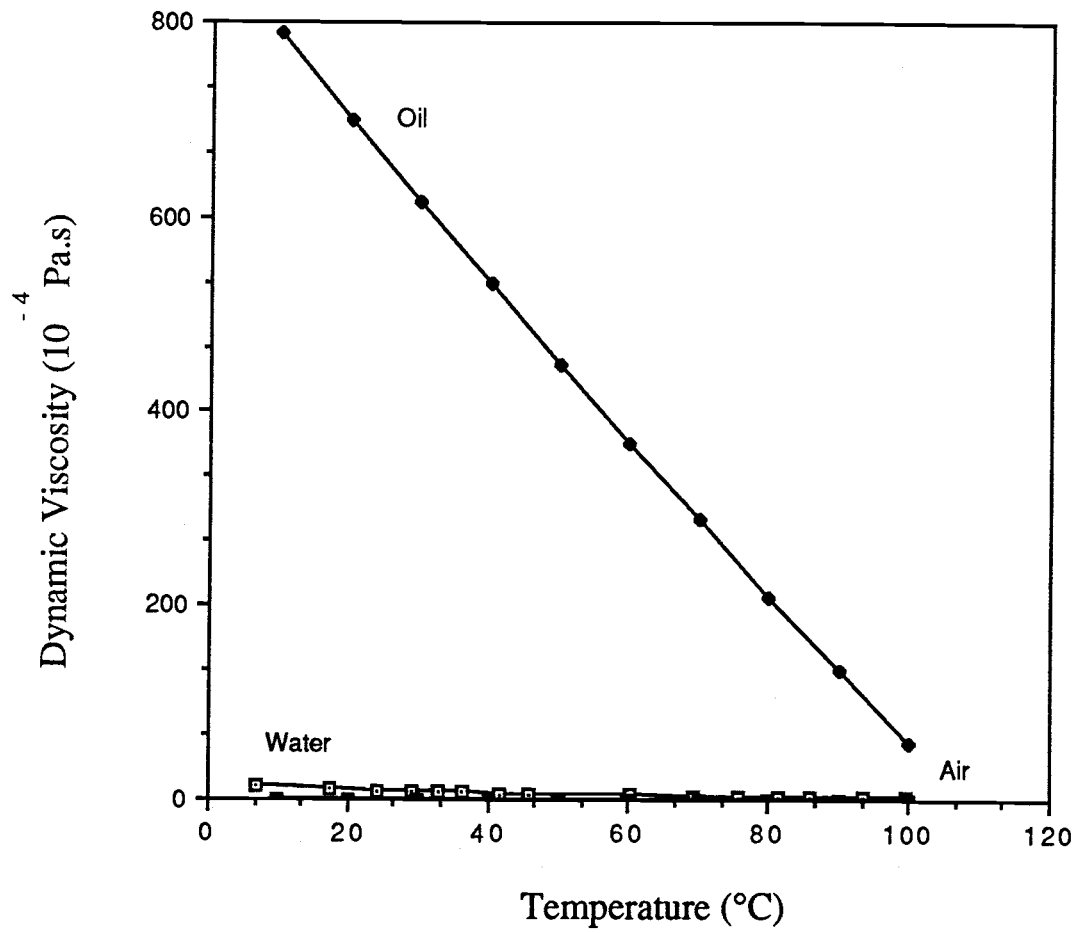


Figure H (e) Dynamic Viscosity-Temperature Variation

APPENDIX I

CORRELATION PROGRAM

```

PROGRAM LEASTSQ
CHARACTER*64 OFNAM8,OFNAM9
DIMENSION X(4,1010),C(3),S(5,5),ANP(5),RNRL(810),GRX(1010)
DIMENSION RNRLS(1010),RAM(810),XNU(1010),BH(4)
C   DETERMINE THE COEFFICIENTS OF FUNCTIONAL FORMS BY LEAST-
C   SQUARES CURVE FITTING METHOD WITH CURFT AND ERROR SUBROUTINES
HE=7.50
BH(1)=4.250/HE
BH(2)=2.686/HE
BH(3)=1.250/HE
BH(4)=0.781/HE
OPEN(19, FILE=' ', STATUS='NEW')
WRITE(*,111)
111  FORMAT(' ENTER FILE FOR FUNCTIONAL FORMS: ')
READ(*,112) OFNAM8
OPEN(18, FILE=OFNAM8)
112  FORMAT(A)
WRITE(*,123)
123  FORMAT(' ENTER # INDEPN VAR, # DATA, # EMPRI EQU, & SPACING: ')
READ(*,100) NVR, NOB, NE, B
100  FORMAT(1X,I1,1X,I3,I2,F6.3)
IF(B.LT.0.10) THEN
WRITE(*,121)
C
C   NSL: # DATA POINT FOR LARGE SPACING CHANNEL
C   NSM: # DATA POINT FOR MEDIUM SPACING CHANNEL +NSL
C   NSS: # DATA POINT FOR SMALL SPACING CHANNEL +NSL+NSM
C   NSV: # DATA POINT FOR VERY SMALL SPACING CHANNEL +NSL+NSM+NSS
C
121  FORMAT(' ENTER NSL, NSM, NSS, NSV: ')
READ(*,101) NSL,NSM,NSS,NSV
101  FORMAT(4(I3))
ELSE
END IF
IF((NOB.GT.808).AND.(NOB.LT.1008)) THEN
WRITE(*,125)
125  FORMAT(' ENTER NA, NW, & NO: ')
READ(*,122) NA, NW, NO
122  FORMAT(2(I3),I4)
ELSE
END IF
NOB=NOB*6
NSL=NSL*6
NSM=NSM*6
NSS=NSS*6
NSV=NSV*6
NSLW=10*6
NSMW=18*6
NSSW=9*6
NSVW=11*6
NSLO=10*6
NSMO=10*6
NSSO=11*6
NSVO=11*6
NA=NA*6
NW=NW*6
NO=NO*6
READ(18,99) (GRX(N),RAM(N),XNU(N),N=1,NGE)
99  FORMAT(6(1X,E8.2,1X,E8.2,1X,F7.2))
DO 3 I=1, NE
DO 1 NV=2,NVR
DO 11 N=1, NOB
X(1,N)=1.0

```

```

      IF(NV-3) 55, 66, 66
55  VARIND=RAM(N)
      IF(I.EQ.2) VARIND=GRX(N)
      X(2,N)=LOG(VARIND)
      GO TO 2
56  IF(B.LE.0.10) THEN
      IF(N.GT.NSV) THEN
      IF(N-1.EQ.NA) THEN
      NSL=NSLW+NA
      NSM=NSMW+NA
      NSS=NSSW+NA
      NSV=NSVW+NA
      ELSE
      END IF
      IF(N-1.EQ.NW) THEN
      NSL=NSLO+NW
      NSM=NSMO+NW
      NSS=NSSO+NW
      NSV=NSVO+NW
      ELSE
      END IF
      ELSE
      END IF
      IF(N.LT.NSL) NS=1
      IF((N.GT.NSL).AND.(N.LT.NSM)) NS=2
      IF((N.GT.NSM).AND.(N.LT.NSS)) NS=3
      IF(N.GT.NSS) NS=4
      ELSE
      NS=1
      BH(NS)=B/HE
      END IF
      VARIND2=RAM(N)/BH(NS)
      X(3,N)=LOG(BH(NS))
      IF(I.EQ.2) VARIND2=GRX(N)/BH(NS)
      X(2,N)=LOG(VARIND2)
      GO TO 2
2    M=NV+1
      X(M,N)=LOG(XNU(N))
11  CONTINUE
      CALL CURFT(NV,NOB,X,C)
      CALL ERROR(NV,NOB,X,C,SSQ)
      C(1)=EXP(C(1))
      IF(NV.EQ.2) THEN
      IF(I.EQ.2) THEN
      IF(B.GT.4.50) THEN
      WRITE(19,88) (C(J), J=1,NV)
      WRITE(*,88) (C(J), J=1,NV)
      ELSE
      WRITE(19,38) (C(J), J=1,NV)
      WRITE(*,38) (C(J), J=1,NV)
      END IF
      ELSE
      IF(B.GT.4.50) THEN
      WRITE(19,89) (C(J), J=1,NV)
      WRITE(*,89) (C(J), J=1,NV)
      ELSE
      WRITE(19,39) (C(J), J=1,NV)
      WRITE(*,39) (C(J), J=1,NV)
      END IF
      END IF
88  FORMAT(/, '      Nu = ',F9.6,' * Gr ** ',F9.6,/)
89  FORMAT(/, '      Nu = ',F9.6,' * Ra ** ',F9.6,/)
38  FORMAT(/, '      Nu = ',F9.6,' * (b/H Gr) ** ',F9.6,/)
39  FORMAT(/, '      Nu = ',F9.6,' * (b/H Ra) ** ',F9.6,/)
      ELSE

```

```

      IF(I.EQ.2) THEN
        WRITE(19,67) (C(J), J=1,NV)
        WRITE(*,67) (C(J), J=1,NV)
      ELSE
        WRITE(19,77) (C(J), J=1,NV)
        WRITE(*,77) (C(J), J=1,NV)
      END IF
67  FORMAT(/, '      Nu = ',F9.6,' * Gr ** ',F9.6,' (b/H) ** ',F9.6,/)
77  FORMAT(/, '      Nu = ',F9.6,' * Ra ** ',F9.6,' (b/H) ** ',F9.6,/)
      END IF
1   CONTINUE
3   CONTINUE
      END

      SUBROUTINE CURFT(NV,NOB,X,C)
        DIMENSION X(4,1010),C(3),S(5,5)
        DOUBLE PRECISION S, D
        C
        LEAST SQUARES - NV INDEPENDENT VARIABLES
        C
        Y=X(NV+1,I) - NOB: # OF OBSERVATIONS
        C
        C(I)=COEFFICIENT OF X(I)
        M=NV+1
        MP=M+1
        DO 1 I=1,M
          DO 1 J=1,MP
1         S(I,J)=0.0000000000
          DO 2 I=1,NOB
            DO 2 J=1,M
              DO 2 K=1,M
2             S(J,K)=S(J,K)+X(J,I)*X(K,I)
            S(1,MP)=1.0000000000
            IF(NV-1) 997,997,998
997          S(1,1)=S(1,2)/S(1,1)
            GO TO 999
998          DO 16 LK=1,NV
11           IF(S(1,1)) 13,12,13
12           WRITE(19,20)
20          FORMAT(' EQUATIONS IN SUBROUTINE CURFT ARE DEPENDENT - IGNORE
*FOLLOWING ERROR ANALYSIS')
            DO 30 III=1,NV
30           C(III)=0.
            GO TO 31
13           DO 14 J=1,M
14           S(M,J)=S(1,J+1)/S(1,1)
            DO 15 I=2,NV
              D=S(I,1)
              DO 15 J=1,M
15             S(I-1,J)=S(I,J+1)-D*S(M,J)
              DO 16 J=1,M
16             S(NV,J)=S(M,J)
999          DO 3 I=1,NV
            C(I)=S(I,1)
3           WRITE(19,4) I,C(I)
4           FORMAT(' ',10X,' COEFFICIENT OF X ',I2,' = ',E15.8)
31          RETURN
        END

        C
        SUBROUTINE ERROR(NV,NOB,X,C,SSQ)
          DIMENSION X(4,1010),C(3),S(5,5),ANP(5),RNRL(1010),RNRLS(1010)
          DOUBLE PRECISION YC, TS, TE
          C
          ERROR ANALYSIS - NOB: # OF OBSERVATIONS
          C
          Y=X(NV+1,I) - SSQ=STANDARD DEVIATION
          C
          C(I) - CONSTANTS
          C
          WRITTEN BY R. E. POWE - MECHANICAL ENGINEERING
          M=NV+1
          TS=0.0000000000
          TE=0.0000000000
          EMX=0.
          DO 5 I=1,5
            ANP(I)=0.
          C
          WRITE(19,1)
1         FORMAT(3X,' Y EXPERIMENTAL ',4X,' Y CALCULATED ',2X,' NUMERICAL ERR
*OR ',3X,' PER CENT ERROR')

```

```

DO 2 I=1, NOB
YE=X(M,I)
C ADD EQUATION FOR YC AT THIS POINT
YC=0.0000000000
DO 20 IJ=1,NU
20 YC=YC+C(IJ)*X(IJ,I)
C YC=C(1)*(X(NU,I))*C(2)
YC=EXP(YC)
YE=EXP(YE)
E=YC-YE
EP=100.*E/YE
EPA=ABS(EP)
IF(EPA-EMX) 6,6,7
7 EMX=EPA
6 DO 8 J=1,5
ACD=J*5
IF(EPA-ACD) 9,9,8
9 ANP(J)=ANP(J)+1.
8 CONTINUE
TS=TS+E*E
TE=TE+ABS(EP)
C WRITE(19,3) YE,YC,E,EP,I
3 FORMAT(4E17.8,IS)
2 CONTINUE
A=NOB
SSQ=SQRT(TS/A)
TE=TE/A
WRITE(19,4) SSQ,TE
4 FORMAT(1X,'STANDARD DEVIATION='E15.8,3X,'AVERAGE % DEVIATION=',
*E15.8)
WRITE(19,10) EMX
10 FORMAT(21X,'MAXIMUM PER CENT DEVIATION='E15.8)
DO 11 I=1,5
XNP=ANP(I)
XNP=100.*XNP/A
ACD=I*5
WRITE(19,12) XNP,ACD
11 CONTINUE
12 FORMAT(1X,E15.8,2X,'% OF DATA WITHIN',2X,E15.8,2X,'% OF EQUATION
*')
WRITE(19,77)
77 FORMAT(' ')
RETURN
END

```